MIMO Radar DOD/DOA Estimation and Performance Analysis in the Presence of SIRP Clutter

Vom Fachbereich 18

Elektrotechnik und Informationstechnik

der Technischen Universität Darmstadt

zur Erlangung der Würde eines

Doktor-Ingenieurs (Dr.-Ing.)

genehmigte Dissertation

von

Xin Zhang, M.Sc.

Geboren am 19. 11. 1987 in Henan, China

Referent:	Prof. Dr. Marius Pesavento
Korreferent:	Prof. Dr. Mohammed Nabil El Korso
Tag der Einreichung:	31. 05. 2016
Tag der mündlichen Prüfung:	17. 08. 2016

D17

Darmstädter Dissertation

2016

Declaration

I, the undersigned, hereby declare that this dissertation is my original work and has not been submitted or accepted for the award of any other degree in any institution.

Erklärung laut §9 der Promotionsordnung

Ich versichere hiermit dass ich die vorliegende Dissertation allein und nur unter Verwendung der angegebenen Literatur verfasst habe. Die Arbeit hat bisher noch nicht zu Prüfungszwecken gedient.

Signature/Unterschrift: .....

Your name here

Place/Ort: .....

Date/Datum: .....

VXORI MEAE FIDELI
OPVSCVLVM DEDICATVM EST

Acknowledgements

I herewith express my deepest and sincerest gratitude to my supervisors

Prof. Dr. Marius Pesavento,

and

Prof. Dr. Mohammed Nabil El Korso,

who are to me not only the best academic mentors, but examples to follow as human beings; and to my colleague

Dr. Ying Liu,

whose help with the numerical integration problems encountered in this work was indispensable; and to

Christian Steffens,

who contributed valuably to the German translation of this work's abstract; and to all my other previous and current colleagues in Communication Systems Group at TU Darmstadt, among whom are (in alphabetical order of last names):

Dr. Samer Alabed, Florian Bahlke, Dr. Nils Bornhorst,
Martin Brossard, Dr. Yong Cheng, Dr. Dana Ciochina,
Ganapati Hegde, Dr. Ka Lung Law, Dr. Liang Li,
Fabio Nikolay, Dr. Pouyan Parvazi, Oscar Dario Ramos Cantor,
Dr. Adrian Schad, Wassim Suleiman, Dima Taleb,
Dr. Xin Wen, Dr. Florian Xaver, Dr. Yang Yang,

not merely for their generous and willing help both in work and in daily life, but also for their company itself; and beg for forgiveness from all of the many who have contributed in various ways to the completion of this tiny piece of work but whose name I fail to mention above.

Xin Zhang

Darmstadt, Nov 15, 2016

圖難於其易，為大於其細。

(See simplicity in the complicated.
Achieve greatness in little things.)

——老子《道德經.為無為章第六十三》

(Lao-Tzu, *Tao Te Ching*, Ch. LXIII,
trans. G.-F. Feng and J. English)

Abstract

This thesis investigates the problem of target parameter estimation and performance analysis of multiple-input multiple-output (MIMO) radar in the presence of non-Gaussian clutter. During the past decades, multiple-input multiple-output (MIMO) radar has become a research subject of growing interest, due to its superior performance in many aspects over the traditional phased-array radar. Conventionally, MIMO radar clutter is modeled as Gaussian-distributed. This modeling, however, becomes unrealistic and inadequate in certain specific scenarios, where the clutter shows distinct non-Gaussianity. In the radar literature, one of the most notable and popular models for such non-Gaussian clutter is the so-called spherically invariant random process (SIRP) model. A SIRP is a complex, compound Gaussian process with random power and can be represented as the product of two components: a complex Gaussian process, called the speckle, and the square root of a positive scalar random process, called the texture. The goal of this thesis is to devise estimation algorithms for target parameters, more specifically, for direction-of-departures/arrivals (DODs/DOAs) of the targets, in a MIMO radar context in the presence of SIRP clutter, and to evaluate the ultimate performance of this estimation problem, in terms of performance bounds and of target resolvability. First, three DOD/DOA estimation algorithms are proposed, which differ from one another in the modeling of the texture, as well as in the respective likelihood functions that they are based on, but have in common that all three algorithms employ the same concept of the stepwise numerical concentration approach and thus have similar iterative procedures. Performance properties like convergence of iterations and computational complexity of the three proposed algorithms are then examined. Next, various Cramér-Rao-type bounds (CRTBs) for the DOD/DOA parameters in this context are derived for performance assessment and their relationships between one another are determined. The respective impacts of the texture parameters on the CRTBs are investigated to illustrate the effect of the clutter spikiness on the same. Then, the estimation performance achievable in the presence of SIRP clutter is studied from another point of view, namely, that of the target resolvability, which is quantified by the concept of the resolution limit (RL). As a result, an analytical, closed-form expression of the RL with respect to (w.r.t.) the angular parameters between two

closely spaced targets in this context is derived based on Smith's criterion. For this aim, non-matrix, closed-form expressions for several of the aforementioned CRTBs w.r.t. the angular spacing between the targets are also obtained as byproducts. Moreover, an alternative, more concrete expression for the RL is propsed for asymptotic scenarios. Like for the CRTBs, the respective impacts of the texture parameters on the RL are also determined. Finally, numerical simulations are provided to assess the performance of the proposed algorithms, to show the validity of the derived RL expressions, as well as to reveal the CRTBs' and the RL's insightful properties.

Zusammenfassung

Die vorliegende Dissertation untersucht das Problem der Zielparameterschätzung und der zugehörigen Genauigkeitsanalyse in einem Multiple-Input Multiple-Output (MIMO)-Radarsystem in Gegenwart von nicht Gaußschen Störechos (*eng.* clutter). Aufgrund seiner in vielen Aspekten dem traditionellen Phased-Array-Radar überlegenen Leistungsfähigkeit sind MIMO-Radarsysteme in den letzten Jahrzehnten ein Forschungsgegenstand von wachsendem Interesse geworden. In herkömmlichen Modellen wird das MIMO-Radar-Clutter gewöhnlich als gaußverteilt modelliert. Jedoch wird diese Modellierung in bestimmten Szenarien, in denen das Clutter von einer Gaußverteilung abweicht, unrealistisch und unzureichend. In der Literatur zur Radartechnik ist eines der weitest verbreiteten Modelle für solch nicht Gaußsches Clutter das Modell des sogenannten sphärisch invarianten Zufallsprozesses (*eng.* spherically invariant random process, kurz SIRP). Ein SIRP ist ein komplexwertiger Verbundgaußprozess mit zufälliger Leistung und kann als das Produkt von zwei Komponenten dargestellt werden: ein komplexwertiger Gaußprozess, im Englischen als “Speckle” bezeichnet, und die Quadratwurzel eines positiven Skalar-Zufallsprozess, im Englischen als “Texture” bezeichnet. Das Ziel dieser Arbeit ist es, Schätzalgorithmen für Zielparameter, genauer gesagt für Aus-/Einfallsrichtungen (*eng.* direction-of-departures/arrivals, kurz DODs/DOAs) der Ziele, in einem MIMO-Radarsystem in Gegenwart von SIRP-Clutter zu entwickeln, und die Leistungsfähigkeit dieser Schätzungsaufgabe in Bezug auf die Güte der Zielparameterschätzung sowie das Zielauflösungsvermögen zu bewerten. Zunächst werden drei DOD/DOA-Schätzalgorithmen vorgestellt, die sich voneinander in der Modellierung des Textures sowie in den jeweilig zugrundeliegenden Wahrscheinlichkeitsfunktionen unterscheiden. Gleichzeitig ist allen drei Algorithmen gemeinsam, den gleichen Ansatz der sukzessiven numerischen Konzentration zu verwenden und somit ähnliche iterative Verfahrensweisen zu besitzen. Daraufhin werden Eigenschaften wie die Konvergenz der Iterationen und die Rechenkomplexität der drei vorgeschlagenen Algorithmen untersucht. Für die Analyse der Schätzgüte werden verschiedene Cramér-Rao-artige Grenzen (*eng.* Cramér-Rao-type bounds, kurz CRTBs) für die DOD/DOA-Parameter abgeleitet und ihre Beziehungen untereinander bestimmt, und die jeweiligen Auswirkungen der Textureparameter auf

die CRTBs werden untersucht. Anschließend wird die erreichbare Schätzgüte in Gegenwart von SIRP-Clutter unter dem Gesichtspunkt des Zielauflösungsvermögens betrachtet, welches sich durch die sogenannte Auflösungsgrenze (*eng.* resolution limit, kurz RL) quantifizieren lässt. Basierend auf dem Smithschen Kriterium wird als Ergebnis dieser Betrachtung ein analytisch geschlossener Ausdruck des RLs mit Bezug auf die Winkelparameter zwischen zwei eng aneinanderliegenden Zielen hergeleitet. Als Nebenprodukte der Herleitung werden analytisch geschlossene Ausdrücke für mehrere der genannten CRTBs bezüglich des Winkelabstands zwischen den Zielen erhalten. Darüber hinaus wird ein alternativer, konkreterer Ausdruck für die RL für asymptotische Szenarien vorgestellt. Wie bereits für die CRTBs werden die Auswirkungen der Textureparameter auf das RL bestimmt. Abschließend werden numerische Ergebnisse dargestellt, um die Güte der vorgestellten Algorithmen zu demonstrieren, die Gültigkeit der abgeleiteten RL-Ausdrücke aufzuweisen sowie die aufschlussreichen Eigenschaften der CRTBs und des RLs aufzuzeigen.

List of Abbreviations

Alg.	algorithm
ARL	angular resolution limit
BCD	block coordinate descent
Ch.	chapter
CM	covariance matrix
CMLE	conventional maximum likelihood estimator
cont'd	continued
CPI	coherent processing interval
CRB	Cramér-Rao bound
CRLB	Cramér-Rao lower bound
CRTB	Cramér-Rao-type bound
DML	deterministic maximum likelihood
DOA	direction-of-arrival
DOD	direction-of-departure
EMCB	extended Miller-Chang bound
Eq.	equation
ESPRIT	estimation of signal parameters via rotational invariance technique
Fig.	figure
FIM	Fisher information matrix
GLRT	generalized likelihood ratio test

GMANOVA	generalized multivariate analysis of variance
HCRB	hybrid Cramér-Rao bound
IEMLE	iterative exact maximum likelihood estimator
i.i.d.	independent and identically distributed
KKT	Karush–Kuhn–Tucker
LF	likelihood function
IMAPE	iterative maximum a posteriori estimator
IMLE	iterative maximum likelihood estimator
LLF	log-likelihood function
MAP	maximum a posteriori
MCB	Miller-Chang bound
MCRB	modified Cramér-Rao bound
MIMO	multiple-input multiple-output
ML	maximum likelihood
MSE	mean squared error
MUSIC	multiple signal classification
PDF	probability density function
PX-EM	parameter-expanded expectation-maximization
RCS	radar cross-section
RL	resolution limit
SCR	signal-to-clutter ratio
Sec.	section
Subsec.	subsection
SIRP	spherically invariant random process
SIRV	spherically invariant random vector
SML	stochastic maximum likelihood
SNR	signal-to-noise ratio

SRL	statistical resolution limit
STAP	space-time adaptive processing
w.r.t.	with respect to

List of Symbols

$\mathbb{Z}$	set of integers
$\bigwedge$	logical conjunction
$\bigvee$	logical disjunction
$\sim$	distributed as
$\propto$	direct proportionality
$\otimes$	Kronecker product
$\odot$	Hadamard product
$\hat{(\cdot)}$	estimate of a parameter
$\hat{(\cdot)}^{(i)}$	estimate of a parameter at the ith iteration
$(\cdot)^T$	transpose of a matrix
$(\cdot)^H$	conjugate transpose of a matrix
$(\cdot)^*$	conjugate of a matrix
$[\cdot]_i$	ith element of a vector
$[\cdot]_{i,j}$	(i,j)th entry of a matrix
$\|\cdot\|$	Euclidean norm
$\mathrm{E}\{\cdot\}$	expectation
$\mathrm{E}_{\boldsymbol{y}}\{\cdot\}$	expectation w.r.t. the parameter $\boldsymbol{y}$
$\mathrm{Re}\{\cdot\}$	real part
$\mathrm{Im}\{\cdot\}$	imaginary part
$\mathrm{tr}\{\cdot\}$	trace of a matrix

$\mathrm{vec}\{\cdot\}$	vectorization of a matrix
$\boldsymbol{A} \succeq \boldsymbol{B}$	$\boldsymbol{A} - \boldsymbol{B}$ is a positive semidefinite matrix
$\Gamma(\cdot)$	gamma function
$\Psi(\cdot)$	digamma function
$K_n(\cdot)$	modified Bessel function of the second kind of order n
δ_{ij}	Kronecker delta
B_i	ith Bernoulli number
$i_{\max}$	maximum number of iterations
x_{o_i}	abscissa of the generalized Gauss-Laguerre quadrature
w_{o_i}	weight of the generalized Gauss-Laguerre quadrature
$O_1^{(\cdot)}$	order of the generalized Gauss-Laguerre quadrature; the number in its subscript denotes the parameter of the corresponding abscissa and weight
$\arg\min_x \{f(x)\}$	value of x that minimizes $f(x)$
$\boldsymbol{P}_{(\cdot)}^{\perp}$	orthogonal projection matrix onto the null space spanned by the columns of a matrix
K	number of radar targets
L	number of radar pulses per CPI
T	number of snapshots per pulse
M	number of sensors at the transmitter
N	number of sensors at the receiver
λ	carrier wavelength
$d_i^{(\mathrm{T})}$	distance between the ith sensor and the reference sensor at the transmitter
$d_i^{(\mathrm{R})}$	distance between the ith sensor and the reference sensor at the receiver
$\boldsymbol{I}_M$	$M \times M$ identity matrix
$\boldsymbol{0}_{M\times N}$	$M \times N$ zero matrix
$\boldsymbol{J}_M$	$M \times M$ all-ones matrix
$\boldsymbol{1}_M$	all-ones column vector of dimension M

$\boldsymbol{e}_L^{l+1}$	$L \times 1$ vector whose $(l+1)$th element is one and others are zero
$\boldsymbol{S}$	signal source waveform matrix
$\boldsymbol{s}(t)$	signal source waveform vector at the tth snapshot (Ch. 7)
$\boldsymbol{Y}(l)$	radar output matrix at the lth pulse before matched filtering
$\boldsymbol{Y}$	radar output matrix before matched filtering in the one pulse per CPI case (Ch. 7)
$\boldsymbol{y}(t)$	radar output vector at the tth snapshot before matched filtering in the one pulse per CPI case (Ch. 7)
$\boldsymbol{M}(l)$	clutter matrix at the lth pulse before matched filtering
$\boldsymbol{M}$	clutter matrix before matched filtering in the one pulse per CPI case (Ch. 7)
$\boldsymbol{m}(t)$	clutter vector at the tth snapshot before matched filtering in the one pulse per CPI case (Ch. 7)
$\boldsymbol{Z}(l)$	radar output matrix at the lth pulse after matched filtering
$\boldsymbol{N}(l)$	clutter matrix at the lth pulse after matched filtering
$\boldsymbol{z}(l)$	vectorized radar output at the lth pulse after matched filtering
$\tilde{\boldsymbol{z}}(l)$	vectorized radar output at the lth pulse after matched filtering, spatially whitened by the square root of the speckle CM inverse
$\boldsymbol{z}$	full observation vector after matched filtering
$\boldsymbol{n}(l)$	vectorized clutter at the lth pulse after matched filtering
$\tau(l)$	texture of the clutter vector $\boldsymbol{n}(l)$
$\bar{\tau}(t)$	texture of the clutter vector $\boldsymbol{m}(t)$ in the one pulse per CPI case (Ch. 7)
$\boldsymbol{\tau}$	vector containing the texture realizations at all L pulses
$\hat{\boldsymbol{\tau}}_{\text{MAP}}$	MAP estimate of the texture realization parameter vector $\boldsymbol{\tau}$
$\boldsymbol{x}(l)$	speckle of the clutter vector $\boldsymbol{n}(l)$
$\bar{\boldsymbol{x}}(t)$	speckle of the clutter vector $\boldsymbol{m}(t)$ in the one pulse per CPI case (Ch. 7)
$\boldsymbol{v}(l)$	vector containing RCS coefficients and normalized Doppler frequency shifts of the targets at the lth pulse
$\boldsymbol{v}$	parameter vector containing the real and imaginary parts of $\boldsymbol{v}(l)$ at all L pulses

$\boldsymbol{H}(l)$	a diagonal matrix composed of the elements of $\boldsymbol{v}(l)$
$\hat{\boldsymbol{P}}$	a matrix composed of functions of $\boldsymbol{v}(l)$ at all L pulses
$\hat{\boldsymbol{Q}}$	a matrix composed of functions of $\tau(l)$ and $\boldsymbol{v}(l)$ at all L pulses
$\alpha_k(l)$	RCS coefficient of the kth target
α_k	RCS coefficient of the kth target in the one pulse per CPI case (Ch. 7)
$\boldsymbol{\alpha}$	complex parameter vector including the RCS coefficients of all K targets
$f_k(l)$	normalized Doppler frequency shift of the kth target
$\boldsymbol{f}$	parameter vector containing the normalized Doppler frequency shifts of all K targets
$\theta_k^{(\mathrm{T})}$	DOD of the kth target
$\theta_k^{(\mathrm{R})}$	DOA of the kth target
$\boldsymbol{a}_{(\mathrm{T})}\left(\theta_k^{(\mathrm{T})}\right)$	transmit steering vector for the kth target
$\boldsymbol{a}_{(\mathrm{R})}\left(\theta_k^{(\mathrm{R})}\right)$	receive steering vector for the kth target
$\boldsymbol{\theta}$	parameter vector containing DODs and DOAs of all K targets
$\hat{\boldsymbol{\theta}}_{\mathrm{CMLE}}$	estimate of $\boldsymbol{\theta}$ by the CMLE
$\hat{\boldsymbol{\theta}}_{\mathrm{IMLE}}$	estimate of $\boldsymbol{\theta}$ by the IMLE
$\hat{\boldsymbol{\theta}}_{\mathrm{IMAPE}}$	estimate of $\boldsymbol{\theta}$ by the IMAPE
$\varepsilon_{\boldsymbol{\theta}}$	convergence threshold w.r.t. $\boldsymbol{\theta}$
$\boldsymbol{a}\left(\theta_k^{(\mathrm{T})}, \theta_k^{(\mathrm{R})}\right)$	steering vector after matched filtering
$\boldsymbol{D}^{(\mathrm{T})}$	a matrix composed of the partial derivatives of the steering vector $\boldsymbol{a}\left(\theta_k^{(\mathrm{T})}, \theta_k^{(\mathrm{R})}\right)$ w.r.t. the DODs
$\boldsymbol{D}^{(\mathrm{R})}$	a matrix composed of the partial derivatives of the steering vector $\boldsymbol{a}\left(\theta_k^{(\mathrm{T})}, \theta_k^{(\mathrm{R})}\right)$ w.r.t. the DOAs
$\boldsymbol{D}$	matrix composed of $\boldsymbol{D}^{(\mathrm{T})}$ and $\boldsymbol{D}^{(\mathrm{R})}$
$\tilde{\boldsymbol{D}}$	matrix $\boldsymbol{D}$ spatially whitened by the square root of the speckle CM inverse
$\boldsymbol{A}(\boldsymbol{\theta})$	steering matrix after matched filtering
$\tilde{\boldsymbol{A}}(\boldsymbol{\theta})$	steering matrix after matched filtering, spatially whitened by the square root of the speckle CM inverse

$\boldsymbol{b}(\boldsymbol{\theta}, l)$	signal part of the observation at lth pulse
$\boldsymbol{\gamma}$	vector composed of the concatenation of $\boldsymbol{b}(\boldsymbol{\theta}, l)$ at all L pulses
a	shape parameter of the clutter texture
b	scale parameter of the clutter texture
Gamma(a, b)	gamma distribution with shape parameter a and scale parameter b
Inv-Gamma(a, b)	inverse-gamma distribution with shape parameter a and scale parameter b
$\boldsymbol{\Sigma}$	CM of the clutter speckle
σ^2	a factor to adjust speckle power
$\boldsymbol{\Sigma}_{\text{n}}$	normalized clutter speckle CM
$\text{tr}\{\boldsymbol{\Sigma}\}_{\text{a}}$	an alternatively assumed trace value for the speckle CM other than the one in Eq. (2.17
r	ratio between the alternatively and the originally assumed speckle CM trace and the one assumed in Eq. (2.17)
$\hat{(\cdot)}'$	counterpart of a parameter resulting from the alternative assumption on the speckle CM trace
$\boldsymbol{\rho}(l)$	clutter realization at the lth pulse with its speckle spatially whitened by the square root of the speckle CM inverse
$g_{MN}\left(\|\boldsymbol{\rho}(l)\|^2, a, b\right)$	characteristic function of SIRP clutter
$h_{MN}\left(\|\boldsymbol{\rho}(l)\|^2, a, b\right)$	a function based the clutter characteristic function and its partial derivative w.r.t. its first argument $\|\boldsymbol{\rho}(l)\|^2$
$k_{MN}\left(\|\boldsymbol{\rho}(l)\|^2, a, b\right)$	partial derivative of the clutter characteristic function w.r.t. its second argument (the shape parameter a)
$l_{MN}\left(\|\boldsymbol{\rho}(l)\|^2, a, b\right)$	partial derivative of the clutter characteristic function w.r.t. its third argument (the scale parameter b)
$\boldsymbol{\zeta}$	parameter vector containing the real and imaginary parts of the entries of the lower triangular part of the speckle CM

$\boldsymbol{\chi}$	original unknown parameter vector
$\boldsymbol{\xi}$	transformed unknown parameter vector
$\boldsymbol{\xi}_{\text{det}}$	transformed unknown parameter vector in the deterministic texture case
$\boldsymbol{\xi}_{\text{hyb}}$	transformed hybrid unknown parameter vector
$\boldsymbol{\mu}$	signal parameter vector containing $\boldsymbol{\theta}$ and $\boldsymbol{v}$
$\boldsymbol{\varpi}$	clutter parameter vector containing $\boldsymbol{\zeta}$, a and b
$\boldsymbol{\varpi}_{\text{det}}$	clutter parameter vector in the deterministic texture case
$\boldsymbol{\varpi}_{\text{hyb}}$	augmented hybrid clutter parameter vector
$\bar{\boldsymbol{\xi}}$	unknown parameter vector for the simplified model (Ch. 7)
$\boldsymbol{\psi}$	transformed unknown parameter vector that does not contain the texture parameters
$p(\tau(l); a, b)$	PDF of the clutter texture with parameters a and b
$p(\boldsymbol{\tau}; a, b)$	PDF of the texture realization parameter vector with parameters a and b
$p\left(\boldsymbol{z} \mid \boldsymbol{\tau}; \boldsymbol{\psi}\right)$	conditional PDF of $\boldsymbol{z}$ conditioned on $\boldsymbol{\tau}$ with parameter vector $\boldsymbol{\psi}$
$p\left(\boldsymbol{z}, \boldsymbol{\tau}; \boldsymbol{\xi}\right)$	joint PDF between $\boldsymbol{z}$ and $\boldsymbol{\tau}$ with parameter vector $\boldsymbol{\xi}$
$p\left(\boldsymbol{z}; \boldsymbol{\xi}\right)$	marginal PDF of $\boldsymbol{z}$ with parameter vector $\boldsymbol{\xi}$
Λ_{C}	conditional LLF
Λ_{J}	joint LLF
Λ_{M}	marginal LLF
$\mathbf{CRB}\left(\boldsymbol{\theta}\right)$	CRB w.r.t. the parameter vector $\boldsymbol{\theta}$
$\mathbf{EMCB}\left(\boldsymbol{\theta}\right)$	EMCB w.r.t. the parameter vector $\boldsymbol{\theta}$
$\mathbf{MCB}\left(\boldsymbol{\theta}\right)$	MCB w.r.t. the parameter vector $\boldsymbol{\theta}$
$\mathbf{MCRB}\left(\boldsymbol{\theta}\right)$	MCRB w.r.t. the parameter vector $\boldsymbol{\theta}$
$\mathbf{HCRB}\left(\boldsymbol{\theta}\right)$	HCRB w.r.t. the parameter vector $\boldsymbol{\theta}$
$\boldsymbol{F}$	FIM for the CRB
$\boldsymbol{F}_{\text{EMC}}$	FIM for the EMCB

$\boldsymbol{F}_{\text{MC}}$	FIM for the MCB
$\boldsymbol{F}_{\text{M}}$	FIM for the MCRB
$\boldsymbol{F}_{\text{H}}$	FIM for the HCRB
$\boldsymbol{\Phi}$	block of $\boldsymbol{F}$ w.r.t. the signal parameter vector $\boldsymbol{\mu}$
$\bar{\boldsymbol{\Phi}}$	FIM block w.r.t. the signal parameters for the simplified model (Ch. 7)
$\boldsymbol{\varsigma}$	4×1 lower left block of $\bar{\boldsymbol{\Phi}}$ (Ch. 7)
$\boldsymbol{\Omega}$	4×4 lower right block of $\bar{\boldsymbol{\Phi}}$ (Ch. 7)
$\boldsymbol{\Omega}_i$ $i = 1, 2, 3$	submatrices of $\boldsymbol{\Omega}$ (Ch. 7)
$\boldsymbol{\Theta}_i$ $i = 1, \ldots, 4$	2×2 submatrices of the inverse of $\boldsymbol{\Omega}$ (Ch. 7)
$\boldsymbol{\Phi}_{\boldsymbol{\theta\theta}}$	block of $\boldsymbol{\Phi}$ w.r.t. the parameter vector $\boldsymbol{\theta}$
$\boldsymbol{\Phi}_{\boldsymbol{\theta v}}$	block of $\boldsymbol{\Phi}$ w.r.t. the parameter vectors $\boldsymbol{\theta}$ and $\boldsymbol{v}$
$\boldsymbol{\Phi}_{\text{EMC}}$	block of $\boldsymbol{F}_{\text{EMC}}$ w.r.t. the signal parameter vector $\boldsymbol{\mu}$
$\boldsymbol{\Phi}_{\text{MC}}$	block of $\boldsymbol{F}_{\text{MC}}$ w.r.t. the signal parameter vector $\boldsymbol{\mu}$
$\boldsymbol{\Phi}_{\text{M}}$	block of $\boldsymbol{F}_{\text{M}}$ w.r.t. the signal parameter vector $\boldsymbol{\mu}$
$\boldsymbol{\Phi}_{\text{H}}$	block of $\boldsymbol{F}_{\text{H}}$ w.r.t. the signal parameter vector $\boldsymbol{\mu}$
ϕ_{ij}	entries of $\boldsymbol{\Phi}$
$\bar{\varphi}_{ij}$	entries of $\bar{\boldsymbol{\Phi}}$ (Ch. 7)
ϕ_{ij}^{EMC}	entries of $\boldsymbol{\Phi}_{\text{EMC}}$
ϕ_{ij}^{M}	entries of $\boldsymbol{\Phi}_{\text{M}}$
$\kappa(MN, a, b)$	a factor in the expression of the CRB that contains information from the texture distribution
$\nu(a, b)$	a factor in the expression of the MCRB that contains information from the texture distribution
ω_1	electrical angle of the first target (Ch. 7)
ω_2	electrical angle of the second target (Ch. 7)
Δ	spacing between the two targets w.r.t. the electrical angles (Ch. 7)
σ_Δ	standard deviation of the estimate of Δ (Ch. 7)

δ	ARL of the two targets .r.t. the electrical angles (Ch. 7)
$\boldsymbol{\eta}$	a vector containing the unknown parameters after model linearization (Ch. 7)
$\boldsymbol{C}(t)$	a matrix containing the known angular parameter ω_1 after model linearization (Ch. 7)
$\boldsymbol{R}_i,\ i=1,2,3$	matrices based on transformations of the steering vectors w.r.t. the known angular parameter ω_1 after model linearization (Ch. 7)
$\boldsymbol{\Upsilon}$	block-diagonal matrix composed of the speckle CM inverse (Ch. 7)
$\boldsymbol{\beta}_i(t),\ i=1,2,3$	columns of $\boldsymbol{C}(t)$, obtains as the respective products of $\boldsymbol{R}_i$ and $\boldsymbol{s}(t)$ (Ch. 7)
$\boldsymbol{\beta}_i,\ i=1,2,3$	vectors composed of the concatenation of $\boldsymbol{\beta}_i(t),\ i=1,2,3$, respectively, for all T snapshots (Ch. 7)
$\tilde{\boldsymbol{\beta}}_i$	$\boldsymbol{\beta}_i$ spatially whitened by the square root of $\boldsymbol{\Upsilon}$ (Ch. 7)
$\boldsymbol{y}$	full observation vector (Ch. 7)
$\gamma_{ij},\ i,j=1,2,3$	quadratic forms $\boldsymbol{\beta}_i^H\boldsymbol{\Upsilon}\boldsymbol{\beta}_j$ (Ch. 7)
Q	a factor in the analytical expression of the CRB based on the linearized model (Ch. 7)
$A,\ B,\ C$	coefficients of the quartic equation (transformed Smith's equation) in Eq. (7.42) (Ch. 7)
$\boldsymbol{\Gamma}$	a 3×3 Gramian matrix whose entries are γ_{ij} (Ch. 7)
$\boldsymbol{U}$	a matrix containing the singular vectors of $\boldsymbol{\Sigma}_{\mathrm{n}}^{-1}$ (Ch. 7)
$\lambda_n,\ n=1,\ldots,N$	eigenvalues of $\boldsymbol{\Sigma}_{\mathrm{n}}^{-1}$ (Ch. 7)

Table of Contents

Chapter 1

Introduction

1.1 Background

1.1.1 Multiple-Input Multiple-Output Radar

During the past decade, multiple-input multiple-output (MIMO) radar has been attracting an increasing academic interest [1–5] due to its potential to significantly improve radar performance as compared with the conventional, phased-array radar. MIMO radar, whose concept was first introduced in [6, 7], can be generally defined as a radar that uses multiple antennas to simultaneously transmit diverse (possibly linearly independent, or orthogonal) waveforms and by utilizing multiple antennas to receive the reflected signals [3].

Based on their antenna configurations, MIMO radar systems generally fall into two classes:

I. **MIMO radar with widely separated antennas** (also known as the statistical MIMO radar, distributed MIMO radar, MIMO radar with large aperture arrays, etc.) [4, 5], where the transmit (or both the transmit and the receive) antennas are separated widely enough such that the observed aspect of the target is different for each pair of the transmit/receive antennas. As a result, the total received signal is a superposition of signals from multiple independent fading paths, i.e., paths with statistically independent reflection coefficients. Thus the signal-to-noise ratio (SNR) of the received signal are

relatively constant. This spatial diversity makes the MIMO radar with widely separated antennas more robust against performance deteriorations arising from target scintillations and glint, thereby improves the stability of statistical hypothesis tests, and enhances the resolution and accuracy of target localization [1, 4, 8, 9].

II. **MIMO radar with co-located antennas** (also known as the co-located MIMO radar, coherent MIMO radar, MIMO radar with small aperture arrays, etc.) [2, 3], which has its antennas close to each other both at the transmitter and receiver. Consequently, all the transmit/receive antenna pairs observe the identical radar cross-section (RCS) of the target, which is a measure of power scattered in a given direction when a target is illuminated by an incident wave [10]. By exploiting the waveform diversity, MIMO radar with co-located antenna can utilize virtual sensors to extend its array aperture, thus has the advantages of improved parameter identifiability and estimation accuracy, higher resolution, more flexible beam-pattern design, direct applicability of space-time adaptive processing (STAP) techniques, etc., [3, 11, 12]. Furthermore, MIMO radar with co-located antennas can largely mitigate the time/phase synchronization problem which MIMO radar with widely separated antennas is prone to.

It should be noted that MIMO radar with co-located antennas (with which this thesis is concerned) can either be *monostatic* radar [2, 3, 13, 14] or *bistatic* radar [15–18], whereas MIMO radar with widely separated antennas can be viewed as a type of *multistatic* radar [4]. A monostatic radar is a radar whose transmitter and receiver are co-located, while a bistatic radar is one whose transmitter and receiver are separated by a distance that is comparable to the expected target distance. A multistatic radar, on the other hand, consists of multiple monostatic/bistatic radar components that are spatially diverse. Also note that the concepts of "monostatic" and "bistatic" are concerned with the locations of the transmitter and receiver, instead of the locations of the antennas constituting them, and should not be confused with the concepts of MIMO radars with widely separated and co-located antennas.

1.1.2 Spherically Invariant Random Process Clutter

The term "clutter" in the radar context refers to any unwanted echoes that are caused by scattering objects (e.g., sea, ground, buildings, rain, birds, etc.) other than the targets of interest. Clutter can generally be categorized as either *surface* or *volume* clutter, depending on whether the related scatterer forms a surface or fills a volume. Surface clutter includes ground and sea clutter, etc., while weather and chaff clutter are typical examples of volume clutter. Similar to thermal noise, clutter is random due to the random phases and amplitudes of the scatterers. Since in many scenarios the clutter level is much higher than the thermal noise level at the radar receiver, the radar's detection performance depends on the Signal-to-Clutter Ratio (SCR) instead of the SNR in these cases [19].

In the larger part of the radar literature, the clutter is simply assumed to be a Gaussian stochastic process. Such assumption is generally a good approximation in many cases and has the central limit theorem as its theoretical basis, which requires that the received clutter results from a *large number* of independent and identically distributed (i.i.d.) elementary scatterers. However, in certain specific scenarios where this requirement is not fulfilled, the radar clutter can have an extended tail in the distribution and thus cannot be correctly described by the Gaussian model anymore. As an example, experimental measurements reveal that the ground clutter data heavily deviate from the Gaussian model [20]. This is also true, e.g., for the sea clutter in a high-resolution and low-grazing-angle radar context, where the scatter number is random and the clutter shows nonstationarity [21].

To account for such problems where the clutter is a non-Gaussian process, numerous clutter models have been developed. Among them, the so-called spherically invariant random process (SIRP) model has become the most notable and popular one in radar clutter modeling [20–24]. The concept of SIRPs was first proposed in [25] as a generalization to Gaussian processes, in which a random process is called a SIRP if all the random variables having the same variance in the subspace that is the closed linear span of all the random variables sampled from that process, have the same distribution function. Accordingly, a random vector obtained by sampling a SIRP is called a spherically invariant random vector (SIRV).

A SIRP is a two-scale, complex, compound Gaussian process with random power and

can be represented as the product of two components: a complex Gaussian process with zero mean and unknown covariance matrix (CM), and the square root of a positive scalar random process [22, 23]. In the radar context, the former describes the local scattering and is usually referred to as *speckle*, while the latter, modeling the local power changing, is called *texture*.

Till now, the SIRP model has gained widespread use to treat the heavy-tailed, non-Gaussian distributions of radar clutters [21, 26–29], due to the many advantages that it has, among which are:

I. A SIRP modeling is capable of describing different scales of the clutter roughness.

II. It encompasses a wide variety of non-Gaussian distributions (K-distribution, Student's t-distribution, Laplace, Cauchy and Weibull distribution, etc.).

III. It is mathematically tractable because a SIRP preserves many important properties of a Gaussian process, such as [30]:

   (i) The probability density function (PDF) of a SIRV sampled from a SIRP is uniquely determined by the specification of its mean vector (often assumed as zero vector in practice), its speckle CM, and its speckle PDF (called the *characteristic PDF* of the SIRV).

   (ii) A SIRV is invariant (closed) under a linear transformation, and does not change its characteristic PDF by such a transformation. This property allows a SIRV to be whitened without any penalty.

This thesis deals mainly with two clutter distributions belonging to the SIRP family that are most common in literature and in practical applications, namely:

I. **K-distributed** clutter, in which the texture follows a *gamma distribution*.

II. **Student's t-distributed** clutter, in which the texture follows a *inverse-gamma distribution*.

For clutter of both distributions the texture is characterised by two parameters: the *shape parameter* and the *scale parameter*.

1.1.3 Array Signal Processing

Array signal processing is a branch of signal processing that employs the outputs of an array of sensors to detect signals and to determine signal parameters. Being a topic of growing interest over the past few decades, array signal processing has found wide application in many fields, such as radar, sonar, seismology, radio astronomy, wireless communication, etc. [31, 32].

The quintessential goal of array signal processing in the *estimation of parameters* by jointly exploiting temporal and spatial information obtained from an array of antenna sensors with specific geometric configurations to sample a wavefield that contains information about the parameters characterizing the signal sources (emitters) [31]. Such signal parameters generally include the source number (the estimation of which is also known as *detection* or *signal enumeration*), the directions-of-departure/arrival (DODs/DOAs), the ranges, the velocities, etc., of the signal sources. In order to estimate the unknown parameters of interest, one must firstly set up the observation model and then, based on the model specified, employ a specific estimation algorithm. All of the estimation algorithms fall into two main categories [31]:

I. **Spectral-based methods**, which find the highest peaks of a certain spectrum-like function of the signal parameters as their estimates. These methods can be further classified into:

   (i) *Beamforming techniques*, which steer the antennas to different directions and find those with maximum power as the DOA estimates. Examples of this kind are the *conventional (Bartlett) beamformer*, *Carpon's beamformer*, etc. [31, 33].

   (ii) *Subspace-based techniques*, which exploit properties of the eigenstructure of a certain CM to carry out the analysis. These methods include the multiple signal classification (MUSIC) algorithms and its various extensions [34–38], the estimation of signal parameters via rotational invariance technique (ESPRIT) [39–43], ect.

II. **Parametric methods**, which capitalize, in contrast to the spectral-based methods, more

fully on the underlying data model, and generally require a multidimensional search for the estimates. The so-called *maximum likelihood* (ML) technique, the idea of which consists in finding the values of the parameters that maximize the likelihood function (LF) as their estimates [44], is arguably the most commonly used one of such parametric methods. Based on two different assumptions about the statistics of the source signals, the ML methods can be further divided into:

(i) *Deterministic ML (DML) approach*, which models the signal waveforms as deterministic and unknown [45, 46].

(ii) *Stochastic ML (SML) approach*, which models the signal waveforms as a Gaussian random process [47, 48].

Another estimation approach commonly used in practice and closely related to the ML technique is the so-called *maximum a posteriori* (MAP) technique. Belonging to the family of Bayesian estimators, the MAP approach incorporates a prior distribution followed by the parameter(s) to be estimated into the LF for the ML approach, and maximizes the resulting posteriori LF [44]. The MAP technique can thus be seen as a generalization of the ML technique to the case of unknown random parameters.

The spectral-based methods are computationally more efficient than the parametric methods by avoiding the exhaustive searches for parameter estimates that the latter typically require. The parametric methods, notwithstanding their intrinsic computational complexity, generally provide more accurate results than the spectral-based ones, especially in contexts where highly correlated or coherent signals are involved.

1.1.4 The Cramér-Rao-Type Bounds

The Cramér-Rao bound (CRB), also known as the Cramér-Rao lower bound (CRLB), is one of the most fundamental tools for performance evaluation of estimation problems. Obtained as the inverse of the Fisher information matrix (FIM), the CRB is proved to lower-bound the variance of any *unbiased* estimator [44] (an estimator is called unbiased if the expected value of the estimate it yields of a parameter is equal to the parameter's true value). Thus the

CRB not only offers a benchmark against which the performance of any unbiased estimator can be tested in terms of the mean squared error (MSE) it achieves, but enables to rule out impossible estimators.

An unbiased estimator that attains the CRB is called *efficient*. The SML estimator introduced above in Sec. 1.1.3 is known to be *asymptotically efficient* with respect to (w.r.t.) the number of snapshots, meaning that it achieves in the case of large number of snapshots the CRB calculated under the corresponding model of Gaussian signal waveforms (the stochastic CRB) [31, 44, 49], whereas the DML estimator cannot achieve in this case its corresponding (i.e., the deterministic) CRB calculated by modeling the signal waveforms as deterministic, because the number of unknown parameters increase with the number of snapshots [31]. On the other hand, in the asymptotic case w.r.t. the SNR, and with a fixed number of snapshots, the SML cannot achieve the stochastic CRB [50], while the DML achieves the deterministic CRB [51].

In real-life applications there arises sometimes the task to estimate certain parameter(s) of interest in the presence of unknown random nuisance parameters. This is, for instance, precisely the case for MIMO radar DOD/DOA estimation problems in the presence of SIRP clutter, which this thesis addresses, since the clutter texture is random and unknown. In such cases, the CRB is often difficult or impossible to calculate, because the expressions of the marginal PDF of the observation, with the random nuisance parameters integrated out, are often complicated (sometimes without closed forms) and mathematically intractable. To deal with such difficulties, a number of other lower bounds have been proposed in the literature as alternatives to the CRB [52–57]. All these bounds are similar to the CRB in spirit, but consider, instead of the PDF marginalized w.r.t. the observation, either the joint PDF of the observation and the random nuisance parameters, or the PDF of the former conditioned on the latter, and generally make specific assumptions about or impose certain restrictions on the random nuisance parameters. As a result, these bounds are either looser (lower) than the CRB or apply to a more strict class of estimators, but are easier to calculate as compared with the CRB [52]. Notable examples of these bounds are:

I. **Miller-Chang bound** (MCB) [53], which is obtained by first assuming the random

nuisance parameters as *deterministic* and *known*, calculating the FIM based on the PDF of the observation conditioned on the nuisance parameters, and finally averaging the inverse of the FIM over the random nuisance parameters.

II. **Extended Miller-Chang bound** (EMCB) [52], which is an extension of the MCB, and differs from it in that the EMCB assumes the random nuisance parameters as deterministic but *unknown* in calculating the FIM.

III. **Modified Cramér-Rao bound** (MCRB) [56, 57], which is the same as the MCB in assuming the random nuisance parameters as deterministic and known, but averages over the random nuisance parameters *before* the FIM inversion.

IV. **Hybrid Cramér-Rao bound** (HCRB) [54, 55], which considers the joint PDF of the observation and the random nuisance parameters for the calculation of its FIM (the word "hybrid" in its name signifies that it considers both deterministic and random unknown parameters).

The bounds summarized above were classified in [52] under the name Cramér-Rao-like bounds. Since this name has the same acronym as the Cramér-Rao lower bound, which is more common in the literature, these bounds will be called in this thesis the Cramér-Rao-type bounds (CRTBs) instead, to avoid confusion in nomenclature.

1.1.5 The Resolution Limit

The statistical resolution limit (SRL), or simply the resolution limit (RL), is another common tool to quantify the performance of estimation problems. The RL characterizes the problem of signal resolvability, and is generally defined as the *minimum distance* w.r.t. the parameters of interest (e.g., the DODs/DOAs, frequencies, electrical angles, etc.) that allows distinguishing between two closely spaced signals [58–60].

Till now various methods have been devised to account for the RL, which can be classified, in view of the respective theories they rest on, into the following three approaches:

I. **Mean null spectrum approach** [61, 62], which is based on the mean null spectrum

analysis of the signals, and is always related to a specific high-resolution algorithm. There are two commonly used criteria belonging to this approach:

(i) *Cox's criterion* [61], according to which two signals are resolvable if the mean null spectrum at each of the two signals' parameters of interest is *lower* than the mean null spectrum at the midpoint of the two parameters.

(ii) *Sharman and Durrani's* criterion [62], stating that two signals are resolvable if the second derivative of the mean of the null spectrum at the midpoint of the two signals' parameters of interest is *negative*.

II. **Detection theory approach** [59, 63–67], which employs a *hypothesis test*, e.g., the generalized likelihood ratio test (GLRT) or its asymptotic equivalent, the Bayesian hypothesis test, etc., to decide if one signal or two closely spaced signals are present in the set of the observations. Its idea is to link the *minimum separation* w.r.t. the parameters of interest between two signals that is detectable at a given SNR, to the probability of *false alarm* and/or of *detection*, thereby transforms the problem of resolvability is into that of *detectability*.

III. **Estimation theory approach** [58, 68–71], which capitalizes on the CRB to describe the RL. This is because the CRB is, as mentioned in Sec. 1.1.4, a lower bound for any unbiased estimator, and therefore expresses ultimate estimation accuracy. Two major criteria for the RL based on the CRB have been proposed, namely:

(i) Lee's criterion [68,72], which states that two signals are resolvable if *the larger* of the standard deviations of the estimation of the two signals' parameters of interest is less than *twice* the separation between these two parameters. In practice, the standard deviation can be approximated by the square root of the CRB under mild conditions [73]. One should note that Lee's criterion ignores the coupling effect between the two parameters of interest.

(ii) Smith's criterion [58], which states that two signals are resolvable if the standard deviation of the estimation of the two signals' separation (w.r.t. the parameters of

interest) is less than this separation itself. The standard deviation is also approximated by the CRB. It can be readily seen that Smith's criterion is an extension of Lee's by taking into account the coupling effect between the parameters.

In addressing the resolvability problem in a MIMO radar context in the presence of SIRP clutter, the thesis will adopt the concept of the RL based on Smith's criterion, in view of the following advantages it enjoys:

I. It enjoys generality in contrast to the RL based on the mean null spectrum approach, as the latter is always designed for a specific high-resolution algorithm, but not for a specific signal model itself [74].

II. It is preferable to other criteria derived from the estimation theory, e.g., the one proposed in [68, 72, 75], because it takes the coupling effect between the parameters of interest into account.

III. It is closely related, as revealed in [60], to the RL based on the detection theory approach, meaning that these two approaches can in fact be unified.

1.2 Thesis Overview

This section provides and overview of this thesis. It begins with a brief discussion of the state-of-the-art research progress in each of the field introduced above, and points out the research gaps in the current literature, which make for the motivation and main foci of this thesis. Then, based thereupon, the objectives of the thesis are listed, together with the contributions corresponding to each of them made by this thesis. Finally, an outline of the thesis structure is given by summarizing the content of each of its following chapters.

1.2.1 Thesis Motivation

Till now, abounding works have been dedicated to the research of MIMO radar, either to investigate detection/estimation algorithms or to evaluate radar performance in terms of lower bounds or resolvability [2–4, 11, 12, 15, 18, 76–81]. Specifically, on the topic of DOD/DOA

estimation in a MIMO radar context, not few algorithms, either parametric [11, 17, 82–86] or spectral-based [13–16, 87–95], have been developed, all of which, however, *exclusively* model the radar clutter as Gaussian-distributed. On the other hand, as for estimation problems associated with non-Gaussian, particularly, with SIRP clutter, most of the related works deal *solely* with the estimation of clutter parameters, in which the texture parameter(s) and/or the speckle CM are estimated by assuming the presence of secondary data (known clutter-only realizations) [28, 96–100], instead of considering unknown clutter realizations embedded in and contaminating the transmitted/received signal. On the contrary, in order to estimate radar signal parameters under SIRP clutter, the authors of [98] and [101] devised parameter-expanded expectation-maximization (PX-EM) algorithms, for phased-array and MIMO radar, respectively. Nevertheless, their proposed algorithms are restricted to a special, linear signal model, called the generalized multivariate analysis of variance (GMANOVA) model [102], thus cannot be directly applied to general MIMO radar models, nor to the DOD/DOA estimation problems, which are highly nonlinear [103]. To sum up, there exists no available algorithm in the current literature that addresses the DOD/DOA estimation problem, indeed, that addresses target estimation problems *in general* in a comprehensive manner, in a MIMO radar context in the presence of SIRP clutter.

As an ultimate tool for performance evaluation of estimation problems, the (both stochastic and deterministic) CRB w.r.t. DOA parameters have been derived under a general array signal processing model, respectively in the presence of white Gaussian noise [35, 104, 105], nonuniform Gaussian noise [106], and colored Gaussian noise [107, 108]. On the other hand, notable works investigating the CRB related to SIRP clutter or its certain specific kind (e.g., K-distributed clutter) include, among others, [98, 109, 110]. None of these works, however, provides expressions for the CRB w.r.t. DOD/DOA parameters for a general observation/SIRP clutter model in a systematic, comprehensive manner, as in parallel to the results in [35, 104–108] for Gaussian noise. Furthermore, the expressions and properties of the various CRTBs explored in [52] have not yet been investigated under SIRP clutter, either (except for the HCRB derived *elementwise* under the specific GMANOVA model in [98] with only one clutter texture parameter).

The concept of the other of the aforementioned performance tools, namely, the target resolvability, in terms of the RL, was only recently introduced to the MIMO radar context. Notable results of its investigation in this context can be found in [76–78]. In [76, 77], however, the clutter is modeled as Gaussian-distributed. In [78] the clutter is modeled as a SIRP, but its texture is treated as deterministic and thus the information on the texture distribution is not exploited. Furthermore, the approach in [78] is based on the GLRT (detection theory). No work in the literature has been dedicated to the RL based on the estimation theory (more precisely, on Smith's criterion) in a MIMO radar context under SIRP clutter.

1.2.2 Thesis Objectives, Contributions and Structure

Based on the survey above of the existing gaps in the literature, this thesis undertakes the following tasks as its objectives:

I. Design of DOD/DOA estimation algorithms that are both performant and computationally efficient for co-located MIMO radar targets in the presence of SIRP clutter.

II. Calculation of and comparison between the various CRTBs w.r.t. DOD/DOA parameters in the same context, and investigation of their properties.

III. Derivation of analytical expressions for the RL w.r.t. the angular parameters, namely, the angular RL (ARL), of two closely spaced targets in this context based on Smith's criterion, and exploration into the RL's properties.

The important, original contributions, corresponding to the objectives set above, can be summarized as follows:

I. Three interrelated iterative DOD/DOA estimation algorithms are proposed in a co-located MIMO radar context under SIRP clutter, which differ from one another in the modeling of the clutter texture (as deterministic or stochastic) and in the respective LFs (conditional, joint, or marginal) on which they rest. Performance analysis in terms of convergence and computational complexity are carried out for the proposed algorithms, and in terms of their respective advantages and disadvantages. The three proposed algorithms are:

(i) Iterative maximum likelihood estimator (IMLE) (Ch. 3),

(ii) Iterative maximum a posteriori estimator (IMAPE) (Ch. 4),

(iii) Iterative exact maximum likelihood estimator (IEMLE) (Ch. 5),

all of which have significantly superior performance to that of the conventional ML estimator (CMLE); the latter corresponds to the case where the clutter is assumed to be uniform white Gaussian.

II. Both elementwise and blockwise expressions for the various CRTBs are derived in the same context. Extensive examinations of their relationships and the relationships between them and the texture parameters are provided.

III. An analytical expression for the ARL in this context is derived in Smith's sense based on the CRB, as well as an alternative, more concise expression for it in asymptotic cases. Various properties of the RL revealed by the proposed expressions are carefully inspected. The expressions for the ARL based on other CRTBs are also discussed. In addition, non-matrix, closed-form expressions for certain of the CRTBs are derived as byproducts.

The remaining part of this thesis is organized as follows. Ch. 2 introduces the observation model of the co-located MIMO radar system and specifies the observation statistics. Chs. 3, 4 and 5 are dedicated to the derivation and performance assessment of the IMLE, IMAPE and IEMLE, respectively. Ch. 6 presents the derivation of the expressions for the CRTBs and provides analytical results on their respective properties. Ch. 7 addresses the derivation of analytical expressions for the ARL. Ch. 8 provides the simulation results and discusses the properties that are unmasked by the figures, of the proposed estimators, the CRTBs and the ARL. Finally, Ch. 9 summarizes this thesis and gives an outlook for possible future works.

Chapter 2

MIMO Radar Model Setup

2.1 Observation Model

Consider a bistatic co-located MIMO radar system, illustrated by Fig. 2.1, with linear and possibly nonuniform arrays both at the transmitter and the receiver. Further, assume that K targets are illuminated by the MIMO radar, all modeled as far-field, narrowband, point sources [3]. The radar output at the lth pulse in a coherent processing interval (CPI) is given by [15]:

$$\begin{aligned}\boldsymbol{Y}(l) = &\sum_{k=1}^{K} \alpha_k(l) e^{2j\pi f_k(l) l} \boldsymbol{a}_{(\mathrm{R})}\left(\theta_k^{(\mathrm{R})}\right) \boldsymbol{a}_{(\mathrm{T})}^T\left(\theta_k^{(\mathrm{T})}\right) \boldsymbol{S} \\ &+ \boldsymbol{M}(l), \quad l = 0, \ldots, L-1,\end{aligned} \tag{2.1}$$

where L denotes the number of radar pulses per CPI; $\alpha_k(l)$ and $f_k(l)$ denote a complex coefficient proportional to the RCS and the normalized Doppler frequency shift of the kth target, respectively; $\theta_k^{(\mathrm{T})}$ and $\theta_k^{(\mathrm{R})}$ represent the DOD and DOA of the kth target, respectively (cf. Fig. 2.1 for how these angles are measured); the transmit and receive steering vectors are defined as:

$$\boldsymbol{a}_{(\mathrm{T})}\left(\theta_k^{(\mathrm{T})}\right) = \left[e^{j\frac{2\pi \sin\left(\theta_k^{(\mathrm{T})}\right)}{\lambda} d_1^{(\mathrm{T})}}, \ldots, e^{j\frac{2\pi \sin\left(\theta_k^{(\mathrm{T})}\right)}{\lambda} d_M^{(\mathrm{T})}}\right]^T, \tag{2.2}$$

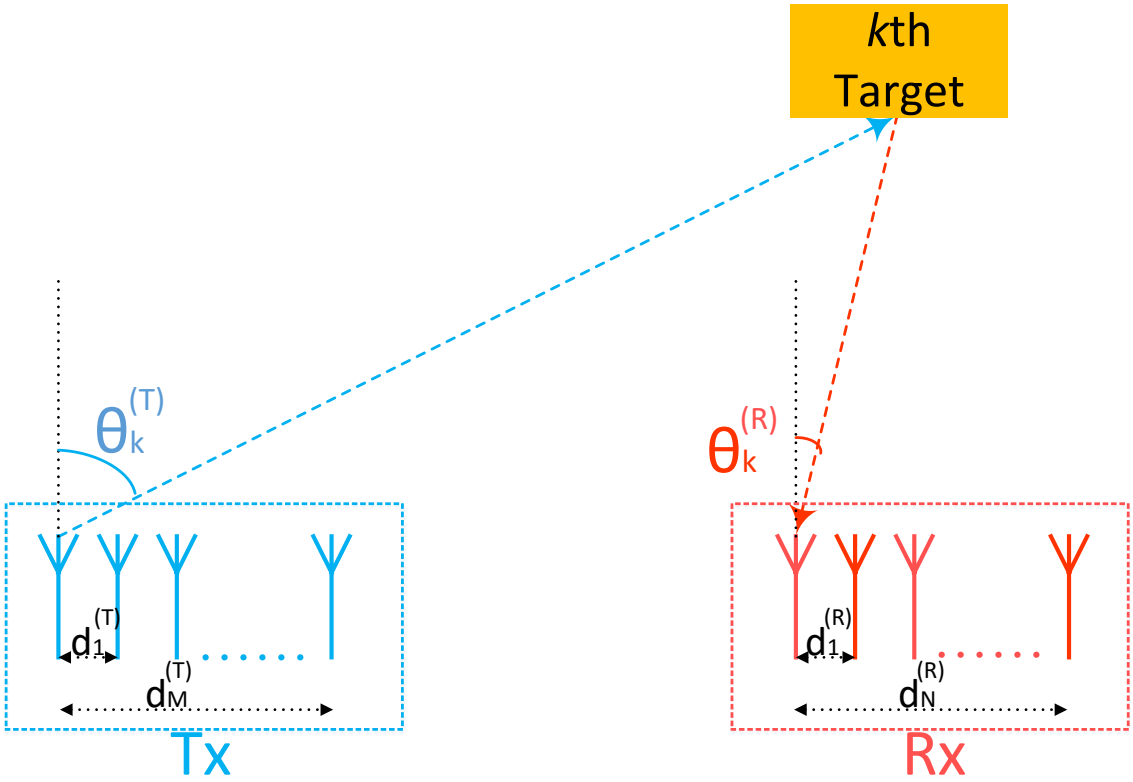

Figure 2.1: Bistatic co-located MIMO radar model.

and

$$\boldsymbol{a}_{(\mathrm{R})}\left(\theta_k^{(\mathrm{R})}\right)=\left[e^{j\frac{2\pi\sin\left(\theta_k^{(\mathrm{R})}\right)}{\lambda}d_1^{(\mathrm{R})}},\ldots,e^{j\frac{2\pi\sin\left(\theta_k^{(\mathrm{R})}\right)}{\lambda}d_N^{(\mathrm{R})}}\right]^T, \tag{2.3}$$

in which M and N represent the number of sensors at the transmitter and the receiver, respectively; $d_i^{(\mathrm{T})}$ and $d_i^{(\mathrm{R})}$ denote the distance between the ith sensor and the reference sensor at the transmitter and the receiver, respectively; λ stands for the carrier wavelength; the $M\times T$ matrix $\boldsymbol{S}$ and the $N\times T$ matrix $\boldsymbol{M}(l)$ denote the signal source waveform matrix and the received clutter matrix at the lth pulse, respectively, where T is the number of snapshots per pulse; and $(\cdot)^T$ denotes the transpose of a matrix.

Since the MIMO radar diversity in terms of waveform coding enables the transmission of orthogonal waveforms [4], such that

$$\boldsymbol{S}\boldsymbol{S}^H=\boldsymbol{S}^*\boldsymbol{S}^T=T\boldsymbol{I}_M, \tag{2.4}$$

in which $(\cdot)^H$ and $(\cdot)^*$ represent the conjugate transpose and the conjugate of a matrix, respectively, and $\boldsymbol{I}_M$ denotes the $M\times M$ identity matrix, the radar output after the matched filtering [111] can be rewritten as:

$$\begin{aligned}\boldsymbol{Z}(l)=&\frac{1}{\sqrt{T}}\boldsymbol{Y}(l)\boldsymbol{S}^H\\ =&\sum_{k=1}^{K}\sqrt{T}\alpha_k(l)e^{2j\pi f_k(l)l}\boldsymbol{a}_{(\mathrm{R})}\left(\theta_k^{(\mathrm{R})}\right)\boldsymbol{a}_{(\mathrm{T})}^T\left(\theta_k^{(\mathrm{T})}\right)+\boldsymbol{N}(l),\\ &l=0,\ldots,L-1,\end{aligned} \tag{2.5}$$

where

$$\boldsymbol{N}(l)=\frac{1}{\sqrt{T}}\boldsymbol{M}(l)\boldsymbol{S}^H \tag{2.6}$$

denotes the clutter matrix at the lth pulse after matched filtering.

By stacking the output in Eq. (2.5) into an $MN\times 1$ vector denoted by $\boldsymbol{z}(l)$, one further has:

$$\begin{aligned}\boldsymbol{z}(l)=&\mathrm{vec}\left\{\boldsymbol{Z}(l)\right\}\\ =&\boldsymbol{A}\left(\boldsymbol{\theta}\right)\boldsymbol{v}(l)+\boldsymbol{n}(l),\quad l=0,\ldots,L-1,\end{aligned} \tag{2.7}$$

in which vec$\{\cdot\}$ stands for the vectorization of a matrix, the $K \times 1$ vector

$$\boldsymbol{v}(l) = \left[\sqrt{T}\alpha_1(l)e^{2j\pi f_1(l)l}, \ldots, \sqrt{T}\alpha_K(l)e^{2j\pi f_K(l)l}\right]^T, \quad l = 0, \ldots, L-1, \tag{2.8}$$

contains the complex-valued RCS coefficients and the normalized Doppler shifts,

$$\boldsymbol{n}(l) = \text{vec}\left\{\boldsymbol{N}(l)\right\}, \quad l = 0, \ldots, L-1, \tag{2.9}$$

denotes the clutter vector after matched filtering at the lth pulse, and

$$\boldsymbol{A}\left(\boldsymbol{\theta}\right) = \left[\boldsymbol{a}\left(\theta_1^{(\text{T})}, \theta_1^{(\text{R})}\right), \ldots, \boldsymbol{a}\left(\theta_K^{(\text{T})}, \theta_K^{(\text{R})}\right)\right] \tag{2.10}$$

denotes the steering matrix after matched filtering, where

$$\boldsymbol{\theta} = \left[\theta_1^{(\text{T})}, \ldots, \theta_K^{(\text{T})}, \theta_1^{(\text{R})}, \ldots, \theta_K^{(\text{R})}\right]^T \tag{2.11}$$

is a $2K \times 1$ parameter vector introduced to incorporate the unknown DODs and DOAs of all K targets, and

$$\begin{aligned} &\boldsymbol{a}\left(\theta_k^{(\text{T})}, \theta_k^{(\text{R})}\right) \\ =&\text{vec}\left\{\boldsymbol{a}_{(\text{R})}\left(\theta_k^{(\text{R})}\right)\boldsymbol{a}_{(\text{T})}^T\left(\theta_k^{(\text{T})}\right)\right\} \\ =&\left(\boldsymbol{I}_M \otimes \boldsymbol{a}_{(\text{R})}\left(\theta_k^{(\text{R})}\right)\right)\boldsymbol{a}_{(\text{T})}\left(\theta_k^{(\text{T})}\right), \quad k = 1, \ldots, K, \end{aligned} \tag{2.12}$$

in which $\otimes$ denotes the Kronecker product.

It is noteworthy that, after the matched filtering and mathematical transformations described above, the co-located MIMO radar model in Eq. (2.7) attains the same expression as the general model for passive array signal processing applications considered in, e.g., [35, 106, 112]. Also note that the considered co-located MIMO radar model can be either bistatic or monostatic. In the latter case one simply has:

$$\theta_k^{(\text{T})} = \theta_k^{(\text{R})} = \theta_k, \quad k = 1, \ldots, K, \tag{2.13}$$

and the direction parameter vector

$$\boldsymbol{\theta} = [\theta_1, \ldots, \theta_K] \tag{2.14}$$

has the size of K.

2.2 Observation Statistics

The clutter vectors $\boldsymbol{n}(l),\ l = 0, \ldots, L-1$, is modeled as i.i.d. SIRVs [22], which can be formulated as the product of two components statistically independent of each other:

$$\boldsymbol{n}(l) = \sqrt{\tau(l)}\boldsymbol{x}(l), \quad l = 0, \ldots, L-1, \tag{2.15}$$

in which the texture terms $\tau(l),\ l = 0, \ldots, L-1$, are i.i.d. positive random variables; the speckle terms $\boldsymbol{x}(l),\ l = 0, \ldots, L-1$, are i.i.d. MN-dimensional circular complex Gaussian vectors with zero mean and second-order moments:

$$\begin{cases} \mathrm{E}\left\{\boldsymbol{x}(i)\boldsymbol{x}^H(j)\right\} = \delta_{ij}\boldsymbol{\Sigma} \\ \mathrm{E}\left\{\boldsymbol{x}(i)\boldsymbol{x}^T(j)\right\} = \mathbf{0}_{MN\times MN}, \quad i,j = 0, \ldots, L-1, \end{cases} \tag{2.16}$$

where $\boldsymbol{\Sigma}$ denotes the speckle CM, $\mathrm{E}\{\cdot\}$ is the expectation operator, δ_{ij} is the Kronecker delta, and $\mathbf{0}_{MN\times MN}$ denotes the $MN \times MN$ zero matrix.

To avoid the ambiguity in the model arising from the scaling effect between the texture and the speckle, thus to make the clutter parameters uniquely identifiable, assume that:

$$\mathrm{tr}\{\boldsymbol{\Sigma}\} = MN, \tag{2.17}$$

in which $\mathrm{tr}\{\cdot\}$ denotes the trace.

As mentioned in Ch. 1, this thesis mainly focuses on two kinds of SIRP clutters that are prevalent in the literature, namely, the K-distributed and the Student's t-distributed clutters. In both cases the texture is characterized by two parameters, the *shape parameter* a and the

scale parameter b (both a and b are positive numbers). Thus, the texture PDF is denoted by $p(\tau(l); a, b)$ for the following clutter models:

- **K-distributed clutter**, in which $\tau(l)$ follows a *gamma distribution* [21, 113–115] (denoted by $\tau(l) \sim \text{Gamma}(a, b)$), with

$$p(\tau(l); a, b) = \frac{1}{\Gamma(a) b^a} \tau(l)^{a-1} e^{-\frac{\tau(l)}{b}}, \tag{2.18}$$

  where $\Gamma(\cdot)$ denotes the gamma function, defined as:

$$\Gamma(a) = \int_0^{+\infty} x^{a-1} e^{-x} \mathrm{d}x. \tag{2.19}$$

  Figs. 2.2 and 2.3 illustrate the PDF of a gamma-distributed texture $\tau(l)$ with various texture parameters, in Fig. 2.2 with fixed b and varying a, and in Fig. 2.3 with fixed a and varying b. In Figs. 2.4 and 2.5, the PDF of a one-dimensional K-distributed clutter (with the clutter power fixed to be 1) is shown with its texture parameters a and b varying in a way corresponding to Figs. 2.2 and 2.3, respectively. Figs. 2.2 and 2.3 show that, either when the shape parameter a or the scale parameter b increases, the gamma-distributed texture becomes more *heavy-tailed*. The K-distributed clutter as a whole, with fixed clutter power, also becomes more *heavy-tailed* when a increases, but does not change its distribution with the change of b, as can be seen from Figs. 2.4 and 2.5.

- **Student's t-distributed clutter**, in which $\tau(l)$ follows an *inverse-gamma distribution* [96, 116–118] (denoted by $\tau(l) \sim \text{Inv-Gamma}(a, b)$[1]), thus:

$$p(\tau(l); a, b) = \frac{b^a}{\Gamma(a)} \tau(l)^{-a-1} e^{-\frac{b}{\tau(l)}}. \tag{2.20}$$

In Figs. 2.6 and 2.7 the PDF of a inverse-gamma-distributed texture $\tau(l)$ is plotted with various texture parameters, in Fig. 2.6 with fixed b and varying a, and in Fig. 2.7 with fixed

[1]Equivalently, $1/\tau(l)$ follows a gamma distribution such that $1/\tau(l) \sim \text{Gamma}(a, 1/b)$.

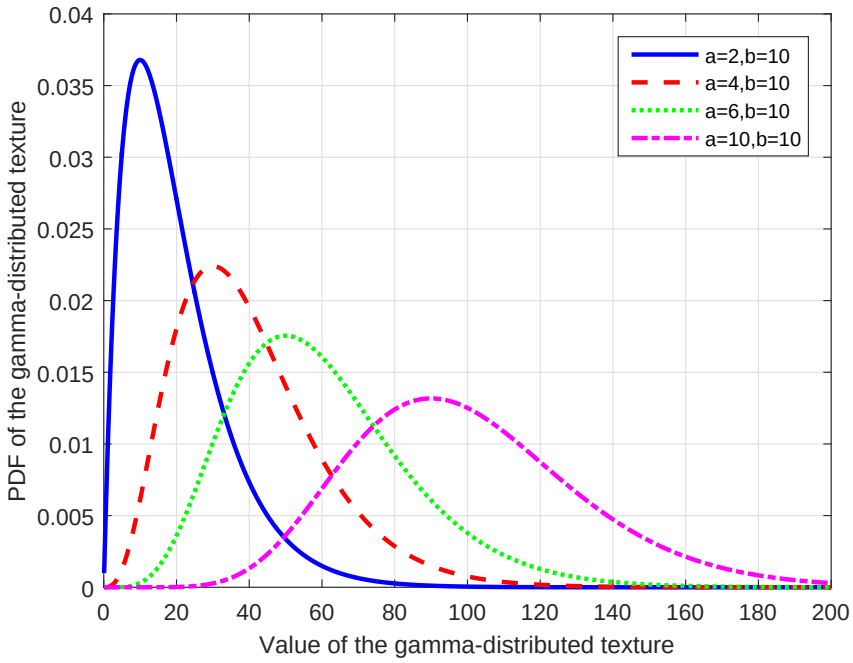

Figure 2.2: PDF of a gamma-distributed texture with with fixed b and varying a.

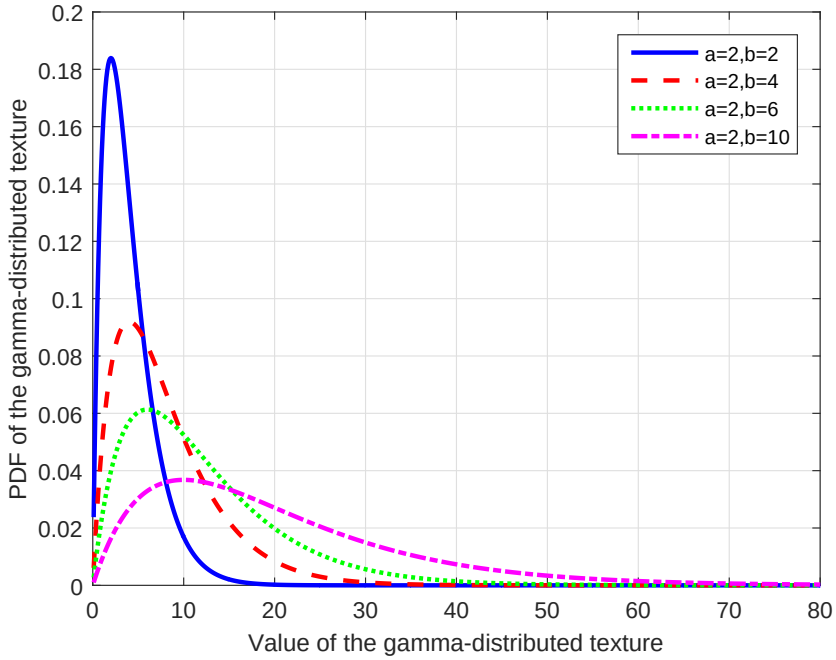

Figure 2.3: PDF of a gamma-distributed texture with with fixed a and varying b.

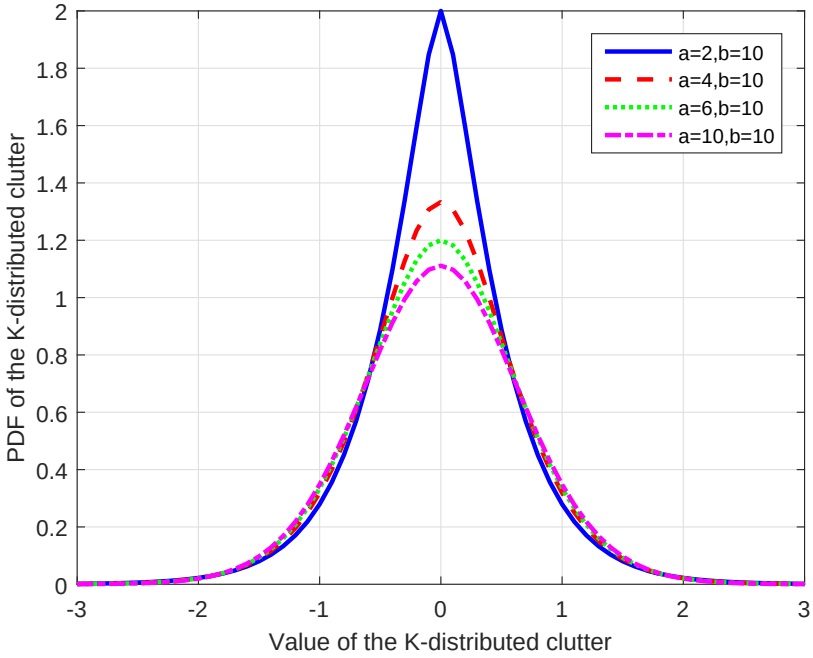

Figure 2.4: PDF of a one-dimensional K-distributed clutter with with fixed b and varying a.

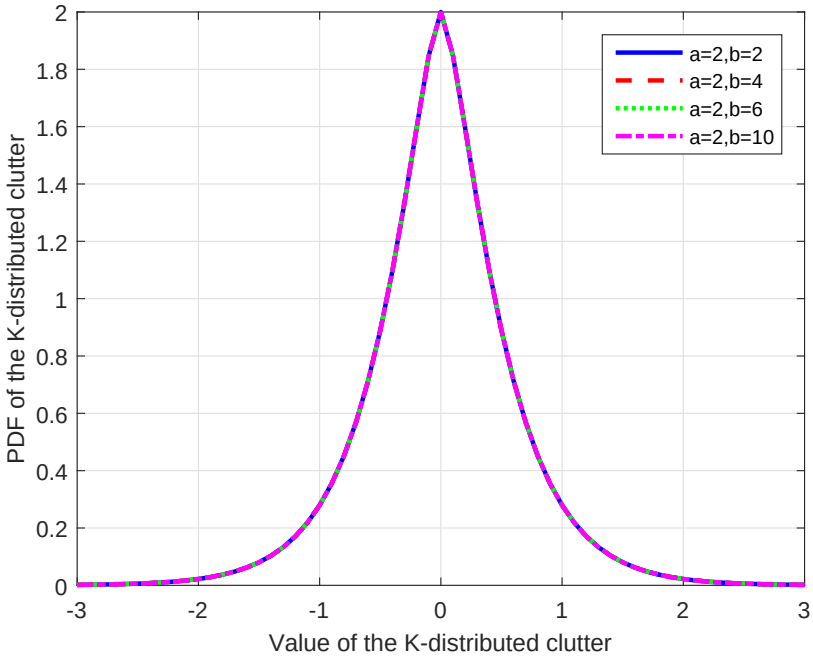

Figure 2.5: PDF of a one-dimensional K-distributed clutter with with fixed a and varying b.

a and varying b. Figs. 2.8 and 2.9 shows the PDF of a one-dimensional t-distributed clutter (also with the clutter power fixed to be 1) with its texture parameters a and b varying in parallel to Figs. 2.6 and 2.7, respectively. One can see from Figs. 2.6 and 2.7 that the inverse gamma-distributed texture becomes more *heavy-tailed*, either when the shape parameter a decreases or when the scale parameter b increases. On the other hand, the t-distributed clutter as a whole, with fixed clutter power, becomes more *heavy-tailed* when a increases, but does not change its distribution with the change of b (cf. Figs. 2.8 and 2.9), similar to the K-distributed clutter in this respect.

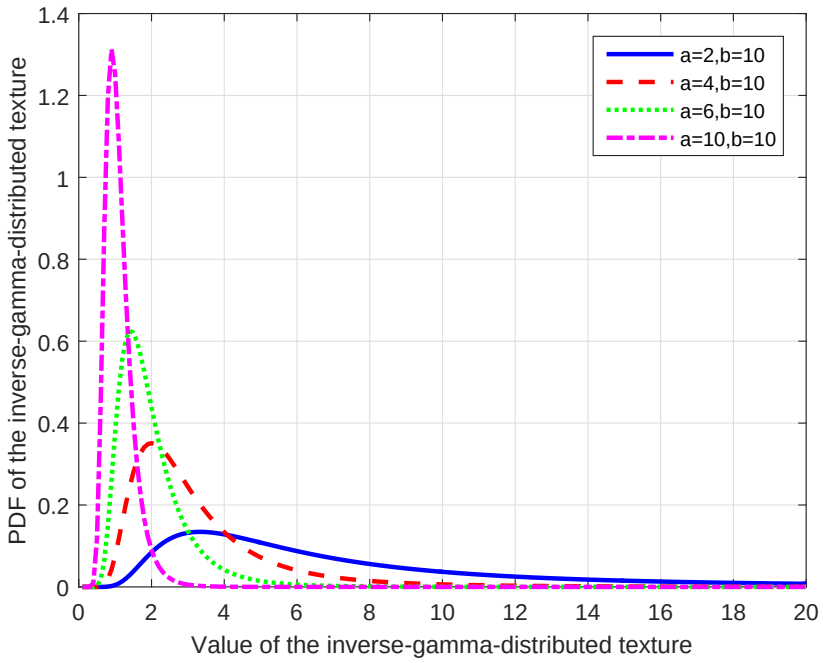

Figure 2.6: PDF of a inverse-gamma-distributed texture with with fixed b and varying a.

2.3 Unknown Parameter Vector

Under the assumptions above, the unknown parameter vector of the problem in question is given by:

$$\boldsymbol{\chi} = \left[\boldsymbol{\theta}^T, \mathrm{Re}\left\{\boldsymbol{\alpha}\right\}^T, \mathrm{Im}\left\{\boldsymbol{\alpha}\right\}^T, \boldsymbol{f}^T, \boldsymbol{\zeta}^T, a, b\right]^T, \tag{2.21}$$

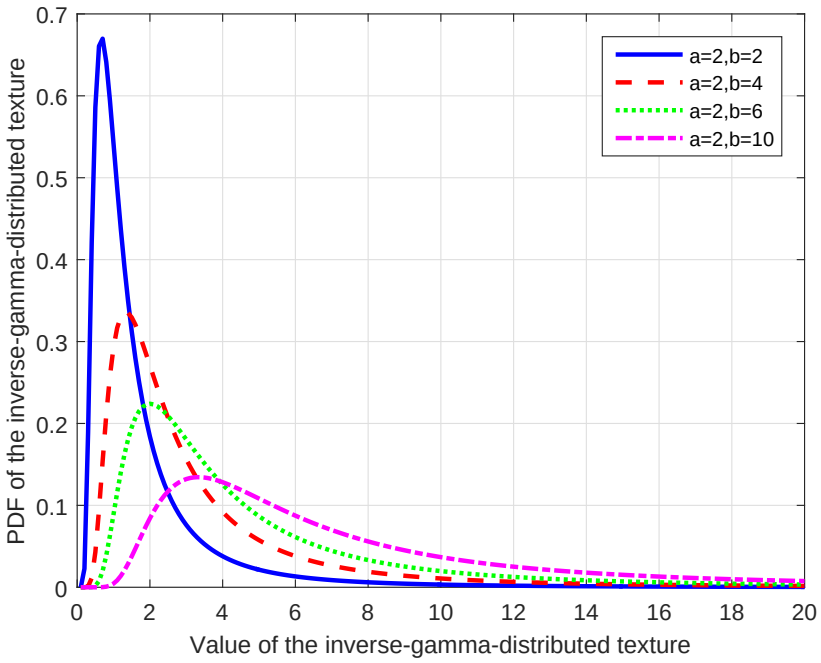

Figure 2.7: PDF of a inverse-gamma-distributed texture with with fixed a and varying b.

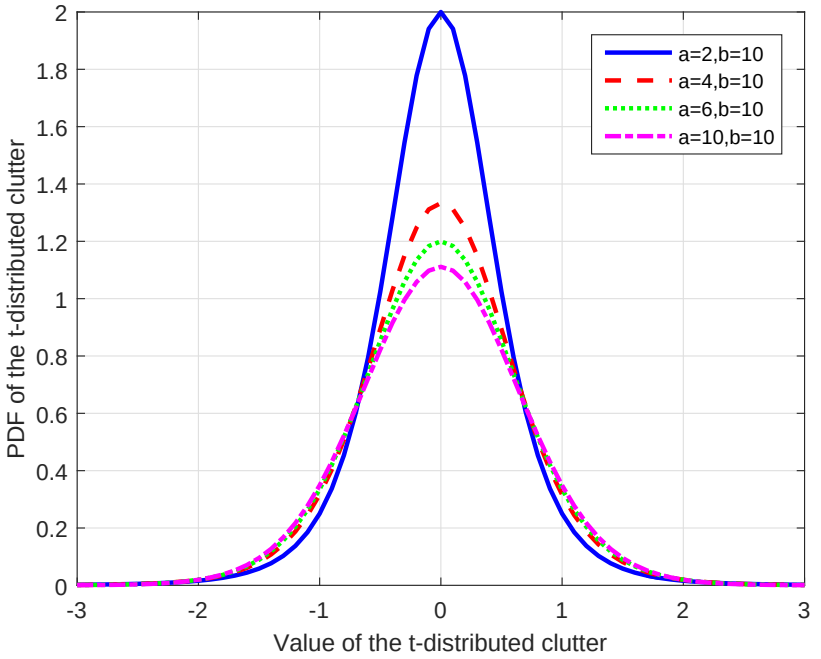

Figure 2.8: PDF of a one-dimensional t-distributed clutter with with fixed b and varying a.

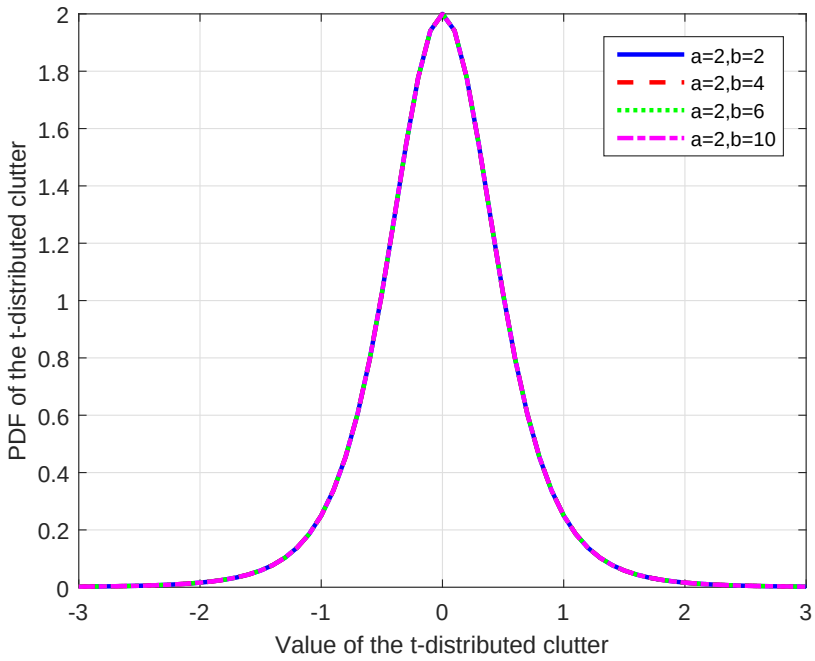

Figure 2.9: PDF of a one-dimensional t-distributed clutter with with fixed a and varying b.

in which

$$\boldsymbol{\alpha} = [\alpha_1(l), \ldots, \alpha_K(l)]^T \tag{2.22}$$

is a complex parameter vector including the RCS coefficients of all K targets,

$$\boldsymbol{f} = [f_1(l), \ldots, f_K(l)]^T \tag{2.23}$$

contains the normalized Doppler frequency shifts of all K targets, $\boldsymbol{\zeta}$ is a M^2N^2-element vector containing the real and imaginary parts of the entries of the lower triangular part of $\boldsymbol{\Sigma}$, $\mathrm{Re}\{\cdot\}$ and $\mathrm{Im}\{\cdot\}$ denote the real and the imaginary part, respectively.

For the considered model above, to make the DOD/DOA estimation problem uniquely identifiable, one needs to estimate the vectors $\boldsymbol{v}(l),\ l = 0, \ldots, L-1$, which are functions of the RCS coefficients $\alpha_k(l),\ k = 1, \ldots, K,\ l = 0, \ldots, L-1$, and the normalized Doppler frequency shifts $f_k(l),\ k = 1, \ldots, K,\ l = 0, \ldots, L-1$, of the targets, instead of estimating $\alpha_k(l)$ and $f_k(l)$ themselves. This approach will be adopted for all three estimators proposed in this thesis. Correspondingly, one considers instead of the original unknown parameter

vector $\boldsymbol{\chi}$ in Eq. (2.21), the transformed new unknown parameter vector:

$$\boldsymbol{\xi} = \left[\boldsymbol{\theta}^T, \boldsymbol{v}^T, \boldsymbol{\zeta}^T, a, b\right]^T, \tag{2.24}$$

in which the $2KL \times 1$ vector

$$\boldsymbol{v} = \left[\mathrm{Re}\left\{\boldsymbol{v}(0)\right\}^T, \mathrm{Im}\left\{\boldsymbol{v}(0)\right\}^T, \ldots, \mathrm{Re}\left\{\boldsymbol{v}(L-1)\right\}^T, \mathrm{Im}\left\{\boldsymbol{v}(L-1)\right\}^T\right]^T, \tag{2.25}$$

is a parameter vector containing the real and imaginary parts of $\boldsymbol{v}(l)$ at all L pulses.

2.4 Likelihood Functions

Let

$$\boldsymbol{z} = \left[\boldsymbol{z}^T(0), ..., \boldsymbol{z}^T(L-1)\right]^T \tag{2.26}$$

denote the full observation vector after matched filtering, further let

$$\boldsymbol{\tau} = [\tau(0), \ldots, \tau(L-1)]^T \tag{2.27}$$

represent the vector containing the texture realizations at all L pulses. Accordingly, the full observation *conditional likelihood* (conditioned on $\boldsymbol{\tau}$) can be written as:

$$p\left(\boldsymbol{z}\,|\boldsymbol{\tau};\boldsymbol{\psi}\right) = \prod_{l=0}^{L-1} \frac{1}{|\pi\boldsymbol{\Sigma}|\,\tau^{MN}(l)} \exp\left(-\frac{\|\boldsymbol{\rho}(l)\|^2}{\tau(l)}\right); \tag{2.28}$$

in which

$$\boldsymbol{\psi} = \left[\boldsymbol{\theta}^T, \boldsymbol{v}^T, \boldsymbol{\zeta}^T\right]^T \tag{2.29}$$

is the unknown parameter vector that does not contain the texture parameters a and b, $\|\cdot\|$ denotes the Euclidean norm, and

$$\boldsymbol{\rho}(l) = \boldsymbol{\Sigma}^{-\frac{1}{2}}\left(\boldsymbol{z}(l) - \boldsymbol{A}\left(\boldsymbol{\theta}\right)\boldsymbol{v}(l)\right), \tag{2.30}$$

represents the clutter realization at the lth pulse with its speckle spatially whitened by the square root of the speckle CM inverse.

Following Bayes' rule, the conditional likelihood in Eq. (2.28), multiplied by the PDF of the texture realization parameter vector, i.e., $p(\boldsymbol{\tau}; a, b)$, leads to the *joint likelihood* between $\boldsymbol{z}$ and $\boldsymbol{\tau}$:

$$\begin{aligned} p\left(\boldsymbol{z}, \boldsymbol{\tau}; \boldsymbol{\xi}\right) &= p\left(\boldsymbol{z} \,|\boldsymbol{\tau}; \boldsymbol{\psi}\,\right) p(\boldsymbol{\tau}; a, b) \\ &= \prod_{l=0}^{L-1} \frac{1}{|\pi\boldsymbol{\Sigma}|\, \tau^{MN}(l)} \exp\left(-\frac{\|\boldsymbol{\rho}(l)\|^2}{\tau(l)}\right) p(\tau(l); a, b). \end{aligned} \tag{2.31}$$

Finally, the full observation *exact (marginal) likelihood*, w.r.t. $\boldsymbol{\xi}$, is obtained by marginalization, i.e., integrating out $\boldsymbol{\tau}$ from the joint likelihood in Eq. (2.31), as:

$$\begin{aligned} p\left(\boldsymbol{z}; \boldsymbol{\xi}\right) &= \int_0^{+\infty} p\left(\boldsymbol{z}, \boldsymbol{\tau}; \boldsymbol{\xi}\right) \mathrm{d}\boldsymbol{\tau} \\ &= \prod_{l=0}^{L-1} \int_0^{+\infty} \frac{1}{|\pi\boldsymbol{\Sigma}|\, \tau^{MN}(l)} \exp\left(-\frac{\|\boldsymbol{\rho}(l)\|^2}{\tau(l)}\right) p(\tau(l); a, b) \mathrm{d}\tau(l). \end{aligned} \tag{2.32}$$

Chapter 3

Iterative Maximum Likelihood DOD and DOA Estimation

The marginal LF in Eq. (2.32) has an integral form and is mathematically difficult to handle. To avoid maximizing the intractable Eq. (2.32), various estimation procedures in the SIRP context have either proposed to use the joint LF in Eq. (2.31) [98] as a tool to achieve the maximization of the marginal LF, or to maximize the conditional LF in Eq. (2.28) [119]. The latter approach treats $\boldsymbol{\tau}$ as *deterministic*, i.e., as one realization from the texture process rather than the process itself. Correspondingly, it takes this realization $\boldsymbol{\tau}$ as one of its unknown parameters to be estimated, while ignores the statistical distribution of the texture as characterized by the texture parameters a and b. In deriving the proposed IMLE, this idea is adopted and the usage of the term "ML" is with regard to this kind of deterministic texture modeling.

Let Λ_{C} denote the conditional log-likelihood function (LLF), which arises from Eq. (2.28), as:

$$\begin{aligned}\Lambda_{\mathrm{C}} &= \ln p\left(\boldsymbol{z}\,|\boldsymbol{\tau};\boldsymbol{\psi}\right)\\ &= -LMN\ln\pi - L\ln|\boldsymbol{\Sigma}|\\ &\quad - MN\sum_{l=0}^{L-1}\ln\tau(l) - \sum_{l=0}^{L-1}\frac{1}{\tau(l)}\boldsymbol{\rho}^{H}(l)\boldsymbol{\rho}(l).\end{aligned} \tag{3.1}$$

3.1 Estimates of the Unknown Parameters

To begin with, let $\partial\Lambda_{\mathrm{C}}/\partial\tau(l) = 0$, the solution of which provides an estimate of the parameter $\tau(l)$ when the parameters $\boldsymbol{\theta}$, $\boldsymbol{v}(l)$ and $\boldsymbol{\Sigma}$ are fixed. Using $\hat{(\cdot)}$ to denote the estimate of a parameter, $\hat{\tau}(l)$ has the following closed-form expression:

$$\begin{aligned}\hat{\tau}(l) &= \frac{1}{MN}\boldsymbol{\rho}^H(l)\boldsymbol{\rho}(l) \\ &= \frac{1}{MN}\boldsymbol{n}^H(l)\boldsymbol{\Sigma}^{-1}\boldsymbol{n}(l),\end{aligned} \tag{3.2}$$

in which the clutter vector at the lth pulse $\boldsymbol{n}(l)$ has, according to Eq. (2.7), the following expression:

$$\boldsymbol{n}(l) = \boldsymbol{z}(l) - \boldsymbol{A}\left(\boldsymbol{\theta}\right)\boldsymbol{v}(l). \tag{3.3}$$

Note that the expression of $\hat{\tau}(l)$ in Eq. (3.2) is *unique* if the matrix $\boldsymbol{\Sigma}$ is invertible, i.e., if the number of pulses per CPI $L \geq MN$.

On the other hand, the estimate of $\boldsymbol{\Sigma}$, when $\boldsymbol{\theta}$, $\boldsymbol{v}(l)$ and $\tau(l)$ are fixed, can be found by applying Lemma 3.2.2. in [120] to Eq. (3.1), as:

$$\hat{\boldsymbol{\Sigma}} = \frac{1}{L}\sum_{l=0}^{L-1}\frac{1}{\tau(l)}\boldsymbol{n}(l)\boldsymbol{n}^H(l), \tag{3.4}$$

which is *unique*, and in which replacing $\tau(l)$ by the expression of $\hat{\tau}(t)$ in Eq. (3.2) leads to the following expression of $\hat{\boldsymbol{\Sigma}}$:

$$\hat{\boldsymbol{\Sigma}} = \frac{MN}{L}\sum_{l=0}^{L-1}\frac{\boldsymbol{n}(l)\boldsymbol{n}^H(l)}{\boldsymbol{n}^H(l)\hat{\boldsymbol{\Sigma}}^{-1}\boldsymbol{n}(l)}. \tag{3.5}$$

One can calculate Eq. (3.5) iteratively by transforming it into:

$$\hat{\boldsymbol{\Sigma}}^{(i+1)} = \frac{MN}{L}\sum_{l=0}^{L-1}\frac{\boldsymbol{n}(l)\boldsymbol{n}^H(l)}{\boldsymbol{n}^H(l)\left(\hat{\boldsymbol{\Sigma}}^{(i)}\right)^{-1}\boldsymbol{n}(l)}, \tag{3.6}$$

in which $\hat{(\cdot)}^{(i)}$ ($i \geq 0$, and $i \in \mathbb{Z}$) stands for the estimate of a parameter at the ith iteration,

where $\mathbb{Z}$ represents the set of integers. The identity matrix $\boldsymbol{I}_{MN}$ is chosen to serve as the initialization matrix $\hat{\boldsymbol{\Sigma}}^{(0)}$.

Iteration (3.6) was derived in [121], and then proved in [97] to be the exact ML estimator of $\hat{\boldsymbol{\Sigma}}$ when the vector $\boldsymbol{\tau}$ is assumed to be deterministic, as is in the case under discussion. The convergence properties of the iteration have been analyzed in [97, 121].

Recalling the disambiguating assumption on the speckle CM trace in Eq. (2.17), one further needs to normalize $\hat{\boldsymbol{\Sigma}}^{(i+1)}$ in Eq. (3.6) to make $\mathrm{tr}\{\boldsymbol{\Sigma}\} = MN$. Let $\hat{\boldsymbol{\Sigma}}_{\mathrm{n}}^{(i+1)}$ denote the normalized estimate $\hat{\boldsymbol{\Sigma}}^{(i+1)}$, which is obtained by:

$$\hat{\boldsymbol{\Sigma}}_{\mathrm{n}}^{(i+1)} = MN \frac{\hat{\boldsymbol{\Sigma}}^{(i+1)}}{\mathrm{tr}\left\{\hat{\boldsymbol{\Sigma}}^{(i+1)}\right\}}. \tag{3.7}$$

Next, one considers the estimate of $\boldsymbol{v}(l)$, which can be found by solving $\partial\Lambda/\partial\boldsymbol{v}(l) = 0$ and has the following closed-form expression:

$$\hat{\boldsymbol{v}}(l) = \left(\tilde{\boldsymbol{A}}^H(\boldsymbol{\theta})\,\tilde{\boldsymbol{A}}(\boldsymbol{\theta})\right)^{-1}\tilde{\boldsymbol{A}}^H(\boldsymbol{\theta})\,\tilde{\boldsymbol{z}}(l), \tag{3.8}$$

in which

$$\tilde{\boldsymbol{A}}(\boldsymbol{\theta}) = \boldsymbol{\Sigma}^{-\frac{1}{2}}\boldsymbol{A}(\boldsymbol{\theta}), \tag{3.9}$$

and

$$\tilde{\boldsymbol{z}}(l) = \boldsymbol{\Sigma}^{-\frac{1}{2}}\boldsymbol{z}(l), \tag{3.10}$$

represent the steering matrix and the observation at the lth pulse, both spatially whitened by the square root of the speckle CM inverse, respectively. The expression of $\hat{\boldsymbol{v}}(l)$ in Eq. (3.8) is *unique* if $K \leq MN$ (K is the number of targets) [122].

3.2 Stepwise Numerical Concentration Approach

From Eqs. (3.2), (3.6) and (3.8) one can observe that the estimation of the involved parameters are *mutually dependent*, in the sense that the expression for the estimate of any of these parameters contains all the remaining parameters, as well as the parameter itself for

the case of $\boldsymbol{\Sigma}$ (cf. Eq. (3.5)). In [98] and [101], the authors overcame the similar difficulty by exploiting the special structure of their GMANOVA model and obtained an expression of $\hat{\boldsymbol{\Sigma}}$ independent of their unknown signal parameters. However, such analytical concentration approach is inapplicable to the estimation problem under consideration. Therefore, the estimation algorithms proposed in this thesis adopts the so-called *stepwise numerical concentration* method, of which the concept was introduced and employed, in the context of nonuniform white Gaussian noise in [106], and of colored Gaussian noise in [123].

The idea of the stepwise concentration consists in the concentration of the LLF w.r.t. certain unknown parameters in an iterative manner. For the problem under discussion, the proposed procedure is to assume, for each iteration, that $\boldsymbol{\Sigma}$ and $\boldsymbol{\tau}$ are fixed and known, and to use their values to compute the estimate of $\hat{\boldsymbol{v}}(l)$, which is then used, in its turn, to update the values of $\boldsymbol{\Sigma}$ and $\boldsymbol{\tau}$ for the next iteration. This sequential updating procedure is then continued until convergence of the parameters of interest, which can be defined, e.g., by the criterion that the difference between the values of estimates obtained from consecutive iterations falls below a certain predefined small threshold.

This general procedure borne in mind, one finally returns to the LLF in Eq. (3.1) for the estimation of $\boldsymbol{\theta}$, the parameter of interest in the problem under discussion, by considering the values of $\boldsymbol{\Sigma}$ and $\boldsymbol{\tau}$ as fixed and known estimates obtained from the previous iteration. Thus, by neglecting the constant terms, the conditional LLF in Eq. (3.1) can be reformulated as:

$$\Lambda_{\mathrm{C}} = -\sum_{l=0}^{L-1} \frac{1}{\tau(l)} \boldsymbol{\rho}^H(l)\boldsymbol{\rho}(l). \tag{3.11}$$

By inserting Eq. (3.8) into Eq. (3.11) and maximizing the resulting expression w.r.t. $\boldsymbol{\theta}$, one obtains the estimate of $\boldsymbol{\theta}$ for each iteration, as:

$$\hat{\boldsymbol{\theta}} = \arg\min_{\boldsymbol{\theta}} \left\{ \sum_{l=0}^{L-1} \frac{1}{\tau(l)} \left\| \boldsymbol{P}^{\perp}_{\tilde{\boldsymbol{A}}(\boldsymbol{\theta})}(t)\tilde{\boldsymbol{z}}(l) \right\|^2 \right\}, \tag{3.12}$$

in which $\arg\min_{\boldsymbol{\theta}} \{f(\boldsymbol{\theta})\}$ denotes the value of $\boldsymbol{\theta}$ that minimizes $f(\boldsymbol{\theta})$ (a function of $\boldsymbol{\theta}$), and

$$\boldsymbol{P}^{\perp}_{\tilde{\boldsymbol{A}}(\boldsymbol{\theta})} = \boldsymbol{I}_{MN} - \tilde{\boldsymbol{A}}(\boldsymbol{\theta}) \left(\tilde{\boldsymbol{A}}^H(\boldsymbol{\theta})\tilde{\boldsymbol{A}}(\boldsymbol{\theta}) \right)^{-1} \tilde{\boldsymbol{A}}^H(\boldsymbol{\theta}) \tag{3.13}$$

is the orthogonal projection matrix onto the null space spanned by the columns of the matrix $\tilde{\boldsymbol{A}}(\boldsymbol{\theta})$. Here, one makes the assumption regarding Eq. (3.12) that it is a *unique* optimum, which for the array Khatri-Rao of Vandermonde manifold structure in Eq. (2.12) holds true almost surely if $K \leq MN$ [122].

3.3 Algorithmic Procedure

The whole procedure of the proposed IMLE, consisting of iterations between two steps, is summarized in Alg. 3.1. Note that at the initialization step of the IMLE, the texture realizations are initialized as all ones, corresponding to a Gaussian-distributed clutter.

Algorithm 3.1 Iterative Maximum Likelihood Estimator (IMLE)

Initialization:

- Choose the convergence threshold $\varepsilon_{\boldsymbol{\theta}}$.
- Choose the maximum number of iterations $i_{\max} \geq 1, i \in \mathbb{Z}$.
- Set the iteration index $i = 0$.
- Set $\hat{\tau}^{(0)}(l) = 1,\ l = 0, \ldots, L-1$.
- Set $\hat{\boldsymbol{\Sigma}}_{\mathrm{n}}^{(0)} = \boldsymbol{I}_{MN}$.

Step 1: At ith iteration ($i \geq 0$),

- Calculate $\hat{\boldsymbol{\theta}}^{(i)}$ according to Eq. (3.12) by numerically computing:

$$\hat{\boldsymbol{\theta}}^{(i)} = \arg\min_{\boldsymbol{\theta}} \left\{ \sum_{l=0}^{L-1} \frac{1}{\hat{\tau}^{(i)}(l)} \left\| \boldsymbol{P}^{\perp}_{\hat{\tilde{\boldsymbol{A}}}^{(i)}(\boldsymbol{\theta})}(l) \hat{\tilde{\boldsymbol{z}}}^{(i)}(l) \right\|^2 \right\}, \tag{3.14}$$

  in which (cf. Eq. (3.9) and (3.10))

$$\hat{\tilde{\boldsymbol{z}}}^{(i)}(l) = \left(\hat{\boldsymbol{\Sigma}}_{\mathrm{n}}^{(i)} \right)^{-\frac{1}{2}} \boldsymbol{z}(l), \tag{3.15}$$

$$\hat{\tilde{\boldsymbol{A}}}^{(i)}(\boldsymbol{\theta}) = \left(\hat{\boldsymbol{\Sigma}}_{\mathrm{n}}^{(i)} \right)^{-\frac{1}{2}} \boldsymbol{A}(\boldsymbol{\theta}), \tag{3.16}$$

  and (cf. Eq. (3.13))

$$\boldsymbol{P}^{\perp}_{\hat{\tilde{\boldsymbol{A}}}^{(i)}(\boldsymbol{\theta})}(l) = \boldsymbol{I}_{MN} - \hat{\tilde{\boldsymbol{A}}}^{(i)}(\boldsymbol{\theta}) \left(\left(\hat{\tilde{\boldsymbol{A}}}^{(i)}(\boldsymbol{\theta}) \right)^H \hat{\tilde{\boldsymbol{A}}}^{(i)}(\boldsymbol{\theta}) \right)^{-1} \left(\hat{\tilde{\boldsymbol{A}}}^{(i)}(\boldsymbol{\theta}) \right)^H. \tag{3.17}$$

- Calculate $\hat{\boldsymbol{v}}^{(i)}(l)$ according to Eq. (3.8) by:

$$\hat{\boldsymbol{v}}^{(i)}(l) = \left(\left(\hat{\tilde{\boldsymbol{A}}}^{(i)} \left(\hat{\boldsymbol{\theta}}^{(i)} \right) \right)^H \hat{\tilde{\boldsymbol{A}}}^{(i)} \left(\hat{\boldsymbol{\theta}}^{(i)} \right) \right)^{-1} \left(\hat{\tilde{\boldsymbol{A}}}^{(i)} \left(\hat{\boldsymbol{\theta}}^{(i)} \right) \right)^H \hat{\tilde{\boldsymbol{z}}}^{(i)}(l). \tag{3.18}$$

Algorithm 3.1 Iterative Maximum Likelihood Estimator (IMLE) (cont'd)

Step 2:

- Update $\hat{\boldsymbol{\Sigma}}^{(i+1)}$ according to Eq. (3.6) by:

$$\hat{\boldsymbol{\Sigma}}^{(i+1)} = \frac{MN}{L} \sum_{l=0}^{L-1} \frac{\hat{\boldsymbol{n}}^{(i)}(l) \left(\hat{\boldsymbol{n}}^{(i)}(l)\right)^H}{\left(\hat{\boldsymbol{n}}^{(i)}(l)\right)^H \left(\hat{\boldsymbol{\Sigma}}_{\text{n}}^{(i)}\right)^{-1} \hat{\boldsymbol{n}}^{(i)}(l)},$$

  in which (cf. Eq. (3.3))

$$\hat{\boldsymbol{n}}^{(i)}(l) = \boldsymbol{z}(l) - \boldsymbol{A}\left(\hat{\boldsymbol{\theta}}^{(i)}\right) \hat{\boldsymbol{v}}^{(i)}(l). \tag{3.19}$$

- Calculate $\hat{\boldsymbol{\Sigma}}_{\text{n}}^{(i+1)}$ according to Eq. (3.7) by:

$$\hat{\boldsymbol{\Sigma}}_{\text{n}}^{(i+1)} = MN \frac{\hat{\boldsymbol{\Sigma}}^{(i+1)}}{\text{tr}\left\{\hat{\boldsymbol{\Sigma}}^{(i+1)}\right\}}. \tag{3.20}$$

- Update $\hat{\tau}^{(i+1)}(l)$ according to Eq. (3.2) by:

$$\hat{\tau}^{(i+1)}(l) = \frac{1}{MN} \left(\hat{\boldsymbol{n}}^{(i)}(l)\right)^H \left(\hat{\boldsymbol{\Sigma}}_{\text{n}}^{(i+1)}\right)^{-1} \hat{\boldsymbol{n}}^{(i)}(l).$$

Termination Condition:

if $(i = 0) \bigvee \left((1 \leq i < i_{\max}) \bigwedge \left\|\hat{\boldsymbol{\theta}}^{(i)} - \hat{\boldsymbol{\theta}}^{(i-1)}\right\| > \varepsilon_{\boldsymbol{\theta}}\right)$ **then**

Set $i = i + 1$, and go to **Step 1**.

end if

return $\hat{\boldsymbol{\theta}}^{(i)}$.

The operators $\bigwedge$ and $\bigvee$ in Alg. 3.1 represent logical conjunction and disjunction, respectively. The returned value of $\hat{\boldsymbol{\theta}}^{(i)}$ by Alg. 3.1 is considered to be the estimate of $\boldsymbol{\theta}$ produced by the proposed IMLE, denoted by $\hat{\boldsymbol{\theta}}_{\text{IMLE}}$.

3.4 Performance Analysis

3.4.1 Convergence and Computational Cost

The proposed IMLE algorithm can be viewed as an application of the block coordinate descent (BCD) method [124, 125]. According to Proposition 2.7.1 (together with the text after its proof) in [125], the BCD method converges to a *stationary point* (namely, a Karush–Kuhn–Tucker (KKT) point) if:

i) The objective function is *continuously differentiable*;

ii) The constraint set of the parameters is *compact*;

iii) The function of the ith block-component attains a *unique minimum* over the constraint set.

The first two conditions above hold true for the case of the proposed IMLE; so does the third, under the mild conditions specified respectively below Eqs. (3.2), (3.4), (3.8) and (3.12) to guarantee the uniqueness of the involved parameter estimates. The convergence of the proposed IMLE algorithm to a stationary point is thus proved. In fact, as simulations in Ch. 8 will show, the convergence of the estimate of the unknown parameter $\hat{\boldsymbol{\theta}}$ can be observed, and is generally attainable with as few as two iterations, a result in accordance with those in [106] and [123].

Based on the observation above, one can conclude that the computational cost of the proposed IMLE, which lies mainly in the numerical solution of the highly nonlinear optimization problem in Eq. (3.14), is only a few times of that of the CMLE. The latter corresponds to the case where the clutter is assumed to be uniform white Gaussian, such that Eq. (3.12) degenerate into [35]:

$$\hat{\boldsymbol{\theta}}_{\text{CMLE}} = \arg\min_{\boldsymbol{\theta}} \left\{ \sum_{l=0}^{L-1} \left\| \boldsymbol{P}^{\perp}_{\boldsymbol{A}(\boldsymbol{\theta})} \boldsymbol{z}(l) \right\|^2 \right\}. \tag{3.21}$$

3.4.2 Invariance of the IMLE to Different Speckle CM Trace Assumptions

To deal with the ambiguity arising from the scaling effect between the texture and the speckle in the clutter model Eq. (2.15), an assumption has to be made about the value of the speckle CM trace. In Eq. (2.17) it has been assumed that $\text{tr}\{\boldsymbol{\Sigma}\} = MN$. The proposed IMLE algorithm, however, is invariant to the different choice of values for the assumed speckle CM trace, as will be demonstrated in this subsection.

Let $\text{tr}\{\boldsymbol{\Sigma}\}_{\text{a}}$ stand for an alternatively assumed trace value for the speckle CM other than the one in Eq. (2.17), and in introduce a variable:

$$r = \frac{\text{tr}\{\boldsymbol{\Sigma}\}_{\text{a}}}{\text{tr}\{\boldsymbol{\Sigma}\}}, \tag{3.22}$$

which represents the ratio between the alternatively and the originally (i.e., the one made in Eq. (2.17)) assumed speckle CM trace. Consider the case that

$$r \neq 1. \tag{3.23}$$

Further, let $\hat{(\cdot)}'$ denote the "counterpart" of a parameter resulting from this alternative assumption on the speckle CM trace value. It then follows that:

$$\boldsymbol{\Sigma}' = r\boldsymbol{\Sigma}, \tag{3.24}$$

based on which one has from the speckle covariance expression in Eq. (2.16) that:

$$\boldsymbol{x}'(l) = \sqrt{r}\boldsymbol{x}(l), \quad l = 0, \ldots, L-1, \tag{3.25}$$

and accordingly, from Eq. (2.15), that:

$$\tau'(l) = \frac{1}{r}\tau(l), \quad l = 0, \ldots, L-1, \tag{3.26}$$

such that:

$$\sqrt{\tau'(l)}\boldsymbol{x}'(l) = \sqrt{\tau(l)}\boldsymbol{x}(l), \quad l = 0, \ldots, L-1. \tag{3.27}$$

Alternatively, Eq. (3.26) can be obtained by inserting Eq. (3.24) into Eq. (3.2).

Moreover, by inserting Eq. (3.24) into Eq. (2.30) one has:

$$\boldsymbol{\rho}'(l) = \frac{1}{\sqrt{r}}\boldsymbol{\rho}(l), \quad l = 0, \ldots, L-1. \tag{3.28}$$

Finally, by noticing that the objective function in Eq. (3.12) is in essence the search for $\hat{\boldsymbol{\theta}}$ by:

$$\hat{\boldsymbol{\theta}} = \arg\min_{\boldsymbol{\theta}} \left\{ \sum_{l=0}^{L-1} \frac{1}{\tau(l)} \boldsymbol{\rho}^H(l)\boldsymbol{\rho}(l) \right\}, \tag{3.29}$$

and by substituting Eqs. (3.26) and (3.28) into Eq. (3.29), one obtains:

$$\begin{aligned} \hat{\boldsymbol{\theta}}' &= \arg\min_{\boldsymbol{\theta}} \left\{ \sum_{l=0}^{L-1} \frac{1}{\tau'(l)} \boldsymbol{\rho}'^H(l)\boldsymbol{\rho}'(l) \right\} \\ &= \arg\min_{\boldsymbol{\theta}} \left\{ \sum_{l=0}^{L-1} \frac{1}{\tau(l)} \boldsymbol{\rho}^H(l)\boldsymbol{\rho}(l) \right\} \\ &= \hat{\boldsymbol{\theta}}, \end{aligned} \tag{3.30}$$

which means that, for the IMLE, the estimate of the parameter $\boldsymbol{\theta}$ under the alternative assumption of $\mathrm{tr}\{\boldsymbol{\Sigma}\}$ is equal to that under the original assumption, i.e., that the value of $\hat{\boldsymbol{\theta}}$ is independent of the assumed value of $\mathrm{tr}\{\boldsymbol{\Sigma}\}$. One can thus conclude that the IMLE is invariant to different speckle CM trace assumptions.

Chapter 4

Iterative Maximum A Posteriori DOD and DOA Estimation

The IMLE proposed above, in which one models the texture as deterministic, has the advantage of easier and faster implementation. It is also a natural approach when the texture does not have a closed-form expression of distribution (e.g., in the case of Weibull clutter) or its distribution is unknown. In general cases, however, such approach is *suboptimal* not only in the sense that it is not based on the exact (marginal) likelihood, but that it ignores information regarding the statistical properties (prior distribution) of the texture. As mentioned at the beginning of Sec. 3, another way to avoid the mathematical complexity in maximizing the marginal likelihood in Eq. (2.32) is to maximize the joint likelihood Eq. (2.31) instead. This is, for instance, the approach adopted in [98], where the proposed PX-EM algorithm is based on a “complete data likelihood" that is equivalent to the joint likelihood. Estimators based on the joint likelihood are in essence MAP estimators, as can be readily seen from:

$$\begin{aligned} \hat{\boldsymbol{\tau}}_{\text{MAP}} &= \arg\max_{\boldsymbol{\tau}} p\left(\boldsymbol{\tau}\,|\boldsymbol{z};\boldsymbol{\xi}\right) \\ &= \arg\max_{\boldsymbol{\tau}} \frac{p\left(\boldsymbol{z}\,|\boldsymbol{\tau};\boldsymbol{\psi}\right) p(\boldsymbol{\tau};a,b)}{p\left(\boldsymbol{z};\boldsymbol{\xi}\right)} \\ &= \arg\max_{\boldsymbol{\tau}} p\left(\boldsymbol{z},\boldsymbol{\tau};\boldsymbol{\xi}\right), \end{aligned} \tag{4.1}$$

in which $\hat{\boldsymbol{\tau}}_{\text{MAP}}$ denotes the MAP estimate of $\boldsymbol{\tau}$.

For this reason, the second estimator to be proposed in this chapter, which is based on the joint likelihood and also employs a numerical concentration approach, is justifiably called the IMAPE. By modeling the texture as stochastic and exploiting the its prior distribution, the IMAPE, of which the derivation is presented below, leads to superior performance over the IMLE.

4.1 Estimates of the Unknown Parameters

Let Λ_{J} denote the joint LLF, which is equal to:

$$\begin{aligned}
\Lambda_{\text{J}} &= \ln p\left(\boldsymbol{z}, \boldsymbol{\tau}; \boldsymbol{\xi}\right) = \ln\left(p\left(\boldsymbol{z}\,|\boldsymbol{\tau}; \boldsymbol{\psi}\right) p(\boldsymbol{\tau}; a, b)\right) \\
&= \Lambda_{\text{C}} + \sum_{l=0}^{L-1} \ln p(\tau(l); a, b) \\
&= \begin{cases}
\Lambda_{\text{C}} - L\ln\Gamma(a) - La\ln b + (a-1)\sum\limits_{l=0}^{L-1}\ln\tau(l) \\
\quad - \dfrac{\sum_{l=0}^{L-1}\tau(l)}{b}, \quad \text{K-distributed clutter,} \\
\Lambda_{\text{C}} - L\ln\Gamma(a) + La\ln b - (a+1)\sum\limits_{l=0}^{L-1}\ln\tau(l) \\
\quad - b\sum\limits_{l=0}^{L-1}\dfrac{1}{\tau(l)}, \quad \text{Student's t-distributed clutter.}
\end{cases}
\end{aligned} \tag{4.2}$$

The expression of $\hat{\tau}(l)$, when all the remaining unknown parameters are fixed, can be found by solving $\partial\Lambda_{\text{J}}/\partial\tau(l) = 0$, as:

$$\hat{\tau}(l) = \begin{cases}
\dfrac{1}{2}\left(\left(a - MN - 1\right)b + \sqrt{\left(a - MN - 1\right)^2 b^2 + 4b\boldsymbol{n}^H(l)\boldsymbol{\Sigma}^{-1}\boldsymbol{n}(l)}\right), \\
\text{K-distributed clutter,} \\
\dfrac{\boldsymbol{n}^H(l)\boldsymbol{\Sigma}^{-1}\boldsymbol{n}(l) + b}{a + MN + 1}, \quad \text{Student's t-distributed clutter,}
\end{cases} \tag{4.3}$$

in which $\boldsymbol{n}(l)$ has the same expression as in Eq. (3.3). The expression of $\hat{\tau}(l)$ in Eq. (4.3), in agreement with that in Eq. (3.2) for the IMLE, is *unique* if the matrix $\boldsymbol{\Sigma}$ is invertible, i.e., if

the number of pulses per CPI $L \geq MN$.

A comparison between the expressions of $\hat{\tau}(l)$ in Eq. (3.2) and in Eq. (4.3) reveals that the latter takes into account the statistical properties of the texture. In these expressions, the parameters a and b play the roles of scale/translation factors to enhance the estimation of $\tau(l)$. This is more easily perceptible in the case of a Student's t-distributed clutter, where the expressions for $\hat{\tau}(l)$ in Eq. (3.2) and (4.3) have a similar form. For example, the case of large b and small a corresponds to a more heavily-tailed distribution of the texture and leads to an increased probability of the realization of $\tau(l)$ with large values. In this case, the estimator in Eq. (4.3), in contrast to that in Eq. (3.2), adjusts $\hat{\tau}(l)$ in a way that prevents the occurrence of small values and encourages that of larger ones.

For the next step, one considers the estimates of the texture parameters a and b. The latter can be obtained by solving $\partial\Lambda_{\text{J}}/\partial b = 0$, as:

$$\hat{b} = \begin{cases} \dfrac{\sum_{l=0}^{L-1} \tau(l)}{La}, & \text{K-distributed clutter,} \\ \dfrac{La}{\sum_{l=0}^{L-1} \frac{1}{\tau(l)}}, & \text{Student's t-distributed clutter,} \end{cases} \tag{4.4}$$

which is *unique* for both clutter distributions.

On the other hand, calculating $\partial\Lambda_{\text{J}}/\partial a$ yields:

$$\frac{\partial\Lambda_{\text{J}}}{\partial a} = \begin{cases} -L\Psi(a) - L\ln b + \displaystyle\sum_{l=0}^{L-1} \ln\tau(l), & \text{K-distributed clutter,} \\ -L\Psi(a) + L\ln b - \displaystyle\sum_{l=0}^{L-1} \ln\tau(l), & \text{Student's t-distributed clutter,} \end{cases} \tag{4.5}$$

in which $\Psi(\cdot)$ stands for the digamma function, defined as the logarithmic derivative of the gamma function in Eq. (2.19), namely:

$$\Psi(a) = \frac{\mathrm{d}}{\mathrm{d}a} \ln\Gamma(a). \tag{4.6}$$

From Eq. (4.5) it turns out that $\partial\Lambda_{\text{J}}/\partial a = 0$ does not allow an analytical expression of

the root. By inserting Eq. (4.4) into Eq. (4.5), one obtains:

$$\frac{\partial \Lambda_{\mathrm{J}}}{\partial a} = \begin{cases} -L\Psi(a) - L\ln\left(\dfrac{\sum_{l=0}^{L-1}\tau(l)}{La}\right) + \displaystyle\sum_{l=0}^{L-1}\ln\tau(l), \\ \text{K-distributed clutter}, \\ -L\Psi(a) + L\ln\left(\dfrac{La}{\sum_{l=0}^{L-1}\frac{1}{\tau(l)}}\right) - \displaystyle\sum_{l=0}^{L-1}\ln\tau(l), \\ \text{Student's t-distributed clutter}. \end{cases} \tag{4.7}$$

Thus the expression of $\hat{a}$ can be found by numerically solving Eq. (4.7). As will be demonstrated below in Sec. 4.2, this expression of $\hat{a}$ is also *unique*.

Next, it is to approach the estimation of the parameters $\boldsymbol{v}(l)$ and the speckle CM $\boldsymbol{\Sigma}$. By noticing that $\partial\Lambda_{\mathrm{J}}/\partial\boldsymbol{\Sigma} = \partial\Lambda_{\mathrm{C}}/\partial\boldsymbol{\Sigma}$, and $\partial\Lambda_{\mathrm{J}}/\partial\boldsymbol{v}(l) = \partial\Lambda_{\mathrm{C}}/\partial\boldsymbol{v}(l)$, it follows immediately that the same expressions of $\hat{\boldsymbol{\Sigma}}$ and $\hat{\boldsymbol{v}}(l)$ in Eqs. (3.4) and (3.8), which were obtained for the IMLE algorithm, are also valid in the case of the IMAPE algorithm. Substituting into Eq. (3.4) the new expression of $\hat{\tau}(l)$ in Eq. (4.3) and interpreting the resulting equation also in an iterative form leads to the following expression for $\hat{\boldsymbol{\Sigma}}$:

$$\hat{\boldsymbol{\Sigma}}^{(i+1)} = \begin{cases} \dfrac{2}{L}\displaystyle\sum_{l=0}^{L-1}\boldsymbol{n}(l)\boldsymbol{n}^H(l) \Bigg/ \Bigg((a-MN-1)\,b \\ + \left(4b\boldsymbol{n}^H(l)\left(\hat{\boldsymbol{\Sigma}}^{(i)}\right)^{-1}\boldsymbol{n}(l) + (a-MN-1)^2\,b^2\right)^{\frac{1}{2}}\Bigg), \\ \text{K-distributed clutter}, \\ \dfrac{a+MN+1}{L}\displaystyle\sum_{l=0}^{L-1}\dfrac{\boldsymbol{n}(l)\boldsymbol{n}^H(l)}{b+\boldsymbol{n}^H(l)\left(\hat{\boldsymbol{\Sigma}}^{(i)}\right)^{-1}\boldsymbol{n}(l)}, \\ \text{Student's t-distributed clutter}. \end{cases} \tag{4.8}$$

for which the initialization matrix is also chosen to be $\hat{\boldsymbol{\Sigma}}^{(0)} = \boldsymbol{I}_{MN}$. Similar to the expression of $\hat{\boldsymbol{\Sigma}}^{(i+1)}$ in Eq. (3.6) for the IMLE algorithm, Eq. (4.8) needs also to be substituted into Eq. (3.7) to obtain the normalized estimate of the CM, $\hat{\boldsymbol{\Sigma}}_{\mathrm{n}}^{(i+1)}$, to fulfill the assumption on the CM trace made in Eq. (2.17).

Finally, one addresses the estimation of $\boldsymbol{\theta}$. By adopting the numerical concentration method similar to that in Sec. 3.2, one also assumes here that $\boldsymbol{\Sigma}$ and $\boldsymbol{\tau}$ are known from the previous iteration of the algorithm. Their values are then used to compute the estimate of $\hat{\boldsymbol{v}}(l)$ (like for the IMLE), and of, distinctively for the IMAPE, a and b. These estimates are then jointly used, in their turn, to update the values of $\boldsymbol{\Sigma}$ and $\boldsymbol{\tau}$ for the next iteration.

Since the estimates of a and b are only dependent on $\boldsymbol{\tau}$, these are also fixed for each iteration. This allows one to drop those terms in the expression of the joint LLF Λ_{J} in Eq. (4.2) that contain only these unknown parameters, and thereby to transform it into the same expression as in Eq. (3.11). This means that $\boldsymbol{\theta}$ can be obtained, also for the IMAPE algorithm, from Eq. (3.12).

4.2 Existence and Uniqueness of the Solution for the Shape Parameter

In contrast to the IMLE proposed in Ch. 3, the IMAPE models the texture as stochastic and therefore needs to estimate the shape parameter a (by Eq. (4.5)) and the scale parameter b (by Eq. (4.4)) of the texture distribution. As mentioned below Eq. (4.5), the estimate of a does not allow an analytic expression, but can only be numerically found by solving the equation $\partial\Lambda_{\mathrm{J}}/\partial a = 0$. A theoretical proof of the existence of its unique solution is thus of concern to ensure the validity and feasibility of the proposed algorithm, which is the aim of this section.

4.2.1 K-Distributed Clutter Case

One first considers the case of K-distributed clutter, for which Eq. (4.7) can be transformed, by replacing $\Psi(a)$ by the full series of its asymptotic series expansion:

$$\Psi(a) = \ln(a) - \frac{1}{2a} - \sum_{n=1}^{\infty} \frac{B_{2n}}{2n a^{2n}}, \tag{4.9}$$

where B_{2n} denotes the $2n$th Bernoulli number, into:

$$\frac{\partial \Lambda_{\mathrm{J}}}{\partial a} = L\left(\frac{1}{2a} + \sum_{n=1}^{\infty} \frac{B_{2n}}{2n a^{2n}} + \ln\left(\frac{L}{\sum_{l=0}^{L-1}\tau(l)} \sqrt[L]{\prod_{l=0}^{L-1}\tau(l)}\right)\right). \tag{4.10}$$

From the expression of Eq. (4.10), it follows readily that:

$$\begin{cases} \lim\limits_{a\to 0^{+}} \dfrac{\partial \Lambda_{\mathrm{J}}}{\partial a} = +\infty, \\ \lim\limits_{a\to +\infty} \dfrac{\partial \Lambda_{\mathrm{J}}}{\partial a} = \ln\left(\dfrac{L}{\sum_{l=0}^{L-1}\tau(l)} \sqrt[L]{\prod_{l=0}^{L-1}\tau(l)}\right) \leq \ln(1) = 0. \end{cases} \tag{4.11}$$

The second to last step in the expression above is obtained by applying the *inequality of arithmetic and geometric means*, which states that:

$$\frac{\sum_{l=0}^{L-1}\tau(l)}{L} \geq \sqrt[L]{\prod_{l=0}^{L-1}\tau(l)}, \tag{4.12}$$

where the equality holds only in the extreme case where

$$\tau(0) = \tau(1) = \cdots = \tau(L-1), \tag{4.13}$$

which corresponds to the Gaussian clutter case. For the K-distributed clutter under discussion, this is a *zero probability* occurrence and thus is trivial in reality.

Furthermore, one can also see from Eq. (4.10) that $\partial\Lambda_{\mathrm{J}}/\partial a$ is a continuous, strictly decreasing function of a in the interval $(0, +\infty)$, meaning that there exists *exactly* one value of a in the interval $(0, +\infty)$ that leads to $\partial\Lambda/\partial a = 0$, which corresponds to the global maximum point of Λ_{J} w.r.t. a in the K-distributed clutter case.

4.2.2 Student's t-Distributed Clutter Case

Similarly, when the clutter follows a Student's t-distribution, substituting Eqs. (4.4) and Eq. (4.9) into Eq. (4.5) yields:

$$\frac{\partial \Lambda_{\mathrm{J}}}{\partial a} = L\left(\frac{1}{2a} + \sum_{n=1}^{\infty} \frac{B_{2n}}{2na^{2n}} + \ln\left(\frac{L}{\sum_{l=0}^{L-1} \frac{1}{\tau(l)} \sqrt[L]{\prod_{l=0}^{L-1} \tau(l)}}\right)\right), \tag{4.14}$$

which is also a continuous, strictly decreasing function of a in the interval $(0, +\infty)$.

Applying the *inequality of harmonic and geometric means*:

$$\frac{L}{\sum_{l=0}^{L-1} \frac{1}{\tau(l)}} \leq \sqrt[L]{\prod_{l=0}^{L-1} \tau(l)}, \tag{4.15}$$

to Eq. (4.14), one further has:

$$\begin{cases} \lim\limits_{a \to 0^+} \dfrac{\partial \Lambda_{\mathrm{J}}}{\partial a} = +\infty, \\ \lim\limits_{a \to +\infty} \dfrac{\partial \Lambda_{\mathrm{J}}}{\partial a} = \ln\left(\dfrac{L}{\sum_{l=0}^{L-1} \frac{1}{\tau(l)} \sqrt[L]{\prod_{l=0}^{L-1} \tau(l)}}\right) \leq \ln(1) = 0, \end{cases} \tag{4.16}$$

where, similarly, the equality in the second line holds only in the trivial case of Eq. (4.13).

Thus, one can conclude that, for Student's t-distributed clutter, there also exists *exactly* one root of the equation $\partial\Lambda/\partial a = 0$ w.r.t. a in the interval $(0, +\infty)$, which corresponds to the global maximum point of Λ_{J} w.r.t. a in this case.

4.3 Algorithmic Procedure

The whole procedure of the proposed IMAPE, which also consists of iterations between two steps, is presented in Alg. 4.1. Note that the initialization of the IMAPE does not imply any prior on the texture parameters. Like the IMLE in Alg. 3.1, the IMAPE also initializes the clutter as Gaussian-distributed (with all texture realizations equal to one). Furthermore, at the first iteration (when the iteration index $i = 0$), the IMAPE carries out the same estimation

procedure as the IMLE in Alg. 3.1. Then, based on the obtained estimates from the first iteration, the texture parameters are estimated according to Eqs. (4.7) and (4.4), and are used for the estimation of $\mathbf{\Sigma}$ and $\tau(l)$ (according to Eqs. (4.8) and (4.3), respectively) for the second iteration.

Algorithm 4.1 Iterative Maximum A Posteriori Estimator (IMAPE)

Initialization:

- Choose the convergence threshold $\varepsilon_{\boldsymbol{\theta}}$.
- Choose the maximum number of iterations $i_{\max}$.
- Set the iteration index $i = 0$.
- Set $\hat{\tau}^{(0)}(l) = 1,\ l = 0, \ldots, L-1$.
- $\hat{\boldsymbol{\Sigma}}_{\mathrm{n}}^{(0)} = \boldsymbol{I}_{MN}$.

Step 1: At ith iteration ($i \geq 0$),

- Calculate $\hat{\boldsymbol{\theta}}^{(i)}$ by Eq. (3.14).
- Calculate $\hat{\boldsymbol{v}}^{(i)}(l)$ by Eq. (3.18).

if $i > 0$ **then**

- Calculate $\hat{a}^{(i)}$ according to Eq. (4.7) by numerically solving:

$$-L\Psi(\hat{a}^{(i)}) - L\ln\left(\frac{\sum_{l=0}^{L-1}\hat{\tau}^{(i)}(l)}{L\hat{a}^{(i)}}\right) + \sum_{l=0}^{L-1}\ln\hat{\tau}^{(i)}(l) = 0,$$

for K-distributed clutter; or

$$-L\Psi(\hat{a}^{(i)}) + L\ln\left(\frac{L\hat{a}^{(i)}}{\sum_{l=0}^{L-1}\frac{1}{\hat{\tau}^{(i)}(l)}}\right) - \sum_{l=0}^{L-1}\ln\hat{\tau}^{(i)}(l) = 0,$$

for Student's t-distributed clutter.

- Calculate $\hat{b}^{(i)}$ according to Eq. (4.4) by:

$$\hat{b}^{(i)} = \begin{cases} \dfrac{\sum_{l=0}^{L-1}\hat{\tau}^{(i)}(l)}{L\hat{a}^{(i)}}, & \text{K-distributed clutter,} \\ \dfrac{L\hat{a}^{(i)}}{\sum_{l=0}^{L-1}\frac{1}{\hat{\tau}^{(i)}(l)}}, & \text{Student's t-distributed clutter.} \end{cases}$$

end if

Algorithm 4.1 Iterative Maximum A Posteriori Estimator (IMAPE) (cont'd)

Step 2:

if $i = 0$ **then**

- Update $\hat{\mathbf{\Sigma}}^{(i+1)}$ by Eq. (3.1).
- Calculate $\hat{\mathbf{\Sigma}}_{\mathrm{n}}^{(i+1)}$ by Eq. (3.20).
- Update $\hat{\tau}^{(i+1)}(l)$ by Eq. (3.1).

else

- Update $\hat{\mathbf{\Sigma}}^{(i+1)}$ according to Eq. (4.8) by:

$$\hat{\mathbf{\Sigma}}^{(i+1)} = \begin{cases} \dfrac{2}{L}\displaystyle\sum_{l=0}^{L-1} \hat{\boldsymbol{n}}^{(i)}(l)\left(\hat{\boldsymbol{n}}^{(i)}(l)\right)^H \Bigg/ \Bigg(\left(\hat{a}^{(i)} - MN - 1\right)\hat{b}^{(i)} \\ + \left(4\hat{b}^{(i)}\left(\hat{\boldsymbol{n}}^{(i)}(l)\right)^H \left(\hat{\mathbf{\Sigma}}^{(i)}\right)^{-1} \hat{\boldsymbol{n}}^{(i)}(l) \right. \\ \left. + \left(\hat{a}^{(i)} - MN - 1\right)^2 \left(\hat{b}^{(i)}\right)^2 \right)^{\frac{1}{2}} \Bigg), \quad \text{K-distributed clutter,} \\ \dfrac{\hat{a}^{(i)} + MN + 1}{L} \displaystyle\sum_{l=0}^{L-1} \dfrac{\hat{\boldsymbol{n}}^{(i)}(l)\left(\hat{\boldsymbol{n}}^{(i)}(l)\right)^H}{\hat{b}^{(i)} + \left(\hat{\boldsymbol{n}}^{(i)}(l)\right)^H \left(\hat{\mathbf{\Sigma}}^{(i)}\right)^{-1} \hat{\boldsymbol{n}}^{(i)}(l)}, \\ \text{Student's t-distributed clutter.} \end{cases}$$

  in which $\hat{\boldsymbol{n}}^{(i)}(l)$ is defined in Eq. (3.19).

- Calculate $\hat{\mathbf{\Sigma}}_{\mathrm{n}}^{(i+1)}$ by Eq. (3.20).
- Update $\hat{\tau}^{(i+1)}(l)$ according to Eq. (4.3) by:

$$\hat{\tau}^{(i+1)}(l) = \begin{cases} \dfrac{1}{2}\Bigg(\left(\hat{a}^{(i)} - MN - 1\right)\hat{b}^{(i)} + \Bigg(4\hat{b}^{(i)}\left(\hat{\boldsymbol{n}}^{(i)}(l)\right)^H \left(\hat{\mathbf{\Sigma}}_{\mathrm{n}}^{(i+1)}\right)^{-1} \\ \cdot \hat{\boldsymbol{n}}^{(i)}(l) + \left(\hat{a}^{(i)} - MN - 1\right)^2 \left(\hat{b}^{(i)}\right)^2 \Bigg)^{\frac{1}{2}} \Bigg), \quad \text{K-distributed clutter,} \\ \dfrac{\left(\hat{\boldsymbol{n}}^{(i)}(l)\right)^H \left(\hat{\mathbf{\Sigma}}_{\mathrm{n}}^{(i+1)}\right)^{-1} \hat{\boldsymbol{n}}^{(i)}(l) + \hat{b}^{(i)}}{\hat{a}^{(i)} + MN + 1}, \quad \text{Student's t-distributed clutter.} \end{cases}$$

end if

Algorithm 4.1 Iterative Maximum A Posteriori Estimator (IMAPE) (cont'd)

Termination Condition:

if $(i = 0) \bigvee \left((1 \leq i < i_{\max}) \bigwedge \left\| \hat{\boldsymbol{\theta}}^{(i)} - \hat{\boldsymbol{\theta}}^{(i-1)} \right\| > \varepsilon_{\boldsymbol{\theta}} \right)$ **then**

Set $i = i + 1$, and go to **Step 1**.

end if

return $\hat{\boldsymbol{\theta}}^{(i)}$.

The returned value of $\hat{\boldsymbol{\theta}}^{(i)}$ by Alg. 4.1 is considered to be the estimate of $\boldsymbol{\theta}$ produced by the proposed IMAPE, denoted by $\hat{\boldsymbol{\theta}}_{\text{IMAPE}}$.

4.4 Performance Analysis

4.4.1 Convergence and Computational Cost

The convergence of the proposed IMAPE algorithm to a stationary point can be proved in a similar way to the proof in Subsec. 3.4.1 for the IMLE, i.e., by the fulfilment of the three conditions quoted there. Like for the IMLE, the first two conditions hold true as well for the proposed IMAPE. The third condition, namely the uniqueness of the parameter estimates involved in the IMAPE algorithm, is also fulfilled under the mild conditions specified in Ch. 3 (for those parameters whose expressions are shared by both the IMLE and the IMAPE), as well as below Eq. (4.3) and in Sec. 4.2 (for the rest parameters involved). As simulations in Ch. 8 will show, the convergence of the estimate of the unknown parameter $\hat{\boldsymbol{\theta}}$ is generally attainable, similar to the IMLE proposed in Ch. 3, with as few as two iterations.

Like the IMLE, the computational cost of the proposed IMAPE also lies mainly in the numerical solution of Eq. (3.14), is thus also a few times of that of the CMLE in Eq. (3.21). It is, however, slightly higher than the computational cost of the IMLE, due to the need to numerically solve Eq. (4.7) for the estimation of the shape parameter a, which the IMLE does not involve.

4.4.2 Invariance of the IMAPE to Different Speckle CM Trace Assumptions

The invariance of the IMAPE to different speckle CM trace assumptions can be easily ascertained for the IMAPE. Recall the representation $\hat{(\cdot)}'$ defined in Sec. 3.4.2 that signifies the "counterpart" of a parameter based on an alternatively assumed (i.e., other than the one in Eq. (2.17)) speckle CM trace. It is clear that the relations revealed for the IMLE between $\tau'(l)$ and $\tau(l)$ by Eq. (3.26), and between $\boldsymbol{\rho}'(l)$ and $\boldsymbol{\rho}(l)$ by Eq. (3.28), also directly apply to the IMAPE. Since, additionally, the IMAPE has the same objective function to search for $\hat{\boldsymbol{\theta}}$ as the IMLE, which can be rewritten in the form of Eq. (3.29), the expression of $\boldsymbol{\rho}'(l)$ for the IMAPE can be obtained just in the same way as for the IMLE, namely, by substituting Eqs. (3.26) and (3.28) into Eq. (3.29), and is equal to $\hat{\boldsymbol{\theta}}$, as shown in Eq. (5.29). This shows that $\hat{\boldsymbol{\theta}}$ for the IMAPE is, just like for the IMLE, independent of the value of the assumed speckle CM trace. Thus the IMAPE is, like the IMLE, invariant to different speckle CM trace assumptions.

Chapter 5

Iterative Exact Maximum Likelihood DOD and DOA Estimation

The IMLE proposed in Ch. 3 and the IMAPE in Ch. 4 are based on the conditional (in Eq. (2.28)) and the joint (in Eq. (2.31)) likelihood respectively. In this sense both are *sub-optimal*, and are *alternatives* to an estimator based on the marginal (exact) likelihood of the observation (in Eq. (2.32)) with the texture integrated out. Such an estimator is mathematically intractable and computationally expensive, as it entails the computation of complicated (and numerical, for the K-distributed clutter) integrals and the solution of nonlinear equations containing such integrals. Notwithstanding this drawback, its investigation is still of significant technical interest, in consideration of the following aspects. First, it is not only theoretically the *optimum* estimator, but *in praxi* it will indeed lead to superior performance over both the IMLE and the IMAPE. Especially, this superiority becomes substantially evident in adverse scenarios where one has small SCRs, snapshot numbers, ect. Secondly, it requires fewer iteration numbers than both the other two estimators. In the Student's t-distributed clutter case, where numerical integrals are not involved, this actually indicates faster implementation.

This chapter is dedicated to the derivation of this optimum estimator, which, like the IMLE, also employs the ML technique, but unlike it, models the texture as stochastic. It contrasts with the IMLE also by the fact that it considers only the texture parameters in-

stead of the texture itself (which is integrated out and thus absent in the marginal likelihood), whereas the IMLE considers only the texture realization but ignores its distribution (the texture parameters). As mentioned in Ch. 1, this new estimator, which also adopts the numerical concentration approach and takes an iterative form, is given the name IEMLE, in which the first "E" in the acronym represents the word "exact", for the purpose of differentiating it from the IMLE and emphasizing the *exact* likelihood as its basis.

5.1 Estimates of the Unknown Parameters

Let Λ_{M} denote the marginal (exact) LLF, which is obtained from Eq. (2.32), as:

$$\begin{aligned}\Lambda_{\mathrm{M}} &= \ln p\left(\boldsymbol{z};\boldsymbol{\xi}\right)\\ &= -LMN\ln\pi - L\ln|\boldsymbol{\Sigma}| + \sum_{l=0}^{L-1}\ln g_{MN}\left(\left\|\boldsymbol{\rho}(l)\right\|^2, a, b\right),\end{aligned} \tag{5.1}$$

in which

$$\begin{aligned}&g_{MN}\left(\left\|\boldsymbol{\rho}(l)\right\|^2, a, b\right)\\ &= \int_0^{+\infty}\frac{\exp\left(-\frac{\|\boldsymbol{\rho}(l)\|^2}{\tau(l)}\right)}{\tau^{MN}(l)}p(\tau(l);a,b)\mathrm{d}\tau(l)\\ &= \begin{cases}\dfrac{2\left\|\boldsymbol{\rho}(l)\right\|^{a-MN}K_{a-MN}\left(2\left\|\boldsymbol{\rho}(l)\right\|/b^{\frac{1}{2}}\right)}{b^{\frac{MN+a}{2}}\Gamma(a)}, & \\ \text{K-distributed clutter}, & \\ \dfrac{b^a\Gamma(MN+a)}{\Gamma(a)\left(\left\|\boldsymbol{\rho}(l)\right\|^2+b\right)^{MN+a}}, & \text{Student's t-distributed clutter},\end{cases}\end{aligned} \tag{5.2}$$

is called the *characteristic function* of SIRP clutter, where $K_n(\cdot)$ is the modified Bessel function of the second kind of order n.

To begin with, one looks for the estimates of the clutter parameters, i.e., of the speckle CM $\boldsymbol{\Sigma}$, and the texture parameters a and b. The expression of $\hat{\boldsymbol{\Sigma}}$ when other unknown

parameters are fixed can be obtained by solving the equation: $\partial\Lambda_{\mathrm{M}}/\partial\boldsymbol{\Sigma}=0$, as [121]:

$$\hat{\boldsymbol{\Sigma}}=\frac{1}{L}\sum_{l=0}^{L-1}h_{MN}\left(\left\|\boldsymbol{\rho}(l)\right\|^{2},a,b\right)\boldsymbol{n}(l)\boldsymbol{n}^{H}(l), \tag{5.3}$$

in which

$$\begin{aligned}
&h_{MN}\left(\left\|\boldsymbol{\rho}(l)\right\|^{2},a,b\right)\\
=&-\left(\frac{\partial g_{MN}\left(\left\|\boldsymbol{\rho}(l)\right\|^{2},a,b\right)}{\partial\left\|\boldsymbol{\rho}(l)\right\|^{2}}\right)\Bigg/g_{MN}\left(\left\|\boldsymbol{\rho}(l)\right\|^{2},a,b\right)\\
=&\begin{cases}
\dfrac{K_{a-MN-1}\left(2\left\|\boldsymbol{\rho}(l)\right\|/b^{\frac{1}{2}}\right)}{b^{\frac{1}{2}}\left\|\boldsymbol{\rho}(l)\right\|K_{a-MN}\left(2\left\|\boldsymbol{\rho}(l)\right\|/b^{\frac{1}{2}}\right)}, & \\
\text{K-distributed clutter}, & \\
\dfrac{MN+a}{\left\|\boldsymbol{\rho}(l)\right\|^{2}+b}, & \text{Student's t-distributed clutter}.
\end{cases}
\end{aligned} \tag{5.4}$$

Note that, similar to $\hat{\boldsymbol{\Sigma}}$ for the IMLE in Eq. (3.6) and for the IMAPE in Eq. (4.8), $\hat{\boldsymbol{\Sigma}}$ in Eq. (5.3) for the IEMLE also has an (albeit *inexplicit*) iterative nature, as can be seen from the expression of $\boldsymbol{\rho}(l)$ in Eq. (2.30), which is a function of $\boldsymbol{\Sigma}$. Thus $\hat{\boldsymbol{\Sigma}}$ in Eq. (5.3) is *unique* if the matrix $\boldsymbol{\Sigma}$ is invertible, i.e., if the number of pulses per CPI $L\geq MN$. Furthermore, due to the assumption on the CM trace in Eq. (2.17), $\hat{\boldsymbol{\Sigma}}$ in Eq. (5.3) has also to be normalized by Eq. (3.7) to obtain $\hat{\boldsymbol{\Sigma}}_{\mathrm{n}}^{(i+1)}$.

Meanwhile, the estimates of a and b, when other unknown parameters are fixed, can be found by equating $\partial\Lambda_{\mathrm{M}}/\partial a$ and $\partial\Lambda_{\mathrm{M}}/\partial b$ to zero, respectively, i,e, by solving:

$$\frac{\partial\Lambda_{\mathrm{M}}}{\partial a}=\sum_{l=0}^{L-1}\frac{k_{MN}\left(\left\|\boldsymbol{\rho}(l)\right\|^{2},a,b\right)}{g_{MN}\left(\left\|\boldsymbol{\rho}(l)\right\|^{2},a,b\right)}=0, \tag{5.5}$$

w.r.t. a, and

$$\frac{\partial\Lambda_{\mathrm{M}}}{\partial b}=\sum_{l=0}^{L-1}\frac{l_{MN}\left(\left\|\boldsymbol{\rho}(l)\right\|^{2},a,b\right)}{g_{MN}\left(\left\|\boldsymbol{\rho}(l)\right\|^{2},a,b\right)}=0, \tag{5.6}$$

w.r.t. b, in which

$$
\begin{aligned}
&k_{MN}\left(\|\boldsymbol{\rho}(l)\|^2, a, b\right) \\
=&\frac{\partial g_{MN}\left(\|\boldsymbol{\rho}(l)\|^2, a, b\right)}{\partial a} \\
=&\begin{cases}
-\dfrac{1}{b^a\Gamma(a)}\displaystyle\int_0^{+\infty}\exp\left(-\frac{\|\boldsymbol{\rho}(l)\|^2}{\tau(l)}-\frac{\tau(l)}{b}\right)\tau(l)^{-MN+a-1} \\
\cdot\left(\ln\left(\dfrac{b}{\tau(l)}\right)+\Psi(a)\right)\mathrm{d}\tau(l), \quad \text{K-distributed clutter,} \\
-\dfrac{b^a\Gamma(MN+a)\left(\ln\left(\frac{\|\boldsymbol{\rho}(l)\|^2}{b}+1\right)-\Psi(MN+a)+\Psi(a)\right)}{\Gamma(MN)\left(\|\boldsymbol{\rho}(l)\|^2+b\right)^{MN+a}}, \\
\text{Student's t-distributed clutter,}
\end{cases}
\end{aligned}
\tag{5.7}
$$

and

$$
\begin{aligned}
&l_{MN}\left(\|\boldsymbol{\rho}(l)\|^2, a, b\right) \\
=&\frac{\partial g_{MN}\left(\|\boldsymbol{\rho}(l)\|^2, a, b\right)}{\partial b} \\
=&\begin{cases}
\dfrac{1}{b^{a+2}\Gamma(a)}\displaystyle\int_0^{+\infty}\exp\left(-\frac{\|\boldsymbol{\rho}(l)\|^2}{\tau(l)}-\frac{\tau(l)}{b}\right) \\
\cdot\,\tau(l)^{-MN+a-1}\left(\tau(l)-ab\right)\mathrm{d}\tau(l), \\
\text{K-distributed clutter,} \\
-\dfrac{ab^{a-1}\Gamma(MN+a)\left(-a\|\boldsymbol{\rho}(l)\|^2+MNb\right)}{\Gamma(a+1)\left(\|\boldsymbol{\rho}(l)\|^2+b\right)^{MN+a+1}}, \\
\text{Student's t-distributed clutter.}
\end{cases}
\end{aligned}
\tag{5.8}
$$

Both Eq. (5.5) and Eq. (5.6) can only be numerically solved. A theoretical proof of the existence and uniqueness of their solutions for Student's t-distributed clutter will be given later in Sec. 5.3. For K-distributed clutter, which involves integrals that have no closed-form expressions, a similar, analytical approach of proof seems impossible. The property of the solutions in this case can nevertheless be determined by numerical means.

On the other hand, the estimate of $\boldsymbol{v}(l)$ can be found by solving $\partial\Lambda_{\mathrm{M}}/\partial\boldsymbol{v}(l)=0$, and has the same expression as $\hat{\boldsymbol{v}}(l)$ in Eq. (3.8).

Next, one turns to the estimation of $\boldsymbol{\theta}$. As the expressions in Eqs. (5.3), (5.5), (5.6) and

(3.8) suggest, the estimation of each of the parameters a, b, $\boldsymbol{\Sigma}$ and $\boldsymbol{v}(l)$ requires the knowledge of all the other. To deal with this mutual dependence of the parameter estimation, the numerical concentration approach, which has been employed in Chs. (3) and (4) respectively for the IMLE and the IMAPE, shall also be adopted here. More precisely, for the IEMLE, one assumes that $\hat{\boldsymbol{\Sigma}}$, $\hat{a}$, $\hat{b}$ $\boldsymbol{\theta}$ are known at each iteration, and uses them to compute $\hat{\boldsymbol{v}}(l)$, which is then used in turn to update the values of $\hat{\boldsymbol{\Sigma}}$ and $\hat{a}$ and $\hat{b}$ to be used in the next iteration. This allows us to drop all the constant terms in the LLF, including those terms that contain only $\boldsymbol{\Sigma}$, a and b as unknown parameters, as they are fixed at each iteration. Furthermore, by inserting the expression of $\hat{\boldsymbol{v}}(l)$ in Eq. (3.8) into what remains in the LLF, the estimate of $\boldsymbol{\theta}$ is obtained as:

$$\hat{\boldsymbol{\theta}} = \begin{cases} \arg\min\limits_{\boldsymbol{\theta}} \left\{ \sum\limits_{l=0}^{L-1} \left((MN-a) \ln \left(\left\| \boldsymbol{P}^{\perp}_{\tilde{\boldsymbol{A}}(\boldsymbol{\theta})} \tilde{\boldsymbol{z}}(l) \right\| \right) \right. \right. \\ \left. \left. - \ln K_{a-MN} \left(2 \left\| \boldsymbol{P}^{\perp}_{\tilde{\boldsymbol{A}}(\boldsymbol{\theta})} \tilde{\boldsymbol{z}}(l) \right\| \Big/ b^{\frac{1}{2}} \right) \right) \right\}, \\ \text{K-distributed clutter}, \\ \arg\min\limits_{\boldsymbol{\theta}} \left\{ \sum\limits_{l=0}^{L-1} \ln \left(\left\| \boldsymbol{P}^{\perp}_{\tilde{\boldsymbol{A}}(\boldsymbol{\theta})} \tilde{\boldsymbol{z}}(l) \right\|^2 + b \right) \right\}, \\ \text{Student's t-distributed clutter}. \end{cases} \tag{5.9}$$

in which $\boldsymbol{P}^{\perp}_{\tilde{\boldsymbol{A}}(\boldsymbol{\theta})}$ is defined in Eq. (3.13). One makes the assumption regarding Eq. (5.9) that it is a *unique* optimum, implying that $K \leq MN$ [122].

5.2 Comparison and Interpretation of the Objective Functions for $\hat{\boldsymbol{\theta}}$

At this point one may recall the expression of $\hat{\boldsymbol{\theta}}$ for the CMLE in Eq. (3.21), as well as that for the IMLE and the IMAPE in Eq. (3.12), and compare them with Eq. (5.9).

Eq. (3.21) shows that the CMLE considers simply the *sum* of $\left\| \boldsymbol{P}^{\perp}_{\boldsymbol{A}(\boldsymbol{\theta})} \boldsymbol{z}(l) \right\|^2$ (the square of the norm of the projection of the observation at pulse l onto the null space of the steering

matrix), while the IMLE and IMAPE, as Eq. (3.12) shows, consider the *modified sum* of these terms (pre-whitened by the speckle CM, and weighted by the inverse of the texture realization at each pulse). It is precisely because of this modification that the IMLE and IMAPE gain their advantages in performance over the CMLE.

On the other hand, one can see from Eq. (3.12) that the IEMLE considers neither the direct nor the modified sum of the projections, but the sum of their *logarithms* (modified by some algebraic operations), which is equivalent to the *product* of them. Since a sum is small only if all its terms are small, while a product can be small even if only very few of its terms are small enough, one can conclude that underlying this contrast between *summation* and *multiplication* is an essential difference, namely, that the CMLE, IMLE and IMAPE treat all the pulses "equally", whereas the IEMLE focus only on the "best" pulses, i.e., those corresponding to the texture realizations of small values. In fact, as the simulations in Ch. 8 will show, this difference leads to superior performance of the IEMLE not only hugely over the CMLE, but also over the IMLE and IMAPE, especially in adverse scenarios of small SCR or snapshot numbers.

5.3 Existence and Uniqueness of the Solutions for the Texture Parameters for Student's t-Distributed Clutter

One first considers $\partial\Lambda_{\mathrm{M}}/\partial a$, which can, by applying the following difference equation of the digamma function:

$$\Psi(x+N)-\Psi(x)=\sum_{i=0}^{N-1}\frac{1}{x+i},\quad N\geq 1, N\in\mathbb{Z}, \tag{5.10}$$

be transformed into:

$$\begin{aligned}\frac{\partial\Lambda_{\mathrm{M}}}{\partial a}=&L\left(\Psi(MN+a)-\Psi(a)\right)-\sum_{l=0}^{L-1}\ln\left(\frac{\|\boldsymbol{\rho}(l)\|^2}{b}+1\right)\\ =&\sum_{i=0}^{MN-1}\frac{L}{a+i}-\sum_{l=0}^{L-1}\ln\left(\frac{\|\boldsymbol{\rho}(l)\|^2}{b}+1\right),\end{aligned} \tag{5.11}$$

which is a continuous, strictly decreasing function of a in the interval $(0, +\infty)$ for any $b \in (0, +\infty)$. Furthermore, we have

$$\begin{cases} \lim\limits_{a\to 0^+} \dfrac{\partial \Lambda_{\mathrm{M}}}{\partial a} = +\infty, \\ \lim\limits_{a\to +\infty} \dfrac{\partial \Lambda_{\mathrm{M}}}{\partial a} = -\sum\limits_{l=0}^{L-1} \ln\left(\dfrac{\|\boldsymbol{\rho}(l)\|^2}{b} + 1\right) < 0, \end{cases} \tag{5.12}$$

meaning that for any $b \in (0, +\infty)$, there exists *exactly* one value of a in the interval $(0, +\infty)$ that leads to $\partial\Lambda_{\mathrm{M}}/\partial a = 0$, which corresponds to the global maximum point of Λ_{M} w.r.t. a.

On the other hand, the expression of $\partial\Lambda_{\mathrm{M}}/\partial b$ for Student's t-distributed clutter is:

$$\frac{\partial \Lambda_{\mathrm{M}}}{\partial b} = \frac{La}{b} - \sum_{l=0}^{L-1} \frac{MN + a}{\|\boldsymbol{\rho}(l)\|^2 + b} = \frac{\nu(b)}{\delta(b)}, \tag{5.13}$$

in which

$$\delta(b) = b \prod_{l=0}^{L-1} \left(\|\boldsymbol{\rho}(l)\|^2 + b\right) > 0 \tag{5.14}$$

over the range of b, and

$$\nu(b) = \sum_{i=0}^{L} c_i b^i, \tag{5.15}$$

is a polynomial w.r.t. b, whose coefficients are:

$$c_0 = w_0 \prod_{j=0}^{L-1} \|\boldsymbol{\rho}(j)\|^2, \tag{5.16a}$$

$$c_1 = w_1 \sum_{0\le j_0<\cdots<j_{L-1}\le L-1} \prod_{j=j_0}^{j_{L-1}} \|\boldsymbol{\rho}(j)\|^2, \tag{5.16b}$$

$$\cdots \tag{5.16c}$$

$$c_i = w_i \sum_{0\le j_0<\cdots<j_{L-i}\le L-1} \prod_{j=j_0}^{j_{L-i}} \|\boldsymbol{\rho}(j)\|^2, \tag{5.16d}$$

$$\cdots \tag{5.16e}$$

$$c_{L-1} = w_{L-1} \sum_{j=0}^{L-1} \|\boldsymbol{\rho}(j)\|^2, \tag{5.16f}$$

$$c_L = w_L. \tag{5.16g}$$

in which

$$w_i = (L-i)a - iMN, \quad i = 0, \ldots, L. \tag{5.17}$$

The coefficients $c_0, \ldots, c_L$ can either be positive, zero, or negative, and their respective signs depend of the values of a and N. Upon closer inspection, however, one can observe that, irrespective of the relationship between the value of a and N, there is always at most one sign change between consecutive nonzero coefficients within the entire sequence $c_0, \ldots, c_L$. For example, if

$$\frac{(i-1)MN}{L-i+1} < a < \frac{iMN}{L-i}, \tag{5.18}$$

then one has:

$$\begin{cases} c_j > 0, & j \leq i-1, \\ c_j < 0, & j \geq i. \end{cases} \tag{5.19}$$

Thus, it arises from Descartes' rule of signs [126] that there is always one positive root of $\nu(b)$. Furthermore, since $\delta(b) > 0$ always holds, one arrives at the conclusion that $\partial\Lambda_{\mathrm{M}}/\partial b = 0$ has *exactly* one root w.r.t. b over the range $(0, +\infty)$ for any $a \in (0, +\infty)$.

5.4 Algorithmic Procedure

Similar to the procedures of the IMLE in Alg. 3.1 and the IMAPE in Algs. 4.1, the whole procedure of the proposed IEMLE also comprises iterations between two steps, as presented in Alg. 5.1. The initialization approach for the IEMLE, however, is different from that for the IMLE and the IMAPE. Both the latter two algorithms initialize the texture realizations as all-one-valued, thereby initialize the clutter as Gaussian-distributed. The IEMLE, on the other hand, does not consider the texture realizations as unknown parameters, but only considers the texture parameters a and b. Accordingly, the IEMLE initializes a and b at the beginning of the algorithm, instead of the texture realizations.

Algorithm 5.1 Iterative Exact Maximum Likelihood Estimator (IEMLE)

Initialization:

- Choose the convergence threshold $\varepsilon_{\boldsymbol{\theta}}$.
- Choose the maximum number of iterations $i_{\max}$.
- Set the iteration index $i = 0$.
- Set $\hat{a}^{(0)}$, $\hat{b}^{(0)}$ to be two arbitrary positive numbers.
- Set $\hat{\boldsymbol{\Sigma}}_{\mathrm{n}}^{(0)} = \boldsymbol{I}_{MN}$.

Step 1: At ith iteration ($i \geq 0$),

- Calculate $\hat{\boldsymbol{\theta}}^{(i)}$ according to Eq. (5.9) by:

$$\hat{\boldsymbol{\theta}}^{(i)} = \begin{cases} \arg\min\limits_{\boldsymbol{\theta}} \left\{ \sum\limits_{l=0}^{L-1} \left(\left(MN - \hat{a}^{(i)}\right) \ln\left(\left\| \boldsymbol{P}^{\perp}_{\hat{\tilde{\boldsymbol{A}}}^{(i)}(\boldsymbol{\theta})} \hat{\tilde{\boldsymbol{z}}}^{(i)}(l) \right\| \right) \right. \right. \\ \left. \left. - \ln K_{\hat{a}^{(i)}-MN}\left(2 \left\| \boldsymbol{P}^{\perp}_{\hat{\tilde{\boldsymbol{A}}}^{(i)}(\boldsymbol{\theta})} \hat{\tilde{\boldsymbol{z}}}^{(i)}(t) \right\| \Big/ \left(\hat{b}^{(i)} \right)^{\frac{1}{2}} \right) \right) \right\}, \\ \text{K-distributed clutter}, \\ \arg\min\limits_{\boldsymbol{\theta}} \left\{ \sum\limits_{l=0}^{L-1} \ln\left(\left\| \boldsymbol{P}^{\perp}_{\hat{\tilde{\boldsymbol{A}}}^{(i)}(\boldsymbol{\theta})} \hat{\tilde{\boldsymbol{z}}}^{(i)}(l) \right\|^2 + \hat{b}^{(i)} \right) \right\}, \\ \text{Student's t-distributed clutter}. \end{cases} \tag{5.20}$$

  in which $\hat{\tilde{\boldsymbol{z}}}^{(i)}(l)$, $\hat{\tilde{\boldsymbol{A}}}^{(i)}(\boldsymbol{\theta})$ and $\boldsymbol{P}^{\perp}_{\hat{\tilde{\boldsymbol{A}}}^{(i)}(\boldsymbol{\theta})}(l)$ are defined in Eqs. (3.15), (3.16) and (3.17), respectively.

- Calculate $\hat{\boldsymbol{v}}^{(i)}(l)$ by Eq. (3.18).

Algorithm 5.1 Iterative Exact Maximum Likelihood Estimator (IEMLE) (cont'd)

Step 2:

- Update $\hat{a}^{(i+1)}$ according to Eq. (5.5) by numerically solving:

$$-\frac{\left(\hat{b}^{(i)}\right)^{\frac{MN-\hat{a}^{(i+1)}}{2}}}{2}\sum_{l=0}^{L-1}\frac{\displaystyle\int_0^{+\infty}\exp\left(-\frac{\left\|\hat{\boldsymbol{\rho}}^{(i)}(l)\right\|^2}{\tau(l)}-\frac{\tau(l)}{\hat{b}^{(i)}}\right)\tau(l)^{-MN+\hat{a}^{(i+1)}-1}\left(\ln\left(\frac{\hat{b}^{(i)}}{\tau(l)}\right)+\Psi(\hat{a}^{(i+1)})\right)\mathrm{d}\tau(l)}{\left\|\hat{\boldsymbol{\rho}}^{(i)}(l)\right\|^{\hat{a}^{(i+1)}-MN}K_{\hat{a}^{(i+1)}-MN}\left(2\left\|\hat{\boldsymbol{\rho}}^{(i)}(l)\right\|\Big/\left(\hat{b}^{(i)}\right)^{\frac{1}{2}}\right)}=0,$$

  for K-distributed clutter; or

$$L\left(\Psi(MN+\hat{a}^{(i+1)})-\Psi(\hat{a}^{(i+1)})\right)-\sum_{l=0}^{L-1}\ln\left(\frac{\left\|\hat{\boldsymbol{\rho}}^{(i)}(l)\right\|^2}{\hat{b}^{(i)}}+1\right)=0,$$

  for Student's t-distributed clutter, in which $\hat{\boldsymbol{\rho}}^{(i)}(l) = \left(\hat{\boldsymbol{\Sigma}}_{\mathrm{n}}^{(i)}\right)^{-\frac{1}{2}}\left(\boldsymbol{z}(l)-\boldsymbol{A}\left(\hat{\boldsymbol{\theta}}^{(i)}\right)\hat{\boldsymbol{v}}^{(i)}(l)\right)=0.$

- Update $\hat{b}^{(i+1)}$ according to Eq. (5.6) by numerically solving:

$$\left(\frac{\left(\hat{b}^{(i+1)}\right)^{\frac{MN-\hat{a}^{(i+1)}}{2}}}{2}-1\right)\sum_{l=0}^{L-1}\frac{\displaystyle\int_0^{+\infty}\exp\left(-\frac{\left\|\hat{\boldsymbol{\rho}}^{(i)}(l)\right\|^2}{\tau(l)}-\frac{\tau(l)}{\hat{b}^{(i+1)}}\right)\tau(l)^{-MN+\hat{a}^{(i+1)}-1}\left(\tau(l)-\hat{a}^{(i+1)}\hat{b}^{(i+1)}\right)\mathrm{d}\tau(l)}{\left\|\hat{\boldsymbol{\rho}}^{(i)}(l)\right\|^{\hat{a}^{(i+1)}-MN}K_{\hat{a}^{(i+1)}-MN}\left(2\left\|\hat{\boldsymbol{\rho}}^{(i)}(l)\right\|\Big/\left(\hat{b}^{(i+1)}\right)^{\frac{1}{2}}\right)}=0,$$

  for K-distributed clutter; or

$$\frac{L\hat{a}^{(i+1)}}{\hat{b}^{(i+1)}}-\sum_{l=0}^{L-1}\frac{MN+\hat{a}^{(i+1)}}{\left\|\hat{\boldsymbol{\rho}}^{(i)}(l)\right\|^2+\hat{b}^{(i+1)}}=0,$$

  for Student's t-distributed clutter.

Algorithm 5.1 Iterative Exact Maximum Likelihood Estimator (IEMLE) (cont'd)

Step 2 (cont'd):

- Update $\hat{\boldsymbol{\Sigma}}^{(i+1)}$ according to Eq. (5.3) by:

$$\hat{\boldsymbol{\Sigma}}^{(i+1)} = \frac{1}{L}\sum_{l=0}^{L-1} h_{MN}\left(\left\|\hat{\boldsymbol{\rho}}^{(i)}(l)\right\|^2, \hat{a}^{(i+1)}, \hat{b}^{(i+1)}\right)\hat{\boldsymbol{n}}^{(i)}(l)\left(\hat{\boldsymbol{n}}^{(i)}(l)\right)^H,$$

  where $\hat{\boldsymbol{n}}^{(i)}(l)$ is defined in Eq. (3.19), and

$$h_{MN}\left(\left\|\hat{\boldsymbol{\rho}}^{(i)}(l)\right\|, \hat{a}^{(i+1)}, \hat{b}^{(i+1)}\right) = \begin{cases} \dfrac{K_{\hat{a}^{(i+1)}-MN-1}\left(2\left\|\hat{\boldsymbol{\rho}}^{(i)}(l)\right\| \Big/ \left(\hat{b}^{(i+1)}\right)^{\frac{1}{2}}\right)}{\left(\hat{b}^{(i+1)}\right)^{\frac{1}{2}}\left\|\hat{\boldsymbol{\rho}}^{(i)}(l)\right\| K_{\hat{a}^{(i+1)}-MN}\left(2\left\|\hat{\boldsymbol{\rho}}^{(i)}(l)\right\| \Big/ \left(\hat{b}^{(i+1)}\right)^{\frac{1}{2}}\right)}, \\ \text{K-distributed clutter,} \\ \dfrac{MN+\hat{a}^{(i+1)}}{\left\|\hat{\boldsymbol{\rho}}^{(i)}(l)\right\|^2+\hat{b}^{(i+1)}}, \quad \text{Student's t-distributed clutter.} \end{cases}$$

- Calculate $\hat{\boldsymbol{\Sigma}}_{\text{n}}^{(i+1)}$ by Eq. (3.20).

Termination Condition:

if $(i=0)\bigvee\left((1\le i<i_{\max})\bigwedge\left\|\hat{\boldsymbol{\theta}}^{(i)}-\hat{\boldsymbol{\theta}}^{(i-1)}\right\|>\varepsilon_{\boldsymbol{\theta}}\right)$ **then**

Set $i=i+1$, and go to **Step 1**.

end if

return $\hat{\boldsymbol{\theta}}^{(i)}$.

5.5 Performance Analysis

5.5.1 Convergence and Computational Cost

Similar what has been discussed in Subsecs. 3.4.1 and 4.4.1 for the IMLE and the IMAPE, respectively, the function value convergence of the proposed IEMLE algorithm can be proved

by showing the fulfillment of the three conditions listed in Subsec. 3.4.1 by the IEMLE. The first two conditions are obviously valid. The third condition, i.e., the uniqueness of the parameter estimates, is also fulfilled under the mild conditions specified below Eqs. (5.3), (5.9) and those in Ch. 3 and Sec. 5.3 (for Student's t-distributed clutter). Simulation results in Ch. 8 will show that, to attain the convergence of the estimate of the unknown parameter $\hat{\boldsymbol{\theta}}$, the IEMLE requires still fewer iterations than the IMLE and the IMAPE. Generally one iteration is enough for this purpose.

For t-distributed clutter case, the computational cost of the IEMLE lies mainly in the numerical solution of Eq. (5.20). As the IEMLE requires fewer iterations than the IMLE and the IMAPE, its computational cost is also smaller than them in this case. For K-distributed clutter case, however, since the IEMLE involves numerically solving the nonlinear equations in Eqs. (5.1) and (5.1) that contain numerical integrals, which is computationally highly expensive, it turns out that the computational cost for the IEMLE in this case is much greater than the IMLE and the IMAPE.

5.5.2 Invariance of the IEMLE to Different Speckle CM Trace Assumptions

Introduce the variables $\mathrm{tr}\{\boldsymbol{\Sigma}\}_{\mathrm{a}}$, r and the representation $\hat{(\cdot)}'$ as defined in Sec. 3.4.2, to stand for the alternatively assumed speckle CM trace, the ratio between this alternatively and the originally (namely, in Eq. (2.17)) assumed speckle CM trace, and the "counterpart" of a parameter corresponding to the alternative assumption of $\mathrm{tr}\{\boldsymbol{\Sigma}\}_{\mathrm{a}}$, respectively. The expressions of $\tau'(l)$ in Eq. (3.26) and $\boldsymbol{\rho}'(l)$ in Eq. (3.28) also hold for the IEMLE.

Additionally, it is known from the scaling property of the gamma and the inverse-gamma distributions that, if

$$\tau(l) \sim \text{Gamma}(a, b), \tag{5.21}$$

then

$$\frac{1}{r}\tau(l) \sim \text{Gamma}(a, \frac{1}{r}b), \tag{5.22}$$

and similarly, if

$$\tau(l) \sim \text{Inv-Gamma}(a, b), \tag{5.23}$$

then

$$\frac{1}{r}\tau(l) \sim \text{Inv-Gamma}(a, \frac{1}{r}b). \tag{5.24}$$

Hence

$$a' = a, \tag{5.25}$$

and

$$b' = \frac{1}{r}b, \tag{5.26}$$

for both texture distributions.

By substituting Eqs. (5.25), (5.26) and (3.28) into Eq. (5.2) one obtains that:

$$g_{MN}\left(\left\|\boldsymbol{\rho}'(l)\right\|^2, a', b'\right) = r^{MN} g_{MN}\left(\left\|\boldsymbol{\rho}(l)\right\|^2, a, b\right), \quad l = 0, \ldots, L-1. \tag{5.27}$$

for both clutter distributions.

Furthermore, by noticing that the objective function in Eq. (5.9) is in essence the search for $\hat{\boldsymbol{\theta}}$ by:

$$\hat{\boldsymbol{\theta}} = \arg\max_{\boldsymbol{\theta}} \left\{ \sum_{l=0}^{L-1} \ln g_{MN}\left(\left\|\boldsymbol{\rho}(l)\right\|^2, a, b\right) \right\}, \tag{5.28}$$

and by applying Eq. (5.27), it can be shown that:

$$\begin{aligned}
\hat{\boldsymbol{\theta}}' &= \arg\max_{\boldsymbol{\theta}} \left\{ \sum_{l=0}^{L-1} \ln g_{MN}\left(\left\|\boldsymbol{\rho}'(l)\right\|^2, a', b'\right) \right\} \\
&= \arg\max_{\boldsymbol{\theta}} \left\{ \sum_{l=0}^{L-1} \ln g_{MN}\left(\left\|\boldsymbol{\rho}(l)\right\|^2, a, b\right) + LMN \ln r \right\} \\
&= \arg\max_{\boldsymbol{\theta}} \left\{ \sum_{l=0}^{L-1} \ln g_{MN}\left(\left\|\boldsymbol{\rho}(l)\right\|^2, a, b\right) \right\} \\
&= \hat{\boldsymbol{\theta}},
\end{aligned} \tag{5.29}$$

which shows that the IEMLE is invariant to different speckle CM trace assumptions, as, like

for the IMLE and the IMAPE, the estimated $\boldsymbol{\theta}$ for the IEMLE is also independent of the assumed value of $\mathrm{tr}\{\boldsymbol{\Sigma}\}$.

Chapter 6

Cramér-Rao-Type Bounds

The task of this section is to derive the expressions for various CRTBs, including the CRB, the MCB, the EMCB, the MCRB and the HCRB, w.r.t. the DOD and DOA parameters of the MIMO radar in the presence of SIRP clutter, based on the estimation model given by Eq. (2.7) in Ch. 2. The expressions of these CRTBs are derived first in the elementwise form of the FIM matrices, then the relations between them are determined, as well as the respective impacts of the texture parameters on each of them. Finally, to make their expressions more compact and their calculation more convenient, a blockwise expression is then derived for each of the CRTBs.

To be consistent with the proposed estimators in Chs. 3-5, and for the purpose of parameter identifiability, one considers for the derivation of the CRTBs also the transformed unknown parameter vector in Eq. (2.24), instead of the original one in Eq. (2.21). Namely, one takes $\boldsymbol{v}(l),\ l = 0, \ldots, L-1$ defined in Eq. (2.8) as part of unknown parameters instead of the RCS coefficients $\alpha_k(l),\ k = 1, \ldots, K$, and the normalized Doppler frequency shifts $f_k(l),\ k = 1, \ldots, K$, of the targets.

6.1 The Cramér-Rao Bound

Let $\mathbf{CRB}\,(\boldsymbol{\theta})$ denotes the CRB w.r.t. the DODs and DOAs of the signal, which, like the IEMLE proposed in Ch. 5, considers exactly the parameter vector $\boldsymbol{\xi}$, and is obtained as the

upper-leftmost elements (those corresponding to $\boldsymbol{\theta}$) of the inverse of the Fisher Information Matrix (FIM). The latter, denoted by $\boldsymbol{F}$, is calculated from the marginal (exact) LLF Λ_{M} defined in Eq. (5.1).

The elements of $\boldsymbol{F}$ are given by:

$$[\boldsymbol{F}]_{i,j} = \mathrm{E}_{\boldsymbol{y}} \left\{ \frac{\partial \Lambda_{\mathrm{M}}}{\partial [\boldsymbol{\xi}]_i} \frac{\partial \Lambda_{\mathrm{M}}}{\partial [\boldsymbol{\xi}]_j} \right\}, \quad i,j = 1, \ldots, 2K(L+1) + M^2N^2 + 2, \tag{6.1}$$

in which $\mathrm{E}_{\boldsymbol{y}} \{\cdot\}$ represents the expectation w.r.t. the parameter $\boldsymbol{y}$, $[\cdot]_{i,j}$ denotes the (i,j)th entry of a matrix, and $[\cdot]_i$ denotes the ith element of a vector.

6.1.1 The Score Functions

The computation of Eq. (6.1) requires, in the first place, the expressions of the partial derivatives of Λ_{M} w.r.t. all the elements of $\boldsymbol{\xi}$ (also known as the *score functions*).

First, introduce the $2K(L+1) \times 1$ signal parameter vector:

$$\boldsymbol{\mu} = \left[\boldsymbol{\theta}^T, \boldsymbol{v}^T\right]^T, \tag{6.2}$$

in which $\boldsymbol{\theta}$ and $\boldsymbol{v}$ are defined in Eq. (2.11) and (2.25), respectively. The score functions w.r.t. $[\boldsymbol{\mu}]_i$, $i = 1, \ldots, 2K(L+1)$, and $[\boldsymbol{\zeta}]_i$, $i = 1, \ldots, M^2N^2$ (the parameter vector $\boldsymbol{\zeta}$ is defined in Sec. 2.3 and contains the real and imaginary parts of the entries of the lower triangular part of the speckle CM $\boldsymbol{\Sigma}$), can be calculated as:

$$\begin{aligned}
\frac{\partial \Lambda_{\mathrm{M}}}{\partial [\boldsymbol{\mu}]_i} = & - \sum_{l=0}^{L-1} h_{MN}\left(\|\boldsymbol{\rho}(l)\|^2, a, b\right) \\
& \cdot \left(\boldsymbol{\rho}^H(l) \boldsymbol{\Sigma}^{-\frac{1}{2}} \frac{\partial \boldsymbol{b}(\boldsymbol{\theta}, l)}{\partial [\boldsymbol{\mu}]_i} + \frac{\partial \boldsymbol{b}^H(\boldsymbol{\theta}, l)}{\partial [\boldsymbol{\mu}]_i} \boldsymbol{\Sigma}^{-\frac{1}{2}} \boldsymbol{\rho}(l) \right), \\
& i = 1, \ldots, 2K(L+1),
\end{aligned} \tag{6.3a}$$

$$\begin{aligned}
\frac{\partial \Lambda}{\partial [\boldsymbol{\zeta}]_i} = & - \sum_{l=0}^{L-1} h_{MN}\left(\|\boldsymbol{\rho}(l)\|^2, a, b\right) \left(\boldsymbol{\rho}^H(l) \boldsymbol{\Sigma}^{-\frac{1}{2}} \frac{\partial \boldsymbol{\Sigma}}{\partial [\boldsymbol{\zeta}]_i} \boldsymbol{\Sigma}^{-\frac{1}{2}} \boldsymbol{\rho}(l) \right) \\
& - L \mathrm{tr} \left\{ \boldsymbol{\Sigma}^{-1} \frac{\partial \boldsymbol{\Sigma}}{\partial [\boldsymbol{\zeta}]_i} \right\}, \quad i = 1, \ldots, M^2N^2,
\end{aligned} \tag{6.3b}$$

$$\tag{6.3c}$$

in which

$$\boldsymbol{b}\left(\boldsymbol{\theta},l\right)=\boldsymbol{A}\left(\boldsymbol{\theta}\right)\boldsymbol{v}(l),\quad l=0,\ldots,L-1, \tag{6.4}$$

and $h_{MN}\left(\left\|\boldsymbol{\rho}(l)\right\|^2,a,b\right)$ is defined in Eq. (5.1).

On the other hand, the score functions w.r.t. a and b are given in Eqs. (5.5) and (5.6), respectively.

6.1.2 Calculation of the FIM Entries w.r.t. the Signal Parameters

To begin with, one investigates the FIM entries w.r.t. the signal parameter vector $\boldsymbol{\mu}$, i.e., the entries on the first $2K(L+1)$ rows and columns of $\boldsymbol{F}$. By substituting Eq. (6.3a) into Eq. (6.1), one obtains:

$$\begin{aligned}
\left[\boldsymbol{F}\right]_{i,j}=&\mathrm{E}_{\boldsymbol{\rho}(l)}\Bigg\{\sum_{l=0}^{L-1}h_{MN}^2\left(\left\|\boldsymbol{\rho}(l)\right\|^2,a,b\right)\\
&\cdot\Bigg(\boldsymbol{\rho}^H(l)\boldsymbol{\Sigma}^{-\frac{1}{2}}\frac{\partial\boldsymbol{b}\left(\boldsymbol{\theta},l\right)}{\partial\left[\boldsymbol{\mu}\right]_i}\boldsymbol{\rho}^H(l)\boldsymbol{\Sigma}^{-\frac{1}{2}}\frac{\partial\boldsymbol{b}\left(\boldsymbol{\theta},l\right)}{\partial\left[\boldsymbol{\mu}\right]_j}\\
&+\boldsymbol{\rho}^H(l)\boldsymbol{\Sigma}^{-\frac{1}{2}}\frac{\partial\boldsymbol{b}\left(\boldsymbol{\theta},l\right)}{\partial\left[\boldsymbol{\mu}\right]_i}\frac{\partial\boldsymbol{b}^H\left(\boldsymbol{\theta},l\right)}{\partial\left[\boldsymbol{\mu}\right]_j}\boldsymbol{\Sigma}^{-\frac{1}{2}}\boldsymbol{\rho}(l)\\
&+\frac{\partial\boldsymbol{b}^H\left(\boldsymbol{\theta},l\right)}{\partial\left[\boldsymbol{\mu}\right]_i}\boldsymbol{\Sigma}^{-\frac{1}{2}}\boldsymbol{\rho}(l)\boldsymbol{\rho}^H(l)\boldsymbol{\Sigma}^{-\frac{1}{2}}\frac{\partial\boldsymbol{b}\left(\boldsymbol{\theta},l\right)}{\partial\left[\boldsymbol{\mu}\right]_j}\\
&+\frac{\partial\boldsymbol{b}^H\left(\boldsymbol{\theta},l\right)}{\partial\left[\boldsymbol{\mu}\right]_i}\boldsymbol{\Sigma}^{-\frac{1}{2}}\boldsymbol{\rho}(l)\frac{\partial\boldsymbol{b}^H\left(\boldsymbol{\theta},l\right)}{\partial\left[\boldsymbol{\mu}\right]_j}\boldsymbol{\Sigma}^{-\frac{1}{2}}\boldsymbol{\rho}(l)\Bigg)\Bigg\}\\
&+\mathrm{E}_{\boldsymbol{\rho}(l_1),\boldsymbol{\rho}(l_2)}\Bigg\{\sum_{l_1=0}^{L-1}\sum_{l_2=1,l_2\neq l_1}^{L-1}h_{MN}\left(\left\|\boldsymbol{\rho}(l_1)\right\|^2,a,b\right)h_{MN}\left(\left\|\boldsymbol{\rho}(l_2)\right\|^2,a,b\right)\\
&\cdot\Bigg(\boldsymbol{\rho}^H(l_1)\boldsymbol{\Sigma}^{-\frac{1}{2}}\frac{\partial\boldsymbol{b}\left(\boldsymbol{\theta},l_1\right)}{\partial\left[\boldsymbol{\mu}\right]_i}\boldsymbol{\rho}^H(l_2)\boldsymbol{\Sigma}^{-\frac{1}{2}}\frac{\partial\boldsymbol{b}\left(\boldsymbol{\theta},l_2\right)}{\partial\left[\boldsymbol{\mu}\right]_j}\\
&+\boldsymbol{\rho}^H(l_1)\boldsymbol{\Sigma}^{-\frac{1}{2}}\frac{\partial\boldsymbol{b}\left(\boldsymbol{\theta},l_1\right)}{\partial\left[\boldsymbol{\mu}\right]_i}\frac{\partial\boldsymbol{b}^H\left(\boldsymbol{\theta},l_2\right)}{\partial\left[\boldsymbol{\mu}\right]_j}\boldsymbol{\Sigma}^{-\frac{1}{2}}\boldsymbol{\rho}(l_2)\\
&+\frac{\partial\boldsymbol{b}^H\left(\boldsymbol{\theta},l_1\right)}{\partial\left[\boldsymbol{\mu}\right]_i}\boldsymbol{\Sigma}^{-\frac{1}{2}}\boldsymbol{\rho}(l_1)\boldsymbol{\rho}^H(l_2)\boldsymbol{\Sigma}^{-\frac{1}{2}}\frac{\partial\boldsymbol{b}\left(\boldsymbol{\theta},l_2\right)}{\partial\left[\boldsymbol{\mu}\right]_j}\\
&+\frac{\partial\boldsymbol{b}^H\left(\boldsymbol{\theta},l_1\right)}{\partial\left[\boldsymbol{\mu}\right]_i}\boldsymbol{\Sigma}^{-\frac{1}{2}}\boldsymbol{\rho}(l_1)\frac{\partial\boldsymbol{b}^H\left(\boldsymbol{\theta},l_2\right)}{\partial\left[\boldsymbol{\mu}\right]_j}\boldsymbol{\Sigma}^{-\frac{1}{2}}\boldsymbol{\rho}(l_2)\Bigg)\Bigg\}
\end{aligned}$$

$$
\begin{aligned}
&= \mathrm{E}_{\|\boldsymbol{\rho}(l)\|}\Bigg\{ \sum_{l=0}^{L-1} h_{MN}^2\left(\|\boldsymbol{\rho}(l)\|^2, a, b\right)\|\boldsymbol{\rho}(l)\|^2 \\
&\cdot \mathrm{E}_{\boldsymbol{\rho}(l)\left|\right.\|\boldsymbol{\rho}(l)\|}\Bigg\{\Bigg(\frac{\boldsymbol{\rho}^H(l)}{\|\boldsymbol{\rho}(l)\|}\boldsymbol{\Sigma}^{-\frac{1}{2}}\frac{\partial \boldsymbol{b}\left(\boldsymbol{\theta},l\right)}{\partial\left[\boldsymbol{\mu}\right]_i}\frac{\boldsymbol{\rho}^H(l)}{\|\boldsymbol{\rho}(l)\|}\boldsymbol{\Sigma}^{-\frac{1}{2}}\frac{\partial \boldsymbol{b}\left(\boldsymbol{\theta},l\right)}{\partial\left[\boldsymbol{\mu}\right]_j} \\
&+\frac{\boldsymbol{\rho}^H(l)}{\|\boldsymbol{\rho}(l)\|}\boldsymbol{\Sigma}^{-\frac{1}{2}}\frac{\partial \boldsymbol{b}\left(\boldsymbol{\theta},l\right)}{\partial\left[\boldsymbol{\mu}\right]_i}\frac{\partial \boldsymbol{b}^H\left(\boldsymbol{\theta},l\right)}{\partial\left[\boldsymbol{\mu}\right]_j}\boldsymbol{\Sigma}^{-\frac{1}{2}}\frac{\boldsymbol{\rho}(l)}{\|\boldsymbol{\rho}(l)\|} \\
&+\frac{\partial \boldsymbol{b}^H\left(\boldsymbol{\theta},l\right)}{\partial\left[\boldsymbol{\mu}\right]_i}\boldsymbol{\Sigma}^{-\frac{1}{2}}\frac{\boldsymbol{\rho}(l)}{\|\boldsymbol{\rho}(l)\|}\frac{\boldsymbol{\rho}^H(l)}{\|\boldsymbol{\rho}(l)\|}\boldsymbol{\Sigma}^{-\frac{1}{2}}\frac{\partial \boldsymbol{b}\left(\boldsymbol{\theta},l\right)}{\partial\left[\boldsymbol{\mu}\right]_j} \\
&+\frac{\partial \boldsymbol{b}^H\left(\boldsymbol{\theta},l\right)}{\partial\left[\boldsymbol{\mu}\right]_i}\boldsymbol{\Sigma}^{-\frac{1}{2}}\frac{\boldsymbol{\rho}(l)}{\|\boldsymbol{\rho}(l)\|}\frac{\partial \boldsymbol{b}^H\left(\boldsymbol{\theta},l\right)}{\partial\left[\boldsymbol{\mu}\right]_j}\boldsymbol{\Sigma}^{-\frac{1}{2}}\frac{\boldsymbol{\rho}(l)}{\|\boldsymbol{\rho}(l)\|}\Bigg)\Bigg\}\Bigg\} \\
&+\mathrm{E}_{\|\boldsymbol{\rho}(l_1)\|,\|\boldsymbol{\rho}(l_2)\|}\Bigg\{\sum_{l_1=0}^{L-1}\sum_{l_2=1,l_2\neq l_1}^{L-1} h_{MN}\left(\|\boldsymbol{\rho}(l_1)\|^2, a, b\right) \\
&\cdot h_{MN}\left(\|\boldsymbol{\rho}(l_2)\|^2, a, b\right)\|\boldsymbol{\rho}(l_1)\|\,\|\boldsymbol{\rho}(l_2)\| \\
&\cdot \mathrm{E}_{\boldsymbol{\rho}(l_1),\boldsymbol{\rho}(l_2)\left|\right.\|\boldsymbol{\rho}(l_1)\|,\|\boldsymbol{\rho}(l_2)\|}\Bigg\{\Bigg(\frac{\boldsymbol{\rho}^H(l_1)}{\|\boldsymbol{\rho}(l_1)\|}\boldsymbol{\Sigma}^{-\frac{1}{2}}\frac{\partial \boldsymbol{b}\left(\boldsymbol{\theta},l_1\right)}{\partial\left[\boldsymbol{\mu}\right]_i}\frac{\boldsymbol{\rho}^H(l_2)}{\|\boldsymbol{\rho}(l_2)\|}\boldsymbol{\Sigma}^{-\frac{1}{2}}\frac{\partial \boldsymbol{b}\left(\boldsymbol{\theta},l_2\right)}{\partial\left[\boldsymbol{\mu}\right]_j} \\
&+\frac{\boldsymbol{\rho}^H(l_1)}{\|\boldsymbol{\rho}(l_1)\|}\boldsymbol{\Sigma}^{-\frac{1}{2}}\frac{\partial \boldsymbol{b}\left(\boldsymbol{\theta},l_1\right)}{\partial\left[\boldsymbol{\mu}\right]_i}\frac{\partial \boldsymbol{b}^H\left(\boldsymbol{\theta},l_2\right)}{\partial\left[\boldsymbol{\mu}\right]_j}\boldsymbol{\Sigma}^{-\frac{1}{2}}\frac{\boldsymbol{\rho}(l_2)}{\|\boldsymbol{\rho}(l_2)\|} \\
&+\frac{\partial \boldsymbol{b}^H\left(\boldsymbol{\theta},l_1\right)}{\partial\left[\boldsymbol{\mu}\right]_i}\boldsymbol{\Sigma}^{-\frac{1}{2}}\frac{\boldsymbol{\rho}(l_1)}{\|\boldsymbol{\rho}(l_1)\|}\frac{\boldsymbol{\rho}^H(l_2)}{\|\boldsymbol{\rho}(l_2)\|}\boldsymbol{\Sigma}^{-\frac{1}{2}}\frac{\partial \boldsymbol{b}\left(\boldsymbol{\theta},l_2\right)}{\partial\left[\boldsymbol{\mu}\right]_j} \\
&+\frac{\partial \boldsymbol{b}^H\left(\boldsymbol{\theta},l_1\right)}{\partial\left[\boldsymbol{\mu}\right]_i}\boldsymbol{\Sigma}^{-\frac{1}{2}}\frac{\boldsymbol{\rho}(l_1)}{\|\boldsymbol{\rho}(l_1)\|}\frac{\partial \boldsymbol{b}^H\left(\boldsymbol{\theta},l_2\right)}{\partial\left[\boldsymbol{\mu}\right]_j}\boldsymbol{\Sigma}^{-\frac{1}{2}}\frac{\boldsymbol{\rho}(l_2)}{\|\boldsymbol{\rho}(l_2)\|}\Bigg)\Bigg\}\Bigg\}, \\
&i,j=1,\ldots,2K(L+1).
\end{aligned}
\tag{6.5}
$$

By utilizing the speckle property in Eq. (2.16), namely, that:

$$
\mathrm{E}\left\{\boldsymbol{x}(i)\boldsymbol{x}^T(j)\right\} = \mathbf{0}_{MN\times MN}, \quad i,j=0,\ldots,L-1, \tag{6.6}
$$

and noticing that $\left(\partial \boldsymbol{b}^H(\boldsymbol{\theta},l)/\partial[\boldsymbol{\mu}]_j\right)\boldsymbol{\Sigma}^{-\frac{1}{2}}(\boldsymbol{\rho}(l)/\|\boldsymbol{\rho}(l)\|)$ is a scaler, one further has:

$$\begin{aligned}
&\mathrm{E}_{\boldsymbol{\rho}(l)\left|\|\boldsymbol{\rho}(l)\|\right.}\left\{\frac{\partial \boldsymbol{b}^H(\boldsymbol{\theta},l)}{\partial[\boldsymbol{\mu}]_i}\boldsymbol{\Sigma}^{-\frac{1}{2}}\frac{\boldsymbol{\rho}(l)}{\|\boldsymbol{\rho}(l)\|}\frac{\partial \boldsymbol{b}^H(\boldsymbol{\theta},l)}{\partial[\boldsymbol{\mu}]_j}\boldsymbol{\Sigma}^{-\frac{1}{2}}\frac{\boldsymbol{\rho}(l)}{\|\boldsymbol{\rho}(l)\|}\right\}\\
=&\mathrm{E}_{\boldsymbol{\rho}(l)\left|\|\boldsymbol{\rho}(l)\|\right.}\left\{\frac{\partial \boldsymbol{b}^H(\boldsymbol{\theta},l)}{\partial[\boldsymbol{\mu}]_i}\boldsymbol{\Sigma}^{-\frac{1}{2}}\frac{\boldsymbol{\rho}(l)}{\|\boldsymbol{\rho}(l)\|}\left(\frac{\partial \boldsymbol{b}^H(\boldsymbol{\theta},l)}{\partial[\boldsymbol{\mu}]_j}\boldsymbol{\Sigma}^{-\frac{1}{2}}\frac{\boldsymbol{\rho}(l)}{\|\boldsymbol{\rho}(l)\|}\right)^T\right\}\\
=&\frac{1}{\|\boldsymbol{\rho}(l)\|^2}\frac{\partial \boldsymbol{b}^H(\boldsymbol{\theta},l)}{\partial[\boldsymbol{\mu}]_i}\boldsymbol{\Sigma}^{-\frac{1}{2}}\mathrm{E}_{\boldsymbol{\rho}(l)\left|\|\boldsymbol{\rho}(l)\|\right.}\left\{\boldsymbol{\rho}(l)\boldsymbol{\rho}^T(l)\right\}\left(\boldsymbol{\Sigma}^{-\frac{1}{2}}\right)^T\frac{\partial \boldsymbol{b}^*(\boldsymbol{\theta},l)}{\partial[\boldsymbol{\mu}]_i}\\
=&0,
\end{aligned}\tag{6.7}$$

and moreover, that:

$$\begin{aligned}
&\mathrm{E}_{\boldsymbol{\rho}(l)\left|\|\boldsymbol{\rho}(l)\|\right.}\left\{\frac{\boldsymbol{\rho}^H(l)}{\|\boldsymbol{\rho}(l)\|}\boldsymbol{\Sigma}^{-\frac{1}{2}}\frac{\partial \boldsymbol{b}(\boldsymbol{\theta},l)}{\partial[\boldsymbol{\mu}]_i}\frac{\boldsymbol{\rho}^H(l)}{\|\boldsymbol{\rho}(l)\|}\boldsymbol{\Sigma}^{-\frac{1}{2}}\frac{\partial \boldsymbol{b}(\boldsymbol{\theta},l)}{\partial[\boldsymbol{\mu}]_j}\right.\\
=&\mathrm{E}_{\boldsymbol{\rho}(l)\left|\|\boldsymbol{\rho}(l)\|\right.}\left\{\left(\frac{\partial \boldsymbol{b}^H(\boldsymbol{\theta},l)}{\partial[\boldsymbol{\mu}]_i}\boldsymbol{\Sigma}^{-\frac{1}{2}}\frac{\boldsymbol{\rho}(l)}{\|\boldsymbol{\rho}(l)\|}\frac{\partial \boldsymbol{b}^H(\boldsymbol{\theta},l)}{\partial[\boldsymbol{\mu}]_j}\boldsymbol{\Sigma}^{-\frac{1}{2}}\frac{\boldsymbol{\rho}(l)}{\|\boldsymbol{\rho}(l)\|}\right)^*\right\}\\
=&0.
\end{aligned}\tag{6.8}$$

By following a similar procedure to that above, it can be further obtained, in parallel to Eqs. (6.7) and (6.8), that:

$$\begin{aligned}
&\mathrm{E}_{\boldsymbol{\rho}(l_1),\boldsymbol{\rho}(l_2)\left|\|\boldsymbol{\rho}(l_1)\|,\|\boldsymbol{\rho}(l_2)\|\right.}\left\{\frac{\boldsymbol{\rho}^H(l_1)}{\|\boldsymbol{\rho}(l_1)\|}\boldsymbol{\Sigma}^{-\frac{1}{2}}\frac{\partial \boldsymbol{b}(\boldsymbol{\theta},l_1)}{\partial[\boldsymbol{\mu}]_i}\frac{\boldsymbol{\rho}^H(l_2)}{\|\boldsymbol{\rho}(l_2)\|}\boldsymbol{\Sigma}^{-\frac{1}{2}}\frac{\partial \boldsymbol{b}(\boldsymbol{\theta},l_2)}{\partial[\boldsymbol{\mu}]_j}\right\}\\
=&\mathrm{E}_{\boldsymbol{\rho}(l_1),\boldsymbol{\rho}(l_2)\left|\|\boldsymbol{\rho}(l_1)\|,\|\boldsymbol{\rho}(l_2)\|\right.}\left\{\left(\frac{\partial \boldsymbol{b}^H(\boldsymbol{\theta},l_1)}{\partial[\boldsymbol{\mu}]_i}\boldsymbol{\Sigma}^{-\frac{1}{2}}\frac{\boldsymbol{\rho}(l_1)}{\|\boldsymbol{\rho}(l_1)\|}\frac{\partial \boldsymbol{b}^H(\boldsymbol{\theta},l_2)}{\partial[\boldsymbol{\mu}]_j}\boldsymbol{\Sigma}^{-\frac{1}{2}}\frac{\boldsymbol{\rho}(l_2)}{\|\boldsymbol{\rho}(l_2)\|}\right)^*\right\}\\
=&0.
\end{aligned}\tag{6.9}$$

Inserting Eqs. (6.7), (6.8) and 6.9 into Eq. (6.5), the latter is reduced to:

$$\begin{aligned}
[\boldsymbol{F}]_{i,j}=&\mathrm{E}_{\|\boldsymbol{\rho}(l)\|}\left\{\sum_{l=0}^{L-1}h_{MN}^2\left(\|\boldsymbol{\rho}(l)\|^2,a,b\right)\|\boldsymbol{\rho}(l)\|^2\right.\\
&\cdot\mathrm{E}_{\boldsymbol{\rho}(l)\left|\|\boldsymbol{\rho}(l)\|\right.}\left\{\left(\frac{\boldsymbol{\rho}^H(l)}{\|\boldsymbol{\rho}(l)\|}\boldsymbol{\Sigma}^{-\frac{1}{2}}\frac{\partial \boldsymbol{b}(\boldsymbol{\theta},l)}{\partial[\boldsymbol{\mu}]_i}\frac{\partial \boldsymbol{b}^H(\boldsymbol{\theta},l)}{\partial[\boldsymbol{\mu}]_j}\boldsymbol{\Sigma}^{-\frac{1}{2}}\frac{\boldsymbol{\rho}(l)}{\|\boldsymbol{\rho}(l)\|}\right.\right.\\
&\left.\left.\left.+\frac{\partial \boldsymbol{b}^H(\boldsymbol{\theta},l)}{\partial[\boldsymbol{\mu}]_i}\boldsymbol{\Sigma}^{-\frac{1}{2}}\frac{\boldsymbol{\rho}(l)}{\|\boldsymbol{\rho}(l)\|}\frac{\boldsymbol{\rho}^H(l)}{\|\boldsymbol{\rho}(l)\|}\boldsymbol{\Sigma}^{-\frac{1}{2}}\frac{\partial \boldsymbol{b}(\boldsymbol{\theta},l)}{\partial[\boldsymbol{\mu}]_j}\right)\right\}\right\}
\end{aligned}$$

$$
\begin{aligned}
&+\mathrm{E}_{\|\boldsymbol{\rho}(l_1)\|,\|\boldsymbol{\rho}(l_2)\|}\Bigg\{\sum_{l_1=0}^{L-1}\sum_{l_2=1,l_2\neq l_1}^{L-1} h_{MN}\left(\|\boldsymbol{\rho}(l_1)\|^2,a,b\right)\\
&\cdot h_{MN}\left(\|\boldsymbol{\rho}(l_2)\|^2,a,b\right)\|\boldsymbol{\rho}(l_1)\|\,\|\boldsymbol{\rho}(l_2)\|\\
&\cdot\mathrm{E}_{\boldsymbol{\rho}(l_1),\boldsymbol{\rho}(l_2)\left|\right.\|\boldsymbol{\rho}(l_1)\|,\|\boldsymbol{\rho}(l_2)\|}\Bigg\{\Bigg(\frac{\boldsymbol{\rho}^H(l_1)}{\|\boldsymbol{\rho}(l_1)\|}\boldsymbol{\Sigma}^{-\frac{1}{2}}\frac{\partial\boldsymbol{b}\left(\boldsymbol{\theta},l_1\right)}{\partial\left[\boldsymbol{\mu}\right]_i}\frac{\partial\boldsymbol{b}^H\left(\boldsymbol{\theta},l_2\right)}{\partial\left[\boldsymbol{\mu}\right]_j}\boldsymbol{\Sigma}^{-\frac{1}{2}}\frac{\boldsymbol{\rho}(l_2)}{\|\boldsymbol{\rho}(l_2)\|}\\
&+\frac{\partial\boldsymbol{b}^H\left(\boldsymbol{\theta},l_1\right)}{\partial\left[\boldsymbol{\mu}\right]_i}\boldsymbol{\Sigma}^{-\frac{1}{2}}\frac{\boldsymbol{\rho}(l_1)}{\|\boldsymbol{\rho}(l_1)\|}\frac{\boldsymbol{\rho}^H(l_2)}{\|\boldsymbol{\rho}(l_2)\|}\boldsymbol{\Sigma}^{-\frac{1}{2}}\frac{\partial\boldsymbol{b}\left(\boldsymbol{\theta},l_2\right)}{\partial\left[\boldsymbol{\mu}\right]_j}\Bigg)\Bigg\}\Bigg\}.\\
=&\,\mathrm{E}_{\|\boldsymbol{\rho}(l)\|}\Bigg\{\sum_{l=0}^{L-1}h_{MN}^2\left(\|\boldsymbol{\rho}(l)\|^2,a,b\right)\|\boldsymbol{\rho}(l)\|^2\\
&\cdot 2\mathrm{Re}\Bigg\{\mathrm{E}_{\boldsymbol{\rho}(l)\left|\right.\|\boldsymbol{\rho}(l)\|}\Bigg\{\frac{\boldsymbol{\rho}^H(l)}{\|\boldsymbol{\rho}(l)\|}\boldsymbol{\Sigma}^{-\frac{1}{2}}\frac{\partial\boldsymbol{b}\left(\boldsymbol{\theta},l\right)}{\partial\left[\boldsymbol{\mu}\right]_i}\frac{\partial\boldsymbol{b}^H\left(\boldsymbol{\theta},l\right)}{\partial\left[\boldsymbol{\mu}\right]_j}\boldsymbol{\Sigma}^{-\frac{1}{2}}\frac{\boldsymbol{\rho}(l)}{\|\boldsymbol{\rho}(l)\|}\Bigg\}\Bigg\}\\
&+\mathrm{E}_{\|\boldsymbol{\rho}(l_1)\|,\|\boldsymbol{\rho}(l_2)\|}\Bigg\{\sum_{l_1=0}^{L-1}\sum_{l_2=1,l_2\neq l_1}^{L-1} h_{MN}\left(\|\boldsymbol{\rho}(l_1)\|^2,a,b\right)\\
&\cdot h_{MN}\left(\|\boldsymbol{\rho}(l_2)\|^2,a,b\right)\|\boldsymbol{\rho}(l_1)\|\,\|\boldsymbol{\rho}(l_2)\|\\
&\cdot 2\mathrm{Re}\Bigg\{\mathrm{E}_{\boldsymbol{\rho}(l_1),\boldsymbol{\rho}(l_2)\left|\right.\|\boldsymbol{\rho}(l_1)\|,\|\boldsymbol{\rho}(l_2)\|}\Bigg\{\frac{\boldsymbol{\rho}^H(l_1)}{\|\boldsymbol{\rho}(l_1)\|}\boldsymbol{\Sigma}^{-\frac{1}{2}}\frac{\partial\boldsymbol{b}\left(\boldsymbol{\theta},l_1\right)}{\partial\left[\boldsymbol{\mu}\right]_i}\\
&\frac{\partial\boldsymbol{b}^H\left(\boldsymbol{\theta},l_2\right)}{\partial\left[\boldsymbol{\mu}\right]_j}\boldsymbol{\Sigma}^{-\frac{1}{2}}\frac{\boldsymbol{\rho}(l_2)}{\|\boldsymbol{\rho}(l_2)\|}\Bigg\}\Bigg\},\quad i,j=1,\ldots,2K(L+1).
\end{aligned}
\tag{6.10}
$$

The equality in the last step of Eq. (6.10) is obtained by noticing that:

$$
\begin{aligned}
&\frac{\partial\boldsymbol{b}^H\left(\boldsymbol{\theta},l\right)}{\partial\left[\boldsymbol{\mu}\right]_i}\boldsymbol{\Sigma}^{-\frac{1}{2}}\frac{\boldsymbol{\rho}(l)}{\|\boldsymbol{\rho}(l)\|}\frac{\boldsymbol{\rho}^H(l)}{\|\boldsymbol{\rho}(l)\|}\boldsymbol{\Sigma}^{-\frac{1}{2}}\frac{\partial\boldsymbol{b}\left(\boldsymbol{\theta},l\right)}{\partial\left[\boldsymbol{\mu}\right]_j}\\
&=\left(\frac{\boldsymbol{\rho}^H(l)}{\|\boldsymbol{\rho}(l)\|}\boldsymbol{\Sigma}^{-\frac{1}{2}}\frac{\partial\boldsymbol{b}\left(\boldsymbol{\theta},l\right)}{\partial\left[\boldsymbol{\mu}\right]_i}\frac{\partial\boldsymbol{b}^H\left(\boldsymbol{\theta},l\right)}{\partial\left[\boldsymbol{\mu}\right]_j}\boldsymbol{\Sigma}^{-\frac{1}{2}}\frac{\boldsymbol{\rho}(l)}{\|\boldsymbol{\rho}(l)\|}\right)^*,
\end{aligned}
\tag{6.11}
$$

and

$$
\begin{aligned}
&\frac{\partial\boldsymbol{b}^H\left(\boldsymbol{\theta},l_1\right)}{\partial\left[\boldsymbol{\mu}\right]_i}\boldsymbol{\Sigma}^{-\frac{1}{2}}\frac{\boldsymbol{\rho}(l_1)}{\|\boldsymbol{\rho}(l_1)\|}\frac{\boldsymbol{\rho}^H(l_2)}{\|\boldsymbol{\rho}(l_2)\|}\boldsymbol{\Sigma}^{-\frac{1}{2}}\frac{\partial\boldsymbol{b}\left(\boldsymbol{\theta},l_2\right)}{\partial\left[\boldsymbol{\mu}\right]_j}\\
&=\left(\frac{\boldsymbol{\rho}^H(l_1)}{\|\boldsymbol{\rho}(l_1)\|}\boldsymbol{\Sigma}^{-\frac{1}{2}}\frac{\partial\boldsymbol{b}\left(\boldsymbol{\theta},l_1\right)}{\partial\left[\boldsymbol{\mu}\right]_i}\frac{\partial\boldsymbol{b}^H\left(\boldsymbol{\theta},l_2\right)}{\partial\left[\boldsymbol{\mu}\right]_j}\boldsymbol{\Sigma}^{-\frac{1}{2}}\frac{\boldsymbol{\rho}(l_2)}{\|\boldsymbol{\rho}(l_2)\|}\right)^*.
\end{aligned}
\tag{6.12}
$$

Finally, by applying Lemmata 2 and 3 in [98] (cf. (B.36) & (B.38), ibid.) to Eq. (6.10),

the latter can be further transformed into:

$$\begin{aligned}[\boldsymbol{F}]_{i,j} =& \mathrm{E}_{\|\boldsymbol{\rho}(l)\|}\Bigg\{\sum_{l=0}^{L-1} h_{MN}^2\left(\|\boldsymbol{\rho}(l)\|^2, a, b\right)\|\boldsymbol{\rho}(l)\|^2 \\ &\cdot 2\mathrm{Re}\Bigg\{\mathrm{tr}\Bigg\{\boldsymbol{\Sigma}^{-\frac{1}{2}}\frac{\partial \boldsymbol{b}\left(\boldsymbol{\theta},l\right)}{\partial\left[\boldsymbol{\mu}\right]_i}\frac{\partial \boldsymbol{b}^H\left(\boldsymbol{\theta},l\right)}{\partial\left[\boldsymbol{\mu}\right]_j}\boldsymbol{\Sigma}^{-\frac{1}{2}}\Bigg\}\Bigg\} \\ =& \frac{2\kappa(MN,a,b)}{L}\mathrm{Re}\Bigg\{\mathrm{tr}\left\{\frac{\partial \boldsymbol{b}^H\left(\boldsymbol{\theta},l\right)}{\partial\left[\boldsymbol{\mu}\right]_i}\boldsymbol{\Sigma}^{-1}\frac{\partial \boldsymbol{b}\left(\boldsymbol{\theta},l\right)}{\partial\left[\boldsymbol{\mu}\right]_j}\right\}, \quad i,j=1,\ldots,2K(L+1).\end{aligned} \tag{6.13}$$

in which

$$\kappa(MN,a,b) = \mathrm{E}_{\|\boldsymbol{\rho}(l)\|}\left\{\sum_{l=0}^{L-1} h_{MN}^2\left(\|\boldsymbol{\rho}(l)\|^2, a, b\right)\|\boldsymbol{\rho}(l)\|^2\right\}. \tag{6.14}$$

6.1.3 The Expression of $\kappa(MN,a,b)$

The expression of the factor $\kappa(MN,a,b)$ can be obtained by applying Eqs. (C.48) and (C.49) in [98] to Eq. (6.14) and transforming the latter into:

$$\kappa(MN,a,b) = \frac{\int_0^{+\infty} h_{MN}^2\left(\|\boldsymbol{\rho}(l)\|^2, a, b\right) g_{MN}\left(\|\boldsymbol{\rho}(l)\|^2, a, b\right)\|\boldsymbol{\rho}(l)\|^{2MN+1}\,\mathrm{d}\,\|\boldsymbol{\rho}(l)\|}{\int_0^{+\infty} g_{MN}\left(\|\boldsymbol{\rho}(l)\|^2, a, b\right)\|\boldsymbol{\rho}(l)\|^{2MN-1}\,\mathrm{d}\,\|\boldsymbol{\rho}(l)\|}, \tag{6.15}$$

into which one then substitutes the expressions of $h_{MN}\left(\|\boldsymbol{\rho}(l)\|^2, a, b\right)$ and $g_{MN}\left(\|\boldsymbol{\rho}(l)\|^2, a, b\right)$ in Eqs. (5.2), and (5.1), respectively, leading to:

$$\kappa(MN,a,b) = \begin{cases} \dfrac{\int_0^{+\infty} x^{MN+a-1}\frac{K_{a-MN-1}^2(x)}{K_{a-MN}(x)}\mathrm{d}x}{2^{MN+a-2}b\Gamma(MN)\Gamma(a)}, & \text{K-distributed clutter,} \\ \dfrac{MNa(a+MN)}{b(a+MN+1)}, & \text{Student's t-distributed clutter.} \end{cases} \tag{6.16}$$

in which $K_n(x)$ is the modified Bessel functions of the second kind of order n.

Note that, for Student's t-distributed clutter, Eq. (6.16) is a generalization of the result in [98] to the two texture parameter case. For K-distributed clutter, Eq. (6.16) offers a more compact expression of $\kappa(MN,a,b)$ than [98].

From Eq. (6.16) it is clear that the factor $\kappa(MN,a,b)$ for K-distributed clutter, which takes the form of integration of Bessel functions, has no close-form expression, and can only

be evaluated numerically. One approach to its calculation is to use the generalized Gauss-Laguerre quadrature [98,127,128], transforming its expression for K-distributed clutter into:

$$\kappa(MN,a,b)=\frac{\sum_{o_1=1}^{O_1^{(2MN+1)}}\frac{\left(\sum_{o_2=1}^{O_2^{(a-1)}}\exp\left(-\frac{x_{o_1}^2}{x_{o_2}b}\right)\frac{1}{b}x_{o_2}^{-(MN+1)}w_{o_2}\right)^2}{\sum_{o_3=1}^{O_3^{(a-1)}}\exp\left(-\frac{x_{o_1}^2}{x_{o_3}b}\right)x_{o_3}^{-MN}w_{o_3}}e^{x_{o_1}}w_{o_1}}{\sum_{o_4=1}^{O_4^{(2MN-1)}}\left(\sum_{o_5=1}^{O_5^{(a-1)}}\exp\left(-\frac{x_{o_4}^2}{x_{o_5}b}\right)x_{o_5}^{-MN}w_{o_5}\right)e^{x_{o_4}}w_{o_4}}, \tag{6.17}$$

where $x_{o_i},\ i=1,\ldots,5$, and $w_{o_i},\ i=1,\ldots,5$, represent the abscissae and the weights of the generalized Gauss-Laguerre quadrature, respectively; $O_1^{(2MN+1)}$, $O_2^{(a-1)}$, etc., denote the quadrature orders; with the subscript of each representing the respective parameter of the corresponding abscissa and weight (e.g., $O_1^{(2MN+1)}$ means that x_{o_1} and w_{o_1} have $2MN+1$ as their parameter). The values of these quadrature orders can be empirically chosen. Generally speaking, a value around 160 for all of them is enough for the calculation.

6.1.4 The Expression of the CRB

To obtain the final expression of **CRB** $(\boldsymbol{\theta})$, one has further to determine the expression of the remaining entries of $\boldsymbol{F}$. For succinct documentation, introduce the $(M^2N^2+2)\times 1$ clutter parameter vector:

$$\boldsymbol{\varpi}=\left[\boldsymbol{\zeta}^T,a,b\right]^T. \tag{6.18}$$

First, one explores the values of the FIM cross-term entries between the signal parameter vector $\boldsymbol{\mu}$ and clutter parameter vector $\boldsymbol{\varpi}$.

It is clear from Eq. (6.3a) that, for any $l=0,\ldots,L-1$, and with a fixed $\|\boldsymbol{\rho}(l)\|$,

$$\frac{\partial\Lambda_{\mathrm{M}}}{\partial\left[\boldsymbol{\mu}\right]_i},\quad i=1,\ldots,2K(L+1), \tag{6.19}$$

are *odd* functions of $\boldsymbol{\rho}(l)$, whereas

$$\frac{\partial\Lambda_{\mathrm{M}}}{\partial\left[\boldsymbol{\varpi}\right]_j},\quad j=1,\ldots,M^2N^2+2, \tag{6.20}$$

are, as can be observed from Eqs. (6.3b), (5.5) and (5.6), *even* functions of $\boldsymbol{\rho}(l)$.

As a result,

$$\begin{aligned} &\frac{\partial \Lambda_{\mathrm{M}}}{\partial \left[\boldsymbol{\mu}\right]_i}\frac{\partial \Lambda_{\mathrm{M}}}{\partial \left[\boldsymbol{\varpi}\right]_j}, \\ &i=1,\ldots,2K(L+1), \quad j=1,\ldots,M^2N^2+2, \end{aligned} \tag{6.21}$$

are even functions of $\boldsymbol{\rho}(l)$, hence:

$$\begin{aligned} &\mathrm{E}\left\{\frac{\partial \Lambda_{\mathrm{M}}}{\partial \left[\boldsymbol{\mu}\right]_i}\frac{\partial \Lambda_{\mathrm{M}}}{\partial \left[\boldsymbol{\varpi}\right]_j}\right\} \\ =&\mathrm{E}_{\|\boldsymbol{\rho}(l)\|}\left\{\mathrm{E}_{\boldsymbol{\rho}(l)\left|\right.\|\boldsymbol{\rho}(l)\|}\left\{\frac{\partial \Lambda_{\mathrm{M}}}{\partial \left[\boldsymbol{\mu}\right]_i}\frac{\partial \Lambda_{\mathrm{M}}}{\partial \left[\boldsymbol{\varpi}\right]_j}\right\}\right\} \\ =&0, \end{aligned} \tag{6.22}$$

which reveals that $\boldsymbol{F}$ has the following *block-diagonal* structure:

$$\boldsymbol{F}=\begin{bmatrix} \boldsymbol{\Phi} & \mathbf{0}_{2K(L+1)\times(M^2N^2+2)} \\ \mathbf{0}_{2K(L+1)\times(M^2N^2+2)} & \boldsymbol{\Xi} \end{bmatrix}, \tag{6.23}$$

in which $\boldsymbol{\Phi}$ denotes the $2K(L+1)\times 2K(L+1)$ FIM block w.r.t. the signal parameter vector $\boldsymbol{\mu}$, whose entries, denoted by ϕ_{ij}, are given by:

$$\begin{aligned} \phi_{ij}=&\frac{2\kappa(MN,a,b)}{MN}\sum_{l=0}^{L-1}\mathrm{Re}\left\{\frac{\partial \boldsymbol{b}^H(\boldsymbol{\theta},l)}{\partial \left[\boldsymbol{\mu}\right]_i}\boldsymbol{\Sigma}^{-1}\frac{\partial \boldsymbol{b}(\boldsymbol{\theta},l)}{\partial \left[\boldsymbol{\mu}\right]_j}\right\}, \\ &i,j=1,\ldots,2K(L+1). \end{aligned} \tag{6.24}$$

The matrix $\boldsymbol{\Xi}$ in Eq. (6.23) represents the FIM block w.r.t. the clutter parameter vector $\boldsymbol{\varpi}$. Since the FIM blocks $\boldsymbol{\Phi}$ and $\boldsymbol{\Xi}$ are decoupled from each other (meaning that the achievable performance for the estimation of $\boldsymbol{\Xi}$ and of $\boldsymbol{\varpi}$ and independent from each other), the concrete expressions for the entries of $\boldsymbol{\varpi}$ is not required for the purpose of obtain $\mathbf{CRB}(\boldsymbol{\theta})$, and one simply has:

$$\left[\mathbf{CRB}(\boldsymbol{\theta})\right]_{i,j}=\left[\boldsymbol{\Phi}^{-1}\right]_{i,j}, \quad i,j=1,\ldots,2K. \tag{6.25}$$

as the elementwise expression of $\mathbf{CRB}(\boldsymbol{\theta})$.

6.2 The Remaining Cramér-Rao-Type Bounds

In parallel to the derivation for **CRB** $(\boldsymbol{\theta})$ in Sec. 6.1, this section discusses the expressions for the remaining aforementioned CRTBs, including the EMCB, the MCB, the MCRB and the HCRB, for the DOD/DOA parameter vector $\boldsymbol{\theta}$, denoted by **EMCB** $(\boldsymbol{\theta})$, **MCB** $(\boldsymbol{\theta})$ **MCRB** $(\boldsymbol{\theta})$ and **HCRB** $(\boldsymbol{\theta})$, respectively.

6.2.1 The Extended Miller-Chang Bound

The EMCB was first proposed in [52] as an extension of the Miller-Chang Bound (MCB) [53]. Its general motivation is to first treat the random nuisance parameters (the texture $\boldsymbol{\tau}$, in the case under discussion) as *deterministic* but *unknown*, and to derive the CRB calculated from the conditional LL Λ_{C} in Eq. (3.1). Then in the next step, the assumption of deterministic $\boldsymbol{\tau}$ is relaxed and the previously obtained CRB is averaged over different realizations of $\boldsymbol{\tau}$ drawn from the corresponding random distribution.

This approach has in common with the proposed IMLE in Ch. 3 that the latter also treats $\boldsymbol{\tau}$ to be deterministic. The performance of this algorithm, in terms of the averaged MSE resulting from many independent Monte-Carlo trials, can be evaluated by averaging the CRBs calculated for each of the trials. It is clear that such an averaged CRB, when the trial number becomes large, approaches the EMCB.

Calculation of the EMCB considers the $(2K(L+1)+M^2N^2+L)\times 1$ unknown parameter vector in the deterministic texture case:

$$\boldsymbol{\xi}_{\mathrm{det}} = \left[\boldsymbol{\psi}^T, \boldsymbol{\tau}^T\right]^T, \tag{6.26}$$

which incorporates the texture realization parameter vector $\boldsymbol{\tau}$ but leaves out the texture parameters a and b. The entries of the corresponding FIM, denoted by $\boldsymbol{F}_{\mathrm{EMC}}$, are calculated by:

$$\begin{aligned}\left[\boldsymbol{F}_{\mathrm{EMC}}\right]_{i,j} =& \mathrm{E}_{\boldsymbol{y}|\boldsymbol{\tau}}\left\{\frac{\partial\Lambda_{\mathrm{C}}}{\partial\left[\boldsymbol{\xi}_{\mathrm{det}}\right]_i}\frac{\partial\Lambda_{\mathrm{C}}}{\partial\left[\boldsymbol{\xi}_{\mathrm{det}}\right]_j}\right\},\\ & i,j = 1,\ldots,2K(L+1)+M^2N^2+L.\end{aligned} \tag{6.27}$$

Among the score functions involved in Eq. (6.27), those w.r.t. $[\boldsymbol{\mu}]_i,\ i=1,\ldots,2K(L+1)$, and $[\boldsymbol{\zeta}]_i,\ i=1,\ldots,M^2N^2$, are given above in Eqs. (6.3a) and (6.3b), respectively. The score functions w.r.t. $[\boldsymbol{\tau}]_i,\ i=1,\ldots,L$, i.e., those w.r.t. $\tau(l),\ l=0,\ldots,L-1$, can be calculated as:

$$\frac{\partial \Lambda_{\mathrm{C}}}{\partial \tau(l)} = -\frac{MN}{\tau(l)} + \frac{1}{\tau^2(l)} \left\|\boldsymbol{\rho}(l)\right\|^2, \quad l=0,\ldots,L-1. \tag{6.28}$$

Inserting Eqs. (6.3a), (6.3b) and (6.28) into Eq. (6.27), and noticing that Eq. (6.28) is also an even function of $\boldsymbol{\rho}(l)$, one arrives at the conclusion that, similar to the expression of $\boldsymbol{F}$ in Eq. (6.23), $\boldsymbol{F}_{\mathrm{EMC}}$ also exhibits a block-diagonal structure, where the block w.r.t. the signal parameter vector $\boldsymbol{\mu}$ is decoupled from the block w.r.t. the clutter parameter vector (in the deterministic texture case):

$$\boldsymbol{\varpi}_{\mathrm{det}} = \left[\boldsymbol{\zeta}^T, \boldsymbol{\tau}^T\right]^T. \tag{6.29}$$

Let $\boldsymbol{\Phi}_{\mathrm{EMC}}$ denote the block of $\boldsymbol{F}_{\mathrm{EMC}}$ w.r.t. $\boldsymbol{\mu}$, The entries of $\boldsymbol{\Phi}_{\mathrm{EMC}}$, represented by ϕ_{ij}^{EMC}, have the following expressions:

$$\begin{aligned} \phi_{ij}^{\mathrm{EMC}} =& 2\sum_{l=0}^{L-1} \frac{1}{\tau(l)} \mathrm{Re}\left\{ \frac{\partial \boldsymbol{b}^H(\boldsymbol{\theta},l)}{\partial [\boldsymbol{\mu}]_i} \boldsymbol{\Sigma}^{-1} \frac{\partial \boldsymbol{b}(\boldsymbol{\theta},l)}{\partial [\boldsymbol{\mu}]_j} \right\}, \\ & i,j=1,\ldots,2K(L+1). \end{aligned} \tag{6.30}$$

Consequently, $\mathbf{EMCB}(\boldsymbol{\theta})$ is given by:

$$\left[\mathbf{EMCB}(\boldsymbol{\theta})\right]_{i,j} = \left[\mathrm{E}_{\boldsymbol{\tau}}\left\{\boldsymbol{\Phi}_{\mathrm{EMC}}^{-1}\right\}\right]_{i,j}, \quad i,j=1,\ldots,2K. \tag{6.31}$$

for which no closed-form expression exists.

6.2.2 The Miller-Chang Bound

The MCB proposed in [53], like its generalized version, the EMCB, also consists in calculating the CRB based on the LL conditioned on the nuisance parameters modeled as deterministic, and then averaging the so obtained CRB over the nuisance parameters. It differs from the EMCB only in that it treats the nuisance parameter not only as deterministic but

also as *known*. Thus, the MCB considers the unknown parameters vector as $\boldsymbol{\psi}$, and its FIM, denoted by $\boldsymbol{F}_{\text{MC}}$, is calculated as:

$$\begin{aligned}\left[\boldsymbol{F}_{\text{MC}}\right]_{i,j} =& \mathrm{E}_{\boldsymbol{y}|\boldsymbol{\tau}}\left\{\frac{\partial \Lambda_{\text{C}}}{\partial\left[\boldsymbol{\psi}\right]_i}\frac{\partial \Lambda_{\text{C}}}{\partial\left[\boldsymbol{\psi}\right]_j}\right\}, \\ & i,j=1,\ldots,2K(L+1)+M^2N^2.\end{aligned} \tag{6.32}$$

From Eq. (6.32) it is easily seen that $\boldsymbol{F}_{\text{MC}}$ is equal to the $(2K(L+1)+M^2N^2)\times(2K(L+1)+M^2N^2)$ upper left-most block of the FIM for the EMCB, i.e.,:

$$\boldsymbol{F}_{\text{MC}} = \begin{bmatrix} \left[\boldsymbol{F}_{\text{EMC}}\right]_{1,1} & \cdots & \left[\boldsymbol{F}_{\text{EMC}}\right]_{1,2K(L+1)+M^2N^2} \\ \vdots & \ddots & \vdots \\ \left[\boldsymbol{F}_{\text{EMC}}\right]_{2K(L+1)+M^2N^2,1} & \cdots & \left[\boldsymbol{F}_{\text{EMC}}\right]_{2K(L+1)+M^2N^2,2K(L+1)+M^2N^2} \end{bmatrix}. \tag{6.33}$$

Thus, $\boldsymbol{F}_{\text{MC}}$ also has a block-diagonal structure, and its block w.r.t. the signal parameter vector $\boldsymbol{\mu}$, denoted by $\boldsymbol{\Phi}_{\text{MC}}$, is equal to $\boldsymbol{\Phi}_{\text{EMC}}$.

Generally speaking, it is proved in [52] that the EMCB is *greater than or equal to* the MCB. However, for the problem under discussion, due to the block-diagonal structure of the FIMs, it follows that:

$$\begin{aligned}&\left[\mathbf{MCB}\left(\boldsymbol{\theta}\right)\right]_{i,j} = \left[\mathrm{E}_{\boldsymbol{\tau}}\left\{\boldsymbol{F}_{\text{MC}}^{-1}\right\}\right]_{i,j} = \left[\mathrm{E}_{\boldsymbol{\tau}}\left\{\boldsymbol{\Phi}_{\text{MC}}^{-1}\right\}\right]_{i,j} \\ &= \left[\mathrm{E}_{\boldsymbol{\tau}}\left\{\boldsymbol{\Phi}_{\text{EMC}}^{-1}\right\}\right]_{i,j} = \left[\mathbf{EMCB}\left(\boldsymbol{\theta}\right)\right]_{i,j}, \quad i,j=1,\ldots,2K,\end{aligned} \tag{6.34}$$

namely, the two are equal w.r.t. the DOD/DOA parameter vector $\boldsymbol{\theta}$.

6.2.3 The Modified Cramér-Rao Bound

The MCRB [56, 57], like the MCB, also considers the unknown parameter vector as $\boldsymbol{\psi}$, namely, it models $\boldsymbol{\tau}$ as deterministic and known. Its corresponding FIM, denoted by $\boldsymbol{F}_{\text{M}}$, is likewise calculated from the conditional LL in Eq. (3.1). The MCRB differs from the MCB

only in that it averages over the random parameters before the FIM inversion, namely:

$$\begin{aligned}[\boldsymbol{F}_{\mathrm{M}}]_{i,j} =& \mathrm{E}_{\boldsymbol{y},\boldsymbol{\tau}}\left\{\frac{\partial\Lambda_{\mathrm{C}}}{\partial\left[\boldsymbol{\psi}\right]_i}\frac{\partial\Lambda_{\mathrm{C}}}{\partial\left[\boldsymbol{\psi}\right]_j}\right\}\\ =& \mathrm{E}_{\boldsymbol{\tau}}\left\{\mathrm{E}_{\boldsymbol{y}|\boldsymbol{\tau}}\left\{\frac{\partial\Lambda_{\mathrm{C}}}{\partial\left[\boldsymbol{\psi}\right]_i}\frac{\partial\Lambda_{\mathrm{C}}}{\partial\left[\boldsymbol{\psi}\right]_j}\right\}\right\}\\ =& \mathrm{E}_{\boldsymbol{\tau}}\left\{[\boldsymbol{F}_{\mathrm{MC}}]_{i,j}\right\},\\ & i,j=1,\ldots,2K(L+1)+M^2N^2.\end{aligned} \tag{6.35}$$

Similar to $\boldsymbol{F}$, $\boldsymbol{F}_{\mathrm{EMC}}$ and $\boldsymbol{F}_{\mathrm{MC}}$, the FIM $\boldsymbol{F}_{\mathrm{M}}$ in Eq. (6.35) also has a block-diagonal structure, whose block w.r.t. the signal parameter vector $\boldsymbol{\mu}$, denoted by $\boldsymbol{\Phi}_{\mathrm{M}}$, contains, according to Eq. (6.35), the following entries ϕ_{ij}^{M}:

$$\begin{aligned}\phi_{ij}^{\mathrm{M}} =& \mathrm{E}_{\boldsymbol{\tau}}\left\{\phi_{ij}^{\mathrm{EMC}}\right\}\\ =& 2\nu(a,b)\sum_{l=0}^{L-1}\mathrm{Re}\left\{\frac{\partial\boldsymbol{b}^H(\boldsymbol{\theta},l)}{\partial\left[\boldsymbol{\mu}\right]_i}\boldsymbol{\Sigma}^{-1}\frac{\partial\boldsymbol{b}(\boldsymbol{\theta},l)}{\partial\left[\boldsymbol{\mu}\right]_j}\right\},\\ & i,j=1,\ldots,2K(L+1),\end{aligned} \tag{6.36}$$

in which

$$\nu(a,b)=\mathrm{E}\left\{\frac{1}{\tau(l)}\right\}=\begin{cases}\dfrac{1}{b(a-1)}, & \text{K-distributed clutter, for } a>1,\\ \dfrac{a}{b}, & \text{Student's t-distributed clutter.}\end{cases} \tag{6.37}$$

Thus $\mathbf{MCRB}\left(\boldsymbol{\theta}\right)$ is given by:

$$\left[\mathbf{MCRB}\left(\boldsymbol{\theta}\right)\right]_{i,j}=\left[\boldsymbol{\Phi}_{\mathrm{M}}^{-1}\right]_{i,j},\quad i,j=1,\ldots,2K. \tag{6.38}$$

6.2.4 The Hybrid Cramér-Rao Bound

The HCRB as defined in [54], on the other hand, models the texture as random and considers the $(2K(L+1)+M^2N^2+L+2)\times 1$ hybrid unknown parameter vector:

$$\boldsymbol{\xi}_{\text{hyb}} = [\boldsymbol{\xi}^T, \boldsymbol{\tau}^T]^T, \tag{6.39}$$

where $\boldsymbol{\tau}$ is treated here as a random parameter vector that contains the i.i.d. random parameter $\tau(l)$ at all snapshots. $\boldsymbol{\xi}_{\text{hyb}}$ is called "hybrid" as it contains both deterministic and random parameters. Furthermore, the HCRB uses the joint LL in Eq. (4.2) to obtain its FIM, instead of the conditional LL in Eq. (3.1) that is used in the derivation of the EMCB, MCB and MCRB. It can be easily seen from the description above that the HCRB has the same spirit as the proposed IMAPE in Ch. 4.

Let $\boldsymbol{F}_{\text{H}}$ denote the FIM for the HCRB, of which the entries are calculated by:

$$\begin{aligned}[\boldsymbol{F}_{\text{H}}]_{i,j} =& \text{E}_{\boldsymbol{y},\boldsymbol{\tau}}\left\{\frac{\partial \Lambda_{\text{J}}}{\partial\left[\boldsymbol{\xi}_{\text{hyb}}\right]_i}\frac{\partial \Lambda_{\text{J}}}{\partial\left[\boldsymbol{\xi}_{\text{hyb}}\right]_j}\right\},\\ & i,j = 1,\ldots,2K(L+1)+M^2N^2+L+2.\end{aligned} \tag{6.40}$$

By substituting Eqs. (6.3a), (6.3b), (5.5), (5.6) and (6.28) into Eq. (6.40), one can find that $\boldsymbol{F}_{\text{H}}$ also has a block-diagonal structure, namely, its block w.r.t. $\boldsymbol{\mu}$, denoted by $\boldsymbol{\Phi}_{\text{H}}$, is decoupled from the block w.r.t. the augmented hybrid clutter parameter vector:

$$\boldsymbol{\varpi}_{\text{hyb}} = \left[\boldsymbol{\varpi}^T, \boldsymbol{\tau}^T\right]^T. \tag{6.41}$$

Furthermore, since:

$$\frac{\partial \Lambda_{\text{J}}}{\partial\left[\boldsymbol{\mu}\right]_i} = \frac{\partial \Lambda_{\text{C}}}{\partial\left[\boldsymbol{\mu}\right]_i}, \quad i = 1,\ldots,2K(L+1), \tag{6.42}$$

it holds that:

$$\boldsymbol{\Phi}_{\text{H}} = \boldsymbol{\Phi}_{\text{M}}. \tag{6.43}$$

As a result, one has:

$$[\mathbf{HCRB}(\boldsymbol{\theta})]_{i,j} = [\mathbf{MCRB}(\boldsymbol{\theta})]_{i,j} = \left[\boldsymbol{\Phi}_{\mathrm{M}}^{-1}\right]_{i,j}, \quad i,j = 1,\ldots,2K. \tag{6.44}$$

6.3 The Relationships between the CRTBs

At this point, an analytical comparison between the CRTBs derived above is of interest, which is also conducive to the determination of certain asymptotic properties of them, as will be presented in this section.

6.3.1 The CRB vs. the MCRB/HCRB

It is theoretically proved, in [54] for the scaler and in [57] for the vector parameter case, that the CRB is always larger than the HCRB. Since, according to Eq. (6.44), one also has the equal MCRB and HCRB for the problem under discussion, it follows that:

$$\mathbf{CRB}(\boldsymbol{\theta}) \succeq \mathbf{HCRB}(\boldsymbol{\theta}) = \mathbf{MCRB}(\boldsymbol{\theta}), \tag{6.45}$$

in which $\mathbf{CRB}(\boldsymbol{\theta}) \succeq \mathbf{HCRB}(\boldsymbol{\theta})$ means that $\mathbf{CRB}(\boldsymbol{\theta}) - \mathbf{HCRB}(\boldsymbol{\theta})$ is positive semidefinite.

This relationship becomes apparent when the clutter follows a Student's t-distribution, where $\mathbf{CRB}(\boldsymbol{\theta})$ has a closed-form expression. By comparison of Eqs. (6.24) - (6.16) with Eqs. (6.25), (6.36) and (6.44), one has:

$$\mathbf{CRB}(\boldsymbol{\theta}) = \frac{a+MN+1}{a+MN}\mathbf{MCRB}(\boldsymbol{\theta}) = \frac{a+MN+1}{a+MN}\mathbf{HCRB}(\boldsymbol{\theta}). \tag{6.46}$$

Consequently,

$$\begin{aligned} &\mathbf{CRB}(\boldsymbol{\theta}) - \mathbf{MCRB}(\boldsymbol{\theta}) = \mathbf{CRB}(\boldsymbol{\theta}) - \mathbf{HCRB}(\boldsymbol{\theta}) \\ =&\frac{1}{a+MN}\mathbf{MCRB}(\boldsymbol{\theta}) = \frac{1}{a+MN}\mathbf{HCRB}(\boldsymbol{\theta}) \\ \succeq&\mathbf{0}_{2K\times 2K}, \end{aligned} \tag{6.47}$$

in which the inequality holds because the MCRB and HCRB matrices are *per definitionem* positive semidefinite.

Moreover, since

$$\lim_{MN\to+\infty} \frac{a+MN+1}{a+MN} = 1, \tag{6.48}$$

it follows from Eq. (6.46) that:

$$\lim_{MN\to+\infty} \mathbf{CRB}\left(\boldsymbol{\theta}\right) = \mathbf{MCRB}\left(\boldsymbol{\theta}\right) = \mathbf{HCRB}\left(\boldsymbol{\theta}\right), \tag{6.49}$$

which shows that, for Student's t-distributed clutter, the CRB approaches the MCRB/HCRB in asymptotic cases w.r.t. the number of sensors either at the transmitter or the receiver.

One should note that this asymptotic property of the CRB, as will be demonstrated by simulations, also holds for K-distributed clutter, despite the fact that, for this case, this property seems impossible to be determined in an analytical way similar to that shown above, due to the lack of a closed-form expression for $\kappa(MN, a, b)$, as one can see from Eq. (6.16).

6.3.2 The EMCB/MCB vs. the MCRB/HCRB

The relationship between $\mathbf{EMCB}\left(\boldsymbol{\theta}\right)$ (or $\mathbf{MCB}\left(\boldsymbol{\theta}\right)$) and $\mathbf{MCRB}\left(\boldsymbol{\theta}\right)$ (or $\mathbf{HCRB}\left(\boldsymbol{\theta}\right)$) can be revealed by noticing, according to Eqs. (6.35) and (6.38), that:

$$\left[\mathbf{MCRB}\left(\boldsymbol{\theta}\right)\right]_{i,j} = \left[\boldsymbol{\Phi}_{\mathrm{M}}^{-1}\right]_{i,j} = \left[\left(\mathrm{E}_{\boldsymbol{\tau}}\left\{\boldsymbol{\Phi}_{\mathrm{MC}}\right\}\right)^{-1}\right]_{i,j}, \quad i,j = 1,\ldots,2K. \tag{6.50}$$

Since the quadratic form in $\boldsymbol{\Phi}_{\mathrm{MC}}^{-1}$ is a convex function of the entries of $\boldsymbol{\Phi}_{\mathrm{MC}}$, by *Jensen's inequality*, one has [129]:

$$\mathrm{E}_{\boldsymbol{\tau}}\left\{\boldsymbol{\Phi}_{\mathrm{MC}}^{-1}\right\} - \left(\mathrm{E}_{\boldsymbol{\tau}}\left\{\boldsymbol{\Phi}_{\mathrm{MC}}\right\}\right)^{-1} \succeq \mathbf{0}. \tag{6.51}$$

Combining Eqs. (6.34), (6.50) and (6.51) leads to:

$$\mathbf{EMCB}\left(\boldsymbol{\theta}\right) = \mathbf{MCB}\left(\boldsymbol{\theta}\right) \succeq \mathbf{MCRB}\left(\boldsymbol{\theta}\right) = \mathbf{HCRB}\left(\boldsymbol{\theta}\right). \tag{6.52}$$

Furthermore, since, for both clutter distributions,

$$\lim_{L\to+\infty}\frac{\sum_{l=0}^{L-1}\frac{1}{\tau(l)}}{L}=\mathrm{E}\left\{\frac{1}{\tau(l)}\right\}, \tag{6.53}$$

it follows that:

$$\lim_{L\to+\infty}\boldsymbol{\Phi}_{\mathrm{EMC}}=\lim_{L\to+\infty}\boldsymbol{\Phi}_{\mathrm{MC}}=\boldsymbol{\Phi}_{\mathrm{M}}=\boldsymbol{\Phi}_{\mathrm{H}}, \tag{6.54}$$

and, as a consequence, that:

$$\lim_{L\to+\infty}\mathbf{EMCB}\left(\boldsymbol{\theta}\right)=\lim_{L\to+\infty}\mathbf{MCB}\left(\boldsymbol{\theta}\right)=\mathbf{MCRB}\left(\boldsymbol{\theta}\right)=\mathbf{HCRB}\left(\boldsymbol{\theta}\right), \tag{6.55}$$

viz., the EMCB/MCB approaches the MCRB/HCRB in asymptotic cases w.r.t. the number of pulses.

6.3.3 The CRB vs. the EMCB/MCB

The relationship between $\mathbf{CRB}\left(\boldsymbol{\theta}\right)$ and $\mathbf{EMCB}\left(\boldsymbol{\theta}\right)$ (or $\mathbf{EMCB}\left(\boldsymbol{\theta}\right)$), on the other hand, is *indefinite*. More specifically, depending on the values of L and MN, the EMCB can either be a tighter (larger in value) or looser (lower) bound than the CRB, as will be illustrated by numerical simulations in Ch. 8.

6.4 The CRTBs and the Texture Parameters

This section investigates the respective impacts of the clutter's texture parameters, a and b, on the CRTBs. First, defined the SCR expression as [98, 101]:

$$\mathrm{SCR}=\frac{1}{L}\frac{\sum_{l=0}^{L-1}\left(\boldsymbol{A}\left(\boldsymbol{\theta}\right)\boldsymbol{v}(l)\right)^{H}\left(\boldsymbol{A}\left(\boldsymbol{\theta}\right)\boldsymbol{v}(l)\right)}{\mathrm{E}\{\tau(l)\}\mathrm{tr}\left\{\boldsymbol{\Sigma}\right\}}, \tag{6.56}$$

in which $\mathrm{E}\{\tau(l)\}$ is equal to ab for K-distributed clutter and $b/(a-1)$ for t-distributed clutter (for $a>1$) [130].

It then turns out from Eq. (6.56) that, for a fixed SCR, one has:

$$\frac{1}{\mathrm{tr}\{\boldsymbol{\Sigma}\}} \propto \begin{cases} a, & \text{K-distributed clutter,} \\ \dfrac{1}{a-1}, & \text{Student's t-distributed clutter, for } a > 1, \end{cases} \tag{6.57}$$

and

$$\frac{1}{\mathrm{tr}\{\boldsymbol{\Sigma}\}} \propto b, \quad \text{K-distributed and Student's t-distributed clutters,} \tag{6.58}$$

in which $\propto$ denotes direct proportionality. Note the relationships in Eq. (6.57) and (6.57) hold irrespective of specific assumptions about the value of the speckle CM trace (e.g., the one in Eq. (2.17)).

Furthermore, from Eq. (6.16), it can be found that:

$$\kappa(MN, a, b) \propto \begin{cases} \dfrac{\int_0^{+\infty} x^{MN+a-1} \frac{K^2_{a-MN-1}(x)}{K_{a-MN}(x)} \mathrm{d}x}{2^{MN+a-2}\Gamma(a)}, & \text{K-distributed clutter,} \\ \dfrac{a(a+MN)}{(a+MN+1)}, & \text{Student's t-distributed clutter, for } a > 1, \end{cases} \tag{6.59}$$

and

$$\kappa(MN, a, b) \propto \frac{1}{b}, \quad \text{K-distributed and Student's t-distributed clutters.} \tag{6.60}$$

6.4.1 CRTBs vs. the Shape Parameter a

One begins with the CRB. The expression in Eq. (6.24) can be converted to:

$$\begin{aligned} \phi_{ij} =& \frac{2\kappa(MN, a, b)}{\mathrm{tr}\{\boldsymbol{\Sigma}\}} \sum_{l=0}^{L-1} \mathrm{Re}\left\{ \frac{\partial \boldsymbol{b}^H(\boldsymbol{\theta}, l)}{\partial [\boldsymbol{\mu}]_i} \boldsymbol{\Sigma}_{\mathrm{n}}^{-1} \frac{\partial \boldsymbol{b}(\boldsymbol{\theta}, l)}{\partial [\boldsymbol{\mu}]_j} \right\}, \\ & i, j = 1, \ldots, 2K(L+1), \end{aligned} \tag{6.61}$$

where $\boldsymbol{\Sigma}_{\mathrm{n}}$ is the normalized $\boldsymbol{\Sigma}$ defined in Eq. (3.7).

Eq. (6.61) shows that:

$$\phi_{ij} \propto \frac{\kappa(MN, a, b)}{\mathrm{tr}\{\boldsymbol{\Sigma}\}}, \tag{6.62}$$

to which one applies Eqs. (6.59) and (6.57) and has straightforwardly:

$$\phi_{ij} \propto \begin{cases} \dfrac{a\int_0^{+\infty} x^{MN+a-1}\frac{K^2_{a-MN-1}(x)}{K_{a-MN}(x)}\mathrm{d}x}{2^{MN+a-2}\Gamma(a)}, & \text{K-distributed clutter,} \\ \dfrac{a(a+MN)}{(a+MN+1)(a-1)}, & \text{Student's t-distributed clutter, for } a>1, \end{cases} \tag{6.63}$$

meaning that for both clutter distributions, ϕ_{ij} decreases as a increases[1].

As a result, $[\mathbf{CRB}(\boldsymbol{\theta})]_{i,j}$ $i,j=1,\ldots,2K(L+1)$, increase with a for both clutter distributions, i.e., the CRB is *positively correlated* with the shape parameter a, meaning that the achievable estimation accuracy for the estimation of $\boldsymbol{\theta}$ *diminishes* as a increases. This can be intuitively explained by Figs. 2.4 and 2.8, which show that, for both clutter distributions with a fixed clutter power, the clutter becomes more heavy-tailed as a increases, signifying a larger portion of clutter power being decentralized.

Similarly, one can deduce from Eqs. (6.37) and (6.57) that:

$$\phi^{\mathrm{M}}_{ij} = \phi^{\mathrm{H}}_{ij} \propto \frac{a}{a-1}, \quad \text{K-distributed and Student's t-distributed clutters,} \tag{6.64}$$

which indicates a positive correlation also between the MCRB/HCRB and a, also meaning that an increase in the value of a causes a diminished estimation accuracy that can be achieved for the estimation of $\boldsymbol{\theta}$.

Notice that, as opposed to the CRB, which has different proportionalities to a for K-distributed and for Student's t-distributed clutters respectively, the MCRB/HCRB have the same proportionality for both clutter distributions.

[1]This relationship is obvious for Student's t-distributed clutter, for K-distributed clutter, however, for which ϕ_{ij} does not enjoy a closed-form expression, can only be determined numerically.

Finally, for the EMCB/MCB, one has from Eq. (6.30) and (3.7) that:

$$\begin{aligned}\phi_{ij}^{\text{EMC}} =& \frac{2MN}{\text{tr}\{\boldsymbol{\Sigma}\}} \sum_{l=0}^{L-1} \frac{1}{\tau(l)} \text{Re}\left\{ \frac{\partial \boldsymbol{b}^H(\boldsymbol{\theta}, l)}{\partial [\boldsymbol{\mu}]_i} \boldsymbol{\Sigma}_{\text{n}}^{-1} \frac{\partial \boldsymbol{b}(\boldsymbol{\theta}, l)}{\partial [\boldsymbol{\mu}]_j} \right\} \\ \propto& \frac{1}{\text{tr}\{\boldsymbol{\Sigma}\}} \sum_{l=0}^{L-1} \frac{1}{\tau(l)}, \\ & i, j = 1, \ldots, 2K(L+1).\end{aligned} \tag{6.65}$$

Consequently, it follows from Eq. (6.31) and (6.34) that:

$$\begin{aligned}&[\textbf{EMCB}(\boldsymbol{\theta})]_{i,j} = [\textbf{MCB}(\boldsymbol{\theta})]_{i,j} \propto \text{tr}\{\boldsymbol{\Sigma}\} \text{E}_{\boldsymbol{\tau}} \left\{ \frac{1}{\sum_{l=0}^{L-1} \frac{1}{\tau(l)}} \right\}, \\ &i, j = 1, \ldots, 2K(L+1).\end{aligned} \tag{6.66}$$

It is known for Student's t-distributed clutter that, if

$$\tau(l) \sim \text{Inv-Gamma}(a, b), \tag{6.67}$$

then

$$\frac{1}{\tau(l)} \sim \text{Gamma}(a, \frac{1}{b}). \tag{6.68}$$

Thus, since $\tau(l),\ l = 0, \ldots, L-1$, are i.i.d. variables, it from the property of the gamma distribution that:

$$\frac{1}{\sum_{l=0}^{L-1} \frac{1}{\tau(l)}} \sim \text{Gamma}(La, \frac{1}{b}), \tag{6.69}$$

and consequently, that:

$$\text{E}_{\boldsymbol{\tau}} \left\{ \frac{1}{\sum_{l=0}^{L-1} \frac{1}{\tau(l)}} \right\} = \frac{La}{b}, \quad \text{Student's t-distributed clutter}, \tag{6.70}$$

which, combined with Eqs. (6.57) and (6.66), results in:

$$[\textbf{EMCB}(\boldsymbol{\theta})]_{i,j} = [\textbf{MCB}(\boldsymbol{\theta})]_{i,j} \propto a(a-1), \quad i, j = 1, \ldots, 2K(L+1). \tag{6.71}$$

indicating a positive correlation also between the EMCB/MCB and a.

For K-distributed clutter, an analogous deduction regarding the impact of a on the EMCB/MCB seems, however, impossible or at least complicated, due to the presence of the sum of inverse gamma variables, of which the precise distribution is unknown. The relationship between the EMCB/MCB and a for K-distributed clutter can nevertheless be numerically ascertained, as will be shown in Ch. 8.

6.4.2 CRTBs vs. the Scale Parameter b

Associating Eq. (6.60) with Eq. (6.61), yields:

$$\phi_{ij} \propto \frac{1}{b\text{tr}\{\boldsymbol{\Sigma}\}}, \quad \text{K-distributed and Student's t-distributed clutters.} \tag{6.72}$$

which, combined with Eq. (6.58), shows that ϕ_{ij} is thus independent of b for both clutter distributions, which means that under a fixed SCR, changing b does not give rise to any variation in the value of $\mathbf{CRB}\left(\boldsymbol{\theta}\right)$, meaning that the achievable estimation accuracy for the estimation of $\boldsymbol{\theta}$ is independent of the value of the scale parameter b. This is simply because, as shown in Figs. 2.5 and 2.9, changing b does not result in any change in the PDF of the clutter, for both clutter distributions with fixed clutter power.

The same also holds true for the MCRB/HCRB for both clutter distributions, and can be established by transforming Eq. (6.36) into:

$$\begin{aligned}\phi_{ij}^{\text{M}} =& \frac{2\nu(a,b)MN}{\text{tr}\{\boldsymbol{\Sigma}\}} \sum_{l=0}^{L-1} \text{Re}\left\{ \frac{\partial \boldsymbol{b}^H\left(\boldsymbol{\theta},l\right)}{\partial\left[\boldsymbol{\mu}\right]_i} \boldsymbol{\Sigma}_{\text{n}}^{-1} \frac{\partial \boldsymbol{b}\left(\boldsymbol{\theta},l\right)}{\partial\left[\boldsymbol{\mu}\right]_j} \right\} \\ \propto& \frac{\nu(a,b)}{\text{tr}\{\boldsymbol{\Sigma}\}}, \\ & i,j = 1,\ldots,2K(L+1).\end{aligned} \tag{6.73}$$

Furthermore, since it arises from Eq. (6.37) that:

$$\nu(a,b) \propto \frac{1}{b}, \quad \text{K-distributed and Student's t-distributed clutters,} \tag{6.74}$$

which, inserted together with Eq. (6.58) into Eq. (6.73), demonstrates the independence of the MCRB (thus also of the HCRB) of b, for both clutter distributions.

The independence of the EMCB/MCB of b under Student's t-distributed clutter is straightforwardly confirmable by combining Eqs. (6.58), (6.66) and (6.70). However, under K-distributed clutter, the relationship between the EMCB/MCB and b can only be determined numerically.

In summary, the performance of the estimation, in terms of the lowest achievable CRTBs, is only related to the shape parameter a of the clutter, and decreases as a becomes larger, and is independent of the scale parameter b. This will also be verified by numerical simulations.

6.5 The Blockwise Expressions for the CRTBs

The CRTB expressions derived in Secs. 6.1 and 6.2 are given as the inverses of their respective FIM blocks w.r.t. the signal parameter vector $\boldsymbol{\mu}$, which are calculated *elementwise* by Eqs. (6.24), (6.30), (6.36), ect. As alternatives to this elementwise approach, this section presents the derivation for the *blockwise* expressions for the CRTBs, by reorganizing the elementwise results in Secs. 6.1 and transforming them into matrix-block forms, which are more compact and simpler for calculation, and are especially preferable to the former ones when the size of $\boldsymbol{\mu}$, $2K(L+1)$, is large.

To begin with, one first approaches the CRB. The expression of ϕ_{ij} in Eq. (6.24) can be transformed into:

$$\phi_{ij} = \frac{2\kappa(MN,a,b)}{MN}\mathrm{Re}\left\{\frac{\partial\boldsymbol{\gamma}^H}{\partial\left[\boldsymbol{\mu}\right]_i}\left(\boldsymbol{I}_L\otimes\boldsymbol{\Sigma}^{-1}\right)\frac{\partial\boldsymbol{\gamma}}{\partial\left[\boldsymbol{\mu}\right]_j}\right\}, \tag{6.75}$$

in which the $LMN\times 1$ vector

$$\begin{aligned}\boldsymbol{\gamma} &= \left[\boldsymbol{b}^T\left(\boldsymbol{\theta},0\right),\ldots,\boldsymbol{b}^T\left(\boldsymbol{\theta},L-1\right)\right]^T\\ &= \left[\boldsymbol{v}^T(0)\boldsymbol{A}^T\left(\boldsymbol{\theta}\right),\ldots,\boldsymbol{v}^T(L-1)\boldsymbol{A}^T\left(\boldsymbol{\theta}\right)\right]^T.\end{aligned} \tag{6.76}$$

Furthermore, by straightforward calculations one obtains:

$$\frac{\partial \boldsymbol{\gamma}^H}{\partial \boldsymbol{\theta}} = \left[\boldsymbol{H}^H(0)\boldsymbol{D}^H, \ldots, \boldsymbol{H}^H(L-1)\boldsymbol{D}^H\right], \tag{6.77a}$$

$$\frac{\partial \boldsymbol{\gamma}^H}{\partial \mathrm{Re}\left\{\boldsymbol{v}\right\}(l)} = \left(\boldsymbol{e}_L^{l+1} \otimes \boldsymbol{A}\left(\boldsymbol{\theta}\right)\right)^H, \tag{6.77b}$$

$$\frac{\partial \boldsymbol{\gamma}^H}{\partial \mathrm{Im}\left\{\boldsymbol{v}\right\}(l)} = -j\left(\boldsymbol{e}_L^{l+1} \otimes \boldsymbol{A}\left(\boldsymbol{\theta}\right)\right)^H, \tag{6.77c}$$

in which

$$\boldsymbol{H}(l) = \boldsymbol{I}_2 \otimes \mathrm{diag}\left\{\left[\boldsymbol{v}(l)\right]_1, \ldots, \left[\boldsymbol{v}(l)\right]_K\right\}, \tag{6.78}$$

$\boldsymbol{e}_L^{l+1}$ represents the $L \times 1$ vector whose $(l+1)$th element is one and others are zero, and

$$\boldsymbol{D} = \left[\boldsymbol{D}^{(\mathrm{T})}, \boldsymbol{D}^{(\mathrm{R})}\right], \tag{6.79}$$

where

$$\boldsymbol{D}^{(\mathrm{T})} = \left[\left.\frac{\partial \boldsymbol{a}\left(\theta^{(\mathrm{T})}, \theta^{(\mathrm{R})}\right)}{\partial \theta^{(\mathrm{T})}}\right|_{\theta^{(\mathrm{T})}=\theta_1^{(\mathrm{T})}, \theta^{(\mathrm{R})}=\theta_1^{(\mathrm{R})}}, \ldots, \left.\frac{\partial \boldsymbol{a}\left(\theta^{(\mathrm{T})}, \theta^{(\mathrm{R})}\right)}{\partial \theta^{(\mathrm{T})}}\right|_{\theta^{(\mathrm{T})}=\theta_K^{(\mathrm{T})}, \theta^{(\mathrm{R})}=\theta_K^{(\mathrm{R})}}\right], \tag{6.80}$$

$$\boldsymbol{D}^{(\mathrm{R})} = \left[\left.\frac{\partial \boldsymbol{a}\left(\theta^{(\mathrm{T})}, \theta^{(\mathrm{R})}\right)}{\partial \theta^{(\mathrm{R})}}\right|_{\theta^{(\mathrm{T})}=\theta_1^{(\mathrm{T})}, \theta^{(\mathrm{R})}=\theta_1^{(\mathrm{R})}}, \ldots, \left.\frac{\partial \boldsymbol{a}\left(\theta^{(\mathrm{T})}, \theta^{(\mathrm{R})}\right)}{\partial \theta^{(\mathrm{R})}}\right|_{\theta^{(\mathrm{T})}=\theta_K^{(\mathrm{T})}, \theta^{(\mathrm{R})}=\theta_K^{(\mathrm{R})}}\right]. \tag{6.81}$$

Now, using Eq. (6.75) and Eqs. (6.77a) - (6.77c) to calculate the submatrices of $\boldsymbol{\Phi}$ in Eq. (6.23), one obtains:

$$\boldsymbol{\Phi} = \begin{bmatrix} \boldsymbol{\Phi}_{\boldsymbol{\theta}\boldsymbol{\theta}} & \boldsymbol{\Phi}_{\boldsymbol{\theta}\boldsymbol{v}} \\ \boldsymbol{\Phi}_{\boldsymbol{v}\boldsymbol{\theta}} & \boldsymbol{\Phi}_{\boldsymbol{v}\boldsymbol{v}} \end{bmatrix}, \tag{6.82}$$

in which $\boldsymbol{\Phi}_{\boldsymbol{\theta}\boldsymbol{\theta}}$ denotes the block of $\boldsymbol{\Phi}$ w.r.t. the parameter vector $\boldsymbol{\theta}$, $\boldsymbol{\Phi}_{\boldsymbol{\theta}\boldsymbol{v}}$ denotes the block of $\boldsymbol{\Phi}$ w.r.t. the parameter vectors $\boldsymbol{\theta}$ and $\boldsymbol{v}$, and so on. These submatrices have the following

expressions:

$$\boldsymbol{\Phi}_{\boldsymbol{\theta\theta}} = \frac{2\kappa(MN,a,b)}{MN}\sum_{l=0}^{L-1}\mathrm{Re}\left\{\boldsymbol{H}^H(l)\tilde{\boldsymbol{D}}^H\tilde{\boldsymbol{D}}\boldsymbol{H}(l)\right\}, \tag{6.83}$$

where

$$\tilde{\boldsymbol{D}} = \boldsymbol{\Sigma}^{-\frac{1}{2}}\boldsymbol{D}; \tag{6.84}$$

$$\boldsymbol{\Phi}_{\boldsymbol{\theta v}} = \left[\boldsymbol{\Phi}_{\boldsymbol{\theta v}(0)},\ldots,\boldsymbol{\Phi}_{\boldsymbol{\theta v}(L-1)}\right], \tag{6.85}$$

$$\boldsymbol{\Phi}_{\boldsymbol{v\theta}} = \left[\boldsymbol{\Phi}_{\boldsymbol{v}(0)\boldsymbol{\theta}},\ldots,\boldsymbol{\Phi}_{\boldsymbol{v}(L-1)\boldsymbol{\theta}}\right], \tag{6.86}$$

where

$$\begin{aligned}\boldsymbol{\Phi}_{\boldsymbol{\theta v}(l)} =& \left[\boldsymbol{\Phi}_{\boldsymbol{\theta}\mathrm{Re}\{\boldsymbol{v}(l)\}},\boldsymbol{\Phi}_{\boldsymbol{\theta}\mathrm{Im}\{\boldsymbol{v}(l)\}}\right]\\ =&\frac{2\kappa(MN,a,b)}{MN}\left[\mathrm{Re}\left\{\boldsymbol{H}^H(l)\tilde{\boldsymbol{D}}^H\tilde{\boldsymbol{A}}\left(\boldsymbol{\theta}\right)\right\},\right.\\ &\left.\mathrm{Im}\left\{\boldsymbol{H}^H(l)\tilde{\boldsymbol{D}}^H\tilde{\boldsymbol{A}}\left(\boldsymbol{\theta}\right)\right\}\right],\end{aligned} \tag{6.87}$$

$$\begin{aligned}\boldsymbol{\Phi}_{\boldsymbol{v}(l)\boldsymbol{\theta}} =& \left[\boldsymbol{\Phi}_{\boldsymbol{\theta}\mathrm{Re}\{\boldsymbol{v}(l)\}},\boldsymbol{\Phi}_{\boldsymbol{\theta}\mathrm{Im}\{\boldsymbol{v}(l)\}}\right]\\ =&\frac{2\kappa(MN,a,b)}{MN}\left[\mathrm{Re}\left\{\boldsymbol{H}^H(l)\tilde{\boldsymbol{D}}^H\tilde{\boldsymbol{A}}\left(\boldsymbol{\theta}\right)\right\}^T,\right.\\ &\left.-\mathrm{Im}\left\{\boldsymbol{H}^H(l)\tilde{\boldsymbol{D}}^H\tilde{\boldsymbol{A}}\left(\boldsymbol{\theta}\right)\right\}^T\right];\end{aligned} \tag{6.88}$$

$\boldsymbol{\Phi}_{\boldsymbol{vv}}$ has the following block-diagonal form (meaning that the achievable performance for the estimation of $\boldsymbol{v}(l),\ =0,\ldots,L-1$, and independent from one another):

$$\boldsymbol{\Phi}_{\boldsymbol{vv}} = \begin{bmatrix}\boldsymbol{\Phi}_{\boldsymbol{v}(0)\boldsymbol{v}(0)} & & \boldsymbol{0}\\ & \ddots & \\ \boldsymbol{0} & & \boldsymbol{\Phi}_{\boldsymbol{v}(L-1)\boldsymbol{v}(L-1)}\end{bmatrix}, \tag{6.89}$$

where

$$\begin{aligned}\boldsymbol{\Phi}_{\boldsymbol{v}(l)\boldsymbol{v}(l)} =& \begin{bmatrix}\boldsymbol{\Phi}_{\mathrm{Re}\{\boldsymbol{v}(l)\}\mathrm{Re}\{\boldsymbol{v}(l)\}} & \boldsymbol{\Phi}_{\mathrm{Re}\{\boldsymbol{v}(l)\}\mathrm{Im}\{\boldsymbol{v}(l)\}}\\ \boldsymbol{\Phi}_{\mathrm{Im}\{\boldsymbol{v}(l)\}\mathrm{Re}\{\boldsymbol{v}(l)\}} & \boldsymbol{\Phi}_{\mathrm{Im}\{\boldsymbol{v}(l)\}\mathrm{Im}\{\boldsymbol{v}(l)\}}\end{bmatrix}\\ =&\frac{2\kappa(MN,a,b)}{MN}\begin{bmatrix}\mathrm{Re}\left\{\tilde{\boldsymbol{A}}^H\left(\boldsymbol{\theta}\right)\tilde{\boldsymbol{A}}\left(\boldsymbol{\theta}\right)\right\} & \mathrm{Im}\left\{\tilde{\boldsymbol{A}}^H\left(\boldsymbol{\theta}\right)\tilde{\boldsymbol{A}}\left(\boldsymbol{\theta}\right)\right\}\\ -\mathrm{Im}\left\{\tilde{\boldsymbol{A}}^H\left(\boldsymbol{\theta}\right)\tilde{\boldsymbol{A}}\left(\boldsymbol{\theta}\right)\right\} & \mathrm{Re}\left\{\tilde{\boldsymbol{A}}^H\left(\boldsymbol{\theta}\right)\tilde{\boldsymbol{A}}\left(\boldsymbol{\theta}\right)\right\}\end{bmatrix}.\end{aligned} \tag{6.90}$$

By applying the blockwise matrix inversion formula [131] to Eq. (6.82) and exploiting the submatrices' structures in Eqs. (6.85), (6.86) and (6.89), one has:

$$\begin{aligned}\text{CRB}\left(\boldsymbol{\theta}\right) &= \left(\boldsymbol{\Phi}_{\boldsymbol{\theta\theta}} - \boldsymbol{\Phi}_{\boldsymbol{\theta v}}\boldsymbol{\Phi}_{\boldsymbol{vv}}^{-1}\boldsymbol{\Phi}_{\boldsymbol{v\theta}}\right)^{-1} \\ &= \left(\boldsymbol{\Phi}_{\boldsymbol{\theta\theta}} - \sum_{l=0}^{L-1}\boldsymbol{\Phi}_{\boldsymbol{\theta v}(l)}\boldsymbol{\Phi}_{\boldsymbol{v}(l)\boldsymbol{v}(l)}^{-1}\boldsymbol{\Phi}_{\boldsymbol{v}(l)\boldsymbol{\theta}}\right)^{-1}.\end{aligned} \tag{6.91}$$

Finally, by inserting Eqs. (6.83), (6.87), 6.88 and (6.90), one can obtain, after some manipulations, the following expression for CRB $(\boldsymbol{\theta})$:

$$\begin{aligned}\text{CRB}\left(\boldsymbol{\theta}\right) =& \left(\frac{2\kappa(MN,a,b)}{MN}\text{Re}\left\{\sum_{l=0}^{L-1}\boldsymbol{H}^H(l)\tilde{\boldsymbol{D}}^H\boldsymbol{P}_{\tilde{\boldsymbol{A}}(\boldsymbol{\theta})}^{\perp}\tilde{\boldsymbol{D}}\boldsymbol{H}(l)\right\}\right)^{-1} \\ =& \frac{MN}{2\kappa(MN,a,b)L}\left(\text{Re}\left\{\left(\tilde{\boldsymbol{D}}^H\boldsymbol{P}_{\tilde{\boldsymbol{A}}(\boldsymbol{\theta})}^{\perp}\tilde{\boldsymbol{D}}\right)\odot\hat{\boldsymbol{P}}^T\right\}\right)^{-1},\end{aligned} \tag{6.92}$$

in which $\odot$ stands for the Hadamard product, and

$$\hat{\boldsymbol{P}} = \frac{1}{L}\boldsymbol{J}_2 \otimes \sum_{l=0}^{L-1}\boldsymbol{v}(l)\boldsymbol{v}^H(l), \tag{6.93}$$

where $\boldsymbol{J}_2$ is the 2×2 all-ones matrix.

Following a similar procedure, one can also obtain:

$$\begin{aligned}&\text{MCRB}\left(\boldsymbol{\theta}\right) = \text{HCRB}\left(\boldsymbol{\theta}\right) \\ =& \left(2\nu(a,b)\text{Re}\left\{\sum_{l=0}^{L-1}\boldsymbol{H}^H(l)\tilde{\boldsymbol{D}}^H\boldsymbol{P}_{\tilde{\boldsymbol{A}}(\boldsymbol{\theta})}^{\perp}\tilde{\boldsymbol{D}}\boldsymbol{H}(l)\right\}\right)^{-1} \\ =& \frac{1}{2\nu(a,b)L}\left(\text{Re}\left\{\left(\tilde{\boldsymbol{D}}^H\boldsymbol{P}_{\tilde{\boldsymbol{A}}(\boldsymbol{\theta})}^{\perp}\tilde{\boldsymbol{D}}\right)\odot\hat{\boldsymbol{P}}^T\right\}\right)^{-1},\end{aligned} \tag{6.94}$$

and

$$\begin{aligned}&\text{EMCB}\left(\boldsymbol{\theta}\right) = \text{MCB}\left(\boldsymbol{\theta}\right) \\ =& \text{E}_{\boldsymbol{\tau}}\left\{\left(2\text{Re}\left\{\sum_{l=0}^{L-1}\boldsymbol{H}^H(l)\tilde{\boldsymbol{D}}^H\boldsymbol{P}_{\tilde{\boldsymbol{A}}(\boldsymbol{\theta})}^{\perp}\tilde{\boldsymbol{D}}\boldsymbol{H}(l)\right\}\right)^{-1}\right\} \\ =& \frac{1}{2L}\text{E}_{\boldsymbol{\tau}}\left\{\left(\text{Re}\left\{\left(\tilde{\boldsymbol{D}}^H\boldsymbol{P}_{\tilde{\boldsymbol{A}}(\boldsymbol{\theta})}^{\perp}\tilde{\boldsymbol{D}}\right)\odot\hat{\boldsymbol{Q}}^T\right\}\right)^{-1}\right\},\end{aligned} \tag{6.95}$$

where

$$\hat{\boldsymbol{Q}} = \frac{1}{L}\boldsymbol{J}_2 \otimes \sum_{l=0}^{L-1} \frac{1}{\tau(l)} \boldsymbol{v}(l)\boldsymbol{v}^H(l). \tag{6.96}$$

Eqs. (6.92), (6.94) and (6.95) are the proposed blockwise expressions for the CRTBs.

Chapter 7

The Angular Resolution Limit

This chapter is dedicated to the question of the target resolvability, in terms of an analytical expression for the ARL of two closely spaced MIMO radar targets. For simplicity of description and mathematical manipulation, several restrictions have to be imposed on the co-located MIMO radar model introduced in Ch. 2, leading to a new model, which retains the intrinsic characteristics of the original one, and on which the derivation of the ARL in chapter rests.

7.1 Model Setup

The co-located MIMO radar model specified in Eq. (7.5), before matched filtering, when the following assumptions are further made:

- The MIMO radar is monostatic, namely, the DODs of the targets are equal to the DOAs.
- The MIMO radar has one radar pulse per CPI, i.e., $L = 1$;
- The MIMO radar illuminates *two* closely spaced far-field, narrowband, point sources;
- The steering vectors of the transmitter and the receiver are characterized by, instead of the DODs/DOAs, the electrical angles of the two targets, denoted by ω_1 and ω_2,

respectively. Furthermore, let

$$\Delta = \omega_2 - \omega_1 \tag{7.1}$$

denote the angular spacing between the two targets.

is transformed into:

$$\boldsymbol{Y} = \sum_{k=1}^{2} \alpha_k \boldsymbol{a}_{(\mathrm{R})}(\omega_k)\, \boldsymbol{a}_{(\mathrm{T})}^{T}(\omega_k)\, \boldsymbol{S} + \boldsymbol{M}. \tag{7.2}$$

in which

$$\boldsymbol{a}_{(\mathrm{T})}(\omega_k) = [e^{j\omega_k d_1^{((\mathrm{T}))}}, \ldots, e^{j\omega_k d_M^{((\mathrm{T}))}}]^T, \tag{7.3}$$

and

$$\boldsymbol{a}_{(\mathrm{R})}(\omega_k) = [e^{j\omega_k d_1^{((\mathrm{R}))}}, \ldots, e^{j\omega_k d_N^{((\mathrm{R}))}}]^T, \tag{7.4}$$

$\boldsymbol{Y}$, α_k and $\boldsymbol{M}$ are the equivalents in the one pulse per CPI case to $\boldsymbol{Y}(l)$, $\alpha_k(l)$ and $\boldsymbol{M}(l)$ in Eq. (7.5), and the definitions of the other variables in Eq. (7.2) are the same as in Eq. (7.5).

Reformulate Eq. (7.2) in the vector form, into:

$$\boldsymbol{y}(t) = \sum_{k=1}^{2} \alpha_k \boldsymbol{a}_{(\mathrm{R})}(\omega_k)\, \boldsymbol{a}_{(\mathrm{T})}^{T}(\omega_k)\, \boldsymbol{s}(t) + \boldsymbol{m}(t), \quad t = 1, \ldots, T, \tag{7.5}$$

where $\boldsymbol{y}(t)$ is the tth column of $\boldsymbol{Y}$ and represents the observation vector at the tth snapshot. The same relationship holds true between $\boldsymbol{s}(t)$ and $\boldsymbol{S}$, and between $\boldsymbol{m}(t)$ and $\boldsymbol{M}$.

For the derivation in this chapter, the signal target source vectors $\boldsymbol{s}(t),\ t = 1, \ldots, T$ in Eq. (7.5) are viewed as deterministic, and the received clutter vectors $\boldsymbol{m}(t),\ t = 1, \ldots, T$ before matched filtering are assumed to be i.i.d. SIRVs [22], such that:

$$\boldsymbol{m}(t) = \sqrt{\bar{\tau}(t)}\bar{\boldsymbol{x}}(t), \quad t = 1, \ldots, T. \tag{7.6}$$

in which the statistical properties of the texture $\bar{\tau}(t)$ and the speckle $\bar{\boldsymbol{x}}(t)$[1] resemble, respectively, those of $\tau(l)$ and $\boldsymbol{x}(l)$ introduced below Eq. (2.15); the CM matrix $\boldsymbol{\Sigma}$ in Eq. (2.16) represents here for the new model the CM matrix of $\bar{\boldsymbol{x}}(t)$ and has the size of N.

[1]The modifier $\bar{(\cdot)}$ is used in the symbols $\bar{\tau}(t)$ and $\bar{\boldsymbol{x}}(t)$ to distinguish them from $\tau(l)$ and $\boldsymbol{x}(l)$ used in the previous chapters, thus to avoid notational confusion.

Furthermore, consider the electric angle ω_1 to be known while ω_2 is unknown, which assumption makes good sense in many scenarios, e.g., in those where ω_1 is considered a co-operative target whose position is known and ω_2 represents the unknown position of another, non-cooperative target. Under all the assumptions above, the full unknown parameter vector of the current problem, denoted by $\bar{\boldsymbol{\xi}}$ so as to be distinguished from $\boldsymbol{\xi}$ in Eq. (2.24) for the original model, is given by:

$$\bar{\boldsymbol{\xi}} = \left[\Delta, \mathrm{Re}\{\alpha\}_1, \mathrm{Im}\{\alpha\}_1, \mathrm{Re}\{\alpha\}_2, \mathrm{Im}\{\alpha\}_2, \boldsymbol{\zeta}^T, a, b\right]^T, \tag{7.7}$$

in which the target spacing Δ is the parameter of interest.

7.2 Model Linearization

In order to obtain an analytical expression for the ARL in Smith's sense (as is defined in Sec. 1.1.5), a closed-form (non-matrix) expression for the CRB w.r.t. Δ, denoted by $\mathrm{CRB}(\Delta)$, is required, which, however, cannot be directly obtained based on the model in Eq. (7.5), due to its nonlinearity w.r.t. Δ. One thus has first to linearize the model [59, 65, 76–78], and then derive the FIM expression based on the linearized model that is feasible for analytical inversion. The ARL obtained from the linearized model approximates the exact ARL obtained from the original one.

To linearize the model, one resorts to the second order Taylor expansion around $\Delta = 0$ in Eq. (7.5). This step of approximation is justified by considering the fact that, in asymptotic cases, e.g., those of large SCR or sample size, in which the CRB is a tight bound, the ARL is always very small, i.e., the value of Δ corresponding to the ARL approaches zero ($\Delta \ll 1$) [59, 63–65, 132]. This is also supported by the fact that the ML estimator, and generally all super-resolution estimators, have asymptotically an infinite resolution capability, leading to the ARL asymptotically approaching to 0 [35, 74]. The second order Taylor expansions of $\boldsymbol{a}_{(\mathrm{T})}(\omega_2)$ and $\boldsymbol{a}_{(\mathrm{R})}(\omega_2)$ are respectively given by:

$$\boldsymbol{a}_{(\mathrm{T})}(\omega_2) \approx \boldsymbol{a}_{(\mathrm{T})}(\omega_1) + j\Delta\dot{\boldsymbol{a}}_{(\mathrm{T})}(\omega_1) - \frac{\Delta^2}{2}\ddot{\boldsymbol{a}}_{(\mathrm{T})}(\omega_1), \tag{7.8a}$$

$$\boldsymbol{a}_{(\mathrm{R})}(\omega_2) \approx \boldsymbol{a}_{(\mathrm{R})}(\omega_1) + j\Delta\dot{\boldsymbol{a}}_{(\mathrm{R})}(\omega_1) - \frac{\Delta^2}{2}\ddot{\boldsymbol{a}}_{(\mathrm{R})}(\omega_1), \tag{7.8b}$$

in which

$$\dot{\boldsymbol{a}}_{(\mathrm{T})}(\cdot) = \boldsymbol{a}_{(\mathrm{T})}(\cdot) \odot \boldsymbol{d}_{(\mathrm{T})}, \tag{7.9}$$

$$\dot{\boldsymbol{a}}_{(\mathrm{R})}(\cdot) = \boldsymbol{a}_{(\mathrm{R})}(\cdot) \odot \boldsymbol{d}_{(\mathrm{R})}, \tag{7.10}$$

$$\ddot{\boldsymbol{a}}_{(\mathrm{T})}(\cdot) \triangleq \boldsymbol{a}_{(\mathrm{T})}(\cdot) \odot \boldsymbol{d}_{(\mathrm{T})} \odot \boldsymbol{d}_{(\mathrm{T})}, \tag{7.11}$$

$$\ddot{\boldsymbol{a}}_{(\mathrm{R})}(\cdot) \triangleq \boldsymbol{a}_{(\mathrm{R})}(\cdot) \odot \boldsymbol{d}_{(\mathrm{R})} \odot \boldsymbol{d}_{(\mathrm{R})}, \tag{7.12}$$

where

$$\boldsymbol{d}_{(\mathrm{T})} = [0, d_{(\mathrm{T})}, \ldots, (M-1)d_{(\mathrm{T})}]^T, \tag{7.13}$$

$$\boldsymbol{d}_{(\mathrm{R})} = [0, d_{(\mathrm{R})}, \ldots, (N-1)d_{(\mathrm{R})}]^T. \tag{7.14}$$

One can then approximate Eq. (7.5) as (omitting all terms containing $\Delta^n,\ n > 2$):

$$\boldsymbol{y}(t) \approx \boldsymbol{C}(t)\boldsymbol{\eta} + \boldsymbol{m}(t), \quad t = 1, \ldots, T, \tag{7.15}$$

in which

$$\boldsymbol{\eta} = \left[\alpha_1 + \alpha_2, j\alpha_2\Delta, -\alpha_2\Delta^2\right]^T, \tag{7.16}$$

and

$$\boldsymbol{C}(t) = [\boldsymbol{\beta}_1(t), \boldsymbol{\beta}_2(t), \boldsymbol{\beta}_3(t)], \tag{7.17}$$

in which

$$\boldsymbol{\beta}_i(t) = \boldsymbol{R}_i\boldsymbol{s}(t),\ i, j = 1, 2, 3, \tag{7.18}$$

where

$$\boldsymbol{R}_1 = \boldsymbol{a}_{(\mathrm{R})}(\omega_1)\,\boldsymbol{a}^T_{(\mathrm{T})}(\omega_1), \tag{7.19a}$$

$$\boldsymbol{R}_2 = \dot{\boldsymbol{a}}_{(\mathrm{R})}(\omega_1)\,\boldsymbol{a}^T_{(\mathrm{T})}(\omega_1) + \boldsymbol{a}_{(\mathrm{R})}(\omega_1)\,\dot{\boldsymbol{a}}^T_{(\mathrm{T})}(\omega_1), \tag{7.19b}$$

$$\boldsymbol{R}_3 = \dot{\boldsymbol{a}}_{(\mathrm{R})}(\omega_1)\,\dot{\boldsymbol{a}}^T_{(\mathrm{T})}(\omega_1) + \frac{1}{2}\ddot{\boldsymbol{a}}_{(\mathrm{R})}(\omega_1)\,\boldsymbol{a}^T_{(\mathrm{T})}(\omega_1)$$

$$+\frac{1}{2}\boldsymbol{a}_{(\mathrm{R})}\left(\omega_1\right)\ddot{\boldsymbol{a}}_{(\mathrm{T})}^{T}\left(\omega_1\right). \tag{7.19c}$$

7.3 The Analytical Expression of CRB(Δ)

Let $\boldsymbol{y}=\left[\boldsymbol{y}^T(1),...,\boldsymbol{y}^T(T)\right]^T$ denote the full observation vector. The marginal (exact) PDF (marginalized w.r.t. the full observation) based on the linearized model in Eq. (7.15) is, according to Eq. (2.32), given by:

$$\begin{aligned} p\left(\boldsymbol{y};\bar{\boldsymbol{\xi}}\right)=&\prod_{t=1}^{T}\frac{1}{|\pi\boldsymbol{\Sigma}|}\int_{0}^{+\infty}\frac{\exp\left(-\frac{1}{\bar{\tau}(t)}\left(\boldsymbol{y}(t)-\boldsymbol{C}(t)\boldsymbol{\eta}\right)^{H}\boldsymbol{\Sigma}^{-1}\left(\boldsymbol{y}(t)-\boldsymbol{C}(t)\boldsymbol{\eta}\right)\right)}{\tau^{N}(t)}\\ &\cdot p(\bar{\tau}(t);a,b)\mathrm{d}\bar{\tau}(t). \end{aligned} \tag{7.20}$$

The FIM based on linearized model in Eq. (7.15) can be obtained by following the same procedure as in Sec. 6.1 and using $p\left(\boldsymbol{y};\bar{\boldsymbol{\xi}}\right)$ in Eq. (7.20) for the calculation. The FIM has a similar block-diagonal structure as in Eq. (6.23). Namely, its 5×5 block w.r.t. the signal parameters (Δ, $\mathrm{Re}\{\alpha\}_1$, $\mathrm{Im}\{\alpha\}_1$, $\mathrm{Re}\{\alpha\}_2$ and $\mathrm{Im}\{\alpha\}_2$), denoted by $\bar{\boldsymbol{\Phi}}$ in order to make a distinction between it and $\boldsymbol{\Phi}$ in Eq. (6.23), is decoupled from the FIM block w.r.t. the other parameters (clutter parameters) in the unknown parameter vector $\bar{\boldsymbol{\xi}}$. Furthermore, the calculation shows that the entries of $\bar{\boldsymbol{\Phi}}$, denoted by $\bar{\varphi}_{ij},\ i,j=1,\ldots,5$ (to be distinguished from ϕ_{ij} in Eq. (6.24)), have the following expressions:

$$\bar{\varphi}_{11}=\frac{2\kappa(N,a,b)|\alpha_2|^2}{N}\left(\gamma_{22}-4\Delta\mathrm{Im}\{\gamma_{23}\}+4\Delta^2\gamma_{33}\right) \tag{7.21a}$$

$$\bar{\varphi}_{22}=\bar{\varphi}_{33}=\frac{2\kappa(N,a,b)}{N}\gamma_{11}, \tag{7.21b}$$

$$\begin{aligned} \bar{\varphi}_{44}=\bar{\varphi}_{55}=&\frac{2\kappa(N,a,b)}{N}\big(\gamma_{11}-2\Delta\mathrm{Im}\{\gamma_{12}\}+\Delta^2\gamma_{22}\\ &-2\Delta^2\mathrm{Re}\{\gamma_{13}\}-2\Delta^3\mathrm{Im}\{\gamma_{23}\}+\Delta^4\gamma_{33}\big), \end{aligned} \tag{7.21c}$$

$$\begin{aligned} \bar{\varphi}_{12}=\bar{\varphi}_{21}=&\frac{2\kappa(N,a,b)}{N}\big(-\mathrm{Re}\{\alpha_2\}\mathrm{Im}\{\gamma_{12}\}-\mathrm{Im}\{\alpha_2\}\mathrm{Re}\{\gamma_{12}\}-2\Delta\mathrm{Re}\{\alpha_2\}\mathrm{Re}\{\gamma_{13}\}\\ &+2\Delta\mathrm{Im}\{\alpha_2\}\mathrm{Im}\{\gamma_{13}\}\big), \end{aligned} \tag{7.21d}$$

$$\begin{aligned} \bar{\varphi}_{13}=\bar{\varphi}_{31}=&\frac{2\kappa(N,a,b)}{N}\big(\mathrm{Re}\{\alpha_2\}\mathrm{Re}\{\gamma_{12}\}-\mathrm{Im}\{\alpha_2\}\mathrm{Im}\{\gamma_{12}\}-2\Delta\mathrm{Re}\{\alpha_2\}\mathrm{Im}\{\gamma_{13}\}\\ &-2\Delta\mathrm{Im}\{\alpha_2\}\mathrm{Re}\{\gamma_{13}\}\big), \end{aligned} \tag{7.21e}$$

$$\begin{aligned}\bar{\varphi}_{14} = \bar{\varphi}_{41} = \frac{2\kappa(N,a,b)}{N}\big(&- \mathrm{Re}\{\alpha_2\}\mathrm{Im}\{\gamma_{12}\} - \mathrm{Im}\{\alpha_2\}\mathrm{Re}\{\gamma_{12}\} + \Delta\mathrm{Re}\{\alpha_2\}\gamma_{22} \\ &-2\Delta\mathrm{Re}\{\alpha_2\}\mathrm{Re}\{\gamma_{13}\} + 2\Delta\mathrm{Im}\{\alpha_2\}\mathrm{Im}\{\gamma_{13}\} - \Delta^2\mathrm{Im}\{\alpha_2\}\mathrm{Re}\{\gamma_{23}\} \\ &-3\Delta^2\mathrm{Re}\{\alpha_2\}\mathrm{Im}\{\gamma_{23}\} + 2\Delta^3\mathrm{Re}\{\alpha_2\}\gamma_{33}\big), \end{aligned} \tag{7.21f}$$

$$\begin{aligned}\bar{\varphi}_{15} = \bar{\varphi}_{51} = \frac{2\kappa(N,a,b)}{N}\big(&\mathrm{Re}\{\alpha_2\}\mathrm{Re}\{\gamma_{12}\} - \mathrm{Im}\{\alpha_2\}\mathrm{Im}\{\gamma_{12}\} + \Delta\mathrm{Im}\{\alpha_2\}\gamma_{22} \\ &-2\Delta\mathrm{Re}\{\alpha_2\}\mathrm{Im}\{\gamma_{13}\} - 2\Delta\mathrm{Im}\{\alpha_2\}\mathrm{Re}\{\gamma_{13}\} + \Delta^2\mathrm{Re}\{\alpha_2\}\mathrm{Re}\{\gamma_{23}\} \\ &-3\Delta^2\mathrm{Im}\{\alpha_2\}\mathrm{Im}\{\gamma_{23}\} + 2\Delta^3\mathrm{Im}\{\alpha_2\}\gamma_{33}\big), \end{aligned} \tag{7.21g}$$

$$\bar{\varphi}_{23} = \bar{\varphi}_{32} = \bar{\varphi}_{45} = \bar{\varphi}_{54} = 0, \tag{7.21h}$$

$$\begin{aligned}&\bar{\varphi}_{24} = \bar{\varphi}_{42} = \bar{\varphi}_{35} = \bar{\varphi}_{53} \\ &\quad = \frac{2\kappa(N,a,b)}{N}\left(\gamma_{11} - \Delta\mathrm{Im}\{\gamma_{12}\} - \Delta^2\mathrm{Re}\{\gamma_{13}\}\right), \end{aligned} \tag{7.21i}$$

$$\begin{aligned}&\bar{\varphi}_{25} = \bar{\varphi}_{52} = -\bar{\varphi}_{34} = -\bar{\varphi}_{43} \\ &\quad = \frac{2\kappa(N,a,b)}{N}\left(-\Delta\mathrm{Re}\{\gamma_{12}\} + \Delta^2\mathrm{Im}\{\gamma_{13}\}\right), \end{aligned} \tag{7.21j}$$

in which

$$\gamma_{ij} = \boldsymbol{\beta}_i^H \boldsymbol{\Upsilon} \boldsymbol{\beta}_j, \quad i,j = 1,2,3, \tag{7.22}$$

where

$$\boldsymbol{\Upsilon} = \boldsymbol{I}_T \otimes \boldsymbol{\Sigma}^{-1}, \tag{7.23}$$

$$\boldsymbol{\beta}_i = [\boldsymbol{\beta}_i^T(1), \ldots, \boldsymbol{\beta}_i^T(T)]^T, \quad i = 1,2,3, \tag{7.24}$$

and

$$\boldsymbol{\beta}_j = [\boldsymbol{\beta}_j^T(1), \ldots, \boldsymbol{\beta}_j^T(T)]^T, \quad j = 1,2,3. \tag{7.25}$$

Reformulate $\bar{\boldsymbol{\Phi}}$ into the following expression in terms of submatrices:

$$\bar{\boldsymbol{\Phi}} = \begin{bmatrix} \bar{\varphi}_{11} & \boldsymbol{\varsigma}^T \\ \boldsymbol{\varsigma} & \boldsymbol{\Omega} \end{bmatrix}, \tag{7.26}$$

in which

$$\boldsymbol{\varsigma} = [\bar{\varphi}_{12},\ \bar{\varphi}_{13},\ \bar{\varphi}_{14},\ \bar{\varphi}_{15}]^T, \tag{7.27}$$

and

$$\boldsymbol{\Omega} = \begin{bmatrix} \boldsymbol{\Omega}_1 & \boldsymbol{\Omega}_2 \\ \boldsymbol{\Omega}_2^T & \boldsymbol{\Omega}_3 \end{bmatrix}, \tag{7.28}$$

where

$$\boldsymbol{\Omega}_1 = \bar{\varphi}_{22}\boldsymbol{I}_2, \tag{7.29}$$

$$\boldsymbol{\Omega}_3 = \bar{\varphi}_{44}\boldsymbol{I}_2, \tag{7.30}$$

and

$$\boldsymbol{\Omega}_2 = \begin{bmatrix} \bar{\varphi}_{24} & \bar{\varphi}_{25} \\ -\bar{\varphi}_{25} & \bar{\varphi}_{24} \end{bmatrix}. \tag{7.31}$$

By employing the Block Matrix Inversion Lemma [131] on $\bar{\boldsymbol{\Phi}}$ and on $\boldsymbol{\Omega}$ consecutively, one obtains:

$$\text{CRB}\left(\Delta\right) = \left[\bar{\boldsymbol{\Phi}}^{-1}\right]_{1,1} = \frac{\bar{\varphi}_{11}}{1 - \bar{\varphi}_{11}\boldsymbol{\varsigma}^T\boldsymbol{\Omega}^{-1}\boldsymbol{\varsigma}}, \tag{7.32}$$

in which

$$\boldsymbol{\Omega}^{-1} = \begin{bmatrix} \boldsymbol{\Theta}_1 & \boldsymbol{\Theta}_2 \\ \boldsymbol{\Theta}_3 & \boldsymbol{\Theta}_4 \end{bmatrix}, \tag{7.33}$$

where

$$\boldsymbol{\Theta}_1 = \left(\boldsymbol{\Omega}_1 - \boldsymbol{\Omega}_2\boldsymbol{\Omega}_3^{-1}\boldsymbol{\Omega}_2^T\right)^{-1}, \tag{7.34a}$$

$$\boldsymbol{\Theta}_2 = -\boldsymbol{\Omega}_1^{-1}\boldsymbol{\Omega}_2\left(\boldsymbol{\Omega}_3 - \boldsymbol{\Omega}_2^T\boldsymbol{\Omega}_1^{-1}\boldsymbol{\Omega}_2\right)^{-1}, \tag{7.34b}$$

$$\boldsymbol{\Theta}_3 = -\boldsymbol{\Omega}_3^{-1}\boldsymbol{\Omega}_2^T\left(\boldsymbol{\Omega}_1 - \boldsymbol{\Omega}_2\boldsymbol{\Omega}_3^{-1}\boldsymbol{\Omega}_2^T\right)^{-1}, \tag{7.34c}$$

$$\boldsymbol{\Theta}_4 = \left(\boldsymbol{\Omega}_3 - \boldsymbol{\Omega}_2^T\boldsymbol{\Omega}_1^{-1}\boldsymbol{\Omega}_2\right)^{-1}; \tag{7.34d}$$

are 2×2 matrices.

Inserting Eqs. (7.21a) - (7.21j) into Eq. (7.32) gives rise to the analytical expression for CRB (Δ) as:

$$\text{CRB}\left(\Delta\right) = \frac{1}{\bar{\varphi}_{11} + Q}, \tag{7.35}$$

in which

$$\begin{aligned} Q =&(\bar{\varphi}_{44}\bar{\varphi}_{12}^2 + \bar{\varphi}_{44}\bar{\varphi}_{13}^2 + \bar{\varphi}_{22}\bar{\varphi}_{14}^2 + \bar{\varphi}_{22}\bar{\varphi}_{15}^2 \\ &- 2\bar{\varphi}_{24}\bar{\varphi}_{12}\bar{\varphi}_{14} - 2\bar{\varphi}_{25}\bar{\varphi}_{12}\bar{\varphi}_{15} + 2\bar{\varphi}_{25}\bar{\varphi}_{13}\bar{\varphi}_{15} - 2\bar{\varphi}_{24}\bar{\varphi}_{13}\bar{\varphi}_{15}) \\ &/(\bar{\varphi}_{24}^2 + \bar{\varphi}_{25}^2 - \bar{\varphi}_{22}\bar{\varphi}_{44}). \end{aligned} \tag{7.36}$$

Note that, by a similar derivation procedure to that above, one can also obtain an analytical expression for the MCRB/HCRB w.r.t. Δ, denoted by MCRB (Δ) and HCRB (Δ), based on the linearized model in Eq. (7.15). The resulting MCRB and HCRB retain the same expression as Eq. (7.35), yet with $\bar{\varphi}_{ij}$ in Eqs. (7.21a) - (7.21j) calculated by replacing $\kappa(N, a, b)/N$ with ν in Eq. (6.37). The analytical expression for the EMCB/MCB w.r.t. Δ, however, cannot be attained in an analogous way.

7.4 The Expression of the ARL

Let δ denote the ARL of the two targets in the model under discussion. Assume, without loss of generality, that the spacing between the two targets

$$\Delta > 0. \tag{7.37}$$

In light of Smith's criterion [58], these two targets can be resolved w.r.t. their electrical angles if Δ is *greater* than the standard deviation of the estimate of Δ (denoted by σ_Δ). Hence, the ARL δ, being *per definitionem* the lower limit of Δ that fulfills the above criterion, is identical to the value of Δ for which

$$\Delta^2 = \sigma_\Delta^2 \tag{7.38}$$

holds.

In addition, it is known that under mild conditions [73]:

$$\sigma_\Delta \approx \sqrt{\text{CRB}(\Delta)}, \tag{7.39}$$

therefore the value of δ can computed as the solution to the following equation:

$$\Delta^2 = \text{CRB}(\Delta), \tag{7.40}$$

which is referred to, conventionally, as *Smith's equation*.

The solution of Smith's equation in Eq. (7.40) is given by substituting the analytical expression of CRB (Δ), given in Eq. (7.35), into Eq. (7.40). In doing so, all the terms containing $\Delta^n,\ n > 4$ are omitted to make the equation easier to solve analytically. Besides, it is known from the parameter transformation property of the CRB [44] that:

$$\text{CRB}(\Delta) = \text{CRB}(-\Delta), \tag{7.41}$$

meaning if Δ is a root of (7.40), then $-\Delta$ will also be a root thereof. Thus one can remove those terms in the equation that contain $\Delta^n,\ n = 1, 3$ (odd powers of Δ) without changing its roots.

As a result of the procedure above, one obtains the following quartic equation of Δ:

$$A\Delta^4 - B\Delta^2 - C = 0, \tag{7.42}$$

where

$$\begin{aligned} A = &\frac{2\kappa(N,a,b)|\alpha_2|^2}{N}\big(\gamma_{11}\gamma_{22}\gamma_{33} + 2\text{Re}\left\{\gamma_{13}\gamma_{12}^*\gamma_{23}^*\right\} \\ &-\gamma_{11}|\gamma_{23}|^2 - \gamma_{22}|\gamma_{13}|^2 - \gamma_{33}|\gamma_{12}|^2\big), \end{aligned} \tag{7.43a}$$

$$B = \gamma_{11}\gamma_{33} - |\gamma_{13}|^2, \tag{7.43b}$$

$$C = \gamma_{11}\gamma_{22} - |\gamma_{12}|^2. \tag{7.43c}$$

The ARL δ is taken as the positive real root of Eq. (7.42), namely:

$$\delta = \sqrt{\frac{B + \sqrt{B^2 + 4AC}}{2A}}, \tag{7.44}$$

while the other roots are trivial and rejected.

7.5 The Existence of the Valid Root

The existence of δ in Eq. (7.44) needs to be proved, which is equivalent to prove that the equation in Eq. (7.42) has one and only one positive real root w.r.t. δ. This can be achieved by transforming Eq. (7.43a) into:

$$A = \frac{2\kappa(N,a,b)|\alpha_2|^2}{N} |\mathbf{\Gamma}|, \tag{7.45}$$

in which $\mathbf{\Gamma}$ is a 3×3 Gramian matrix whose entries are:

$$[\mathbf{\Gamma}]_{i,j} = \gamma_{ij} = \tilde{\boldsymbol{\beta}}_i^H \tilde{\boldsymbol{\beta}}_j, \quad i,j = 1,2,3, \tag{7.46}$$

where

$$\tilde{\boldsymbol{\beta}}_i = \mathbf{\Upsilon}^{\frac{1}{2}} \boldsymbol{\beta}_i. \tag{7.47}$$

From Eqs. (7.19a) - (7.19c) it is clear that $\tilde{\boldsymbol{\beta}}_i,\ i,j = 1,2,3$, are linearly independent from one another, unless when

$$\boldsymbol{d}_{(\mathrm{T})} = p\mathbf{1}_M \tag{7.48}$$

and

$$\boldsymbol{d}_{(\mathrm{R})} = q\mathbf{1}_N, \tag{7.49}$$

both hold, where $\mathbf{1}_M$ and $\mathbf{1}_N$ represent the all-ones column vectors of dimension M and N, respectively, and p and q are constants not both zero. The case that $p = q = 0$ occurs only when the inter-sensor spacings at both the transmitter and the receiver all become zero, which is an invalid condition in practice. Thus the Gramian matrix $\mathbf{\Gamma}$ is *positive definite*, and it is always true that:

$$A > 0. \tag{7.50}$$

Meanwhile, one can show that:

$$B > 0, \tag{7.51}$$

and

$$C > 0, \tag{7.52}$$

by employing the Cauchy-Schwarz inequality to Eqs. (7.43b) and (7.43c), where the equality also holds only under the invalid condition explained above.

It thus follows from Eqs. (7.50), (7.51) and (7.52) that:

$$B^2 + 4AC > 0, \tag{7.53}$$

signifying that Eq. (7.42), when viewed as a quadratic equation w.r.t. δ^2, has two real roots, of which one and only one is positive. Equivalently, Eq. (7.42) as a quartic equation w.r.t. δ, has also one and only one positive root, which has the expression in Eq. (7.44)

7.6 The Asymptotic Expression of the ARL

The expression in Eq. (7.44) has room for further simplification. Consider the structure of γ_{ij} in Eq. (7.22):

$$\begin{aligned}
\gamma_{ij} &= \boldsymbol{\beta}_i^H \boldsymbol{\Upsilon} \boldsymbol{\beta}_j \\
&= \frac{N}{\text{tr}\{\boldsymbol{\Sigma}\}} \sum_{t=1}^{T} \boldsymbol{s}^H(t) \boldsymbol{R}_i^H \boldsymbol{\Sigma}_{\text{n}}^{-1} \boldsymbol{R}_j \boldsymbol{s}(t) \\
&= \frac{N}{\text{tr}\{\boldsymbol{\Sigma}\}} \sum_{t=1}^{T} \sum_{n=1}^{N} \lambda_n \left[\boldsymbol{U}\boldsymbol{R}_i \boldsymbol{s}(t)\right]^H \left[\boldsymbol{U}\boldsymbol{R}_j \boldsymbol{s}(t)\right], \quad i,j = 1,2,3.
\end{aligned} \tag{7.54}$$

in which $\boldsymbol{\Sigma}_{\text{n}}$ is the normalized version of the speckle CM $\boldsymbol{\Sigma}$ for the model under discussion, whose trace is N, $\boldsymbol{U}$ is a matrix containing the singular vectors of $\boldsymbol{\Sigma}_{\text{n}}^{-1}$, with corresponding eigenvalues denoted as $\lambda_n,\ n = 1, \ldots, N$.

From Eq. (7.54), it is obvious that in the asymptotic cases, e.g., large T, N, or high SCR

(which signifies large $\sum_{t=1}^{T} \|\boldsymbol{s}(t)\|^2$ or small tr $\{\boldsymbol{\Sigma}\}$), one has:

$$\gamma_{ij} \gg 0, \quad i,j = 1,2,3. \tag{7.55}$$

Furthermore, since from Eqs. (7.43a) - (7.43c) it holds asymptotically that:

$$A = O(\gamma_{ij}^3), \tag{7.56a}$$

$$B = O(\gamma_{ij}^2), \tag{7.56b}$$

$$C = O(\gamma_{ij}^2), \tag{7.56c}$$

thus,

$$\left(\frac{B}{2A}\right)^2 = O(\gamma_{ij}^{-2}) \ll \left(\frac{C}{A}\right) = O(\gamma_{ij}^{-1}), \tag{7.57}$$

which, applied consecutively to Eq. (7.44), results in:

$$\delta = \sqrt{\frac{B}{2A} + \sqrt{\left(\frac{B}{2A}\right)^2 + \frac{C}{A}}} \approx \sqrt[4]{\frac{C}{A}}, \tag{7.58}$$

which is the proposed asymptotic expression for the ARL δ.

7.7 The ARL and the Texture Parameters

Eq. (7.58) is not only more concise in form, but facilitates one's determining the relationship between the ARL and the texture parameters of the clutter. The derivation follows similar steps as in Sec. 6.4.

First of all, it arises from Eq. (7.22) that:

$$\gamma_{ij} \propto \frac{1}{\text{tr}\,\{\boldsymbol{\Sigma}\}}, \tag{7.59}$$

which, applied to Eqs. (7.43a) and (7.43c), leads to

$$A \propto \kappa(N, a, b) \left(\frac{1}{\text{tr}\{\boldsymbol{\Sigma}\}} \right)^3, \tag{7.60}$$

and

$$C \propto \left(\frac{1}{\text{tr}\{\boldsymbol{\Sigma}\}} \right)^2. \tag{7.61}$$

It follows, by substituting Eqs. (7.60) and (7.61) into Eq. (7.58), that:

$$\delta \propto \sqrt[4]{\frac{\text{tr}\{\boldsymbol{\Sigma}\}}{\kappa(N, a, b)}}, \tag{7.62}$$

and moreover, by invoking Eqs. (6.57) and (6.59), that:

$$\delta \propto \begin{cases} \sqrt[4]{\dfrac{2^{N+a-2}\Gamma(a)}{a \int_0^{+\infty} x^{N+a-1} \frac{K_{a-N-1}^2(x)}{K_{a-N}(x)} \mathrm{d}x}}, & \text{K-distributed clutter,} \\ \sqrt[4]{\dfrac{(a+N+1)(a-1)}{a(a+N)}}, & \text{Student's t-distributed clutter, for } a > 1, \end{cases} \tag{7.63}$$

which shows that, in both cases, δ decreases as a increases (though, again, this relationship for K-distributed clutter can only be determined numerically), meaning that the ARL is *positively correlated* with a.

Furthermore, by combining Eqs. (7.62), (6.58) and (6.60), the independence of the ARL of the scale parameter b for both clutter distributions can be easily observed.

The analysis above shows that the respective impacts of the texture parameters on the ARL are in accordance with that on the CRTBs, as will be certified by simulations.

7.8 The ARL Based on the Other CRTBs

Apart from the ARL based on the standard CRB, one can also obtain its variants based on each of the other CRTBs, by equating Δ^2 to the specific CRTB and finding its valid root. For the ARL based on the EMCB, no closed-form expression seems attainable, and its value

can be numerically evaluated by the procedure we used in [128]. For the ARL based on the MCRB/HCRB, on the other hand, one can use the analytical expression of MCRB (Δ) or HCRB (Δ) proposed at the end of Subsec. 7.3 and obtain an analytical expression for δ by following the same procedure as that in Subsec. 7.4. In this case, δ retains the expression as Eqs. (7.44) and (7.58), with only the difference that in the expression of A in Eq. (7.43a) $\kappa(N, a, b)/N$ is replaced by $\nu(a, b)$.

Chapter 8

Numerical Simulations

8.1 The Three Proposed Estimators and the CRTBs

8.1.1 Simulation Context

The context for simulations in relation with the proposed estimators and the CRTBs is based on the general MIMO radar model introduced in Ch. 2. Consider, unless otherwise stipulated, a bistatic co-located MIMO radar, comprising $M = 3$ sensors at the transmitter and $N = 4$ at the receiver, both with half-wave length inter-element spacing. The number of radar pulses per CPI $L = 15$, and each pulse contains $T = 5$ snapshots. Two far-field, narrowband, point-source targets are illuminated by the MIMO radar. The DOD and DOA of the first source are respectively $18°$ and $20°$, and of the second source are $45°$ and $40°$. Both the real and the imaginary parts of the coefficients $\alpha_i(l),\ i = 1, 2,\ l = 0, L-1$, as well as the values of the normalized Doppler frequency shifts $f_i(l),\ i = 1, 2,\ l = 0, L-1$, are randomly drawn from the uniform distribution on the interval $[-1, 1]$. For K-distributed clutter, choose $a = 2$ and $b = 10$; and for t-distributed clutter, $a = 1.1$ and $b = 2$. The entries of the speckle CM $\mathbf{\Sigma}$ are generated by [133]:

$$[\mathbf{\Sigma}]_{m,n} = \sigma^2 0.9^{|m-n|} e^{j\frac{\pi}{2}(m-n)},\ m, n = 1, \ldots, MN, \tag{8.1}$$

in which σ^2 is a factor to adjust speckle power. Each point of the MSEs in the figures is generated by averaging the results of 100 Monte-Carlo trials.

8.1.2 Simulation Results on the Proposed Estimators

Figs. 8.1-8.4 investigates the performance of the three proposed estimators, by comparing their resulting MSEs for the estimation of $\boldsymbol{\theta}$ with the MSEs produced by the CMLE in Eq. (3.21), as well as with the CRB derived in Ch. 6. In Figs. 8.1 and 8.2, the MSEs under K-distributed clutter are plotted, versus the pulse number L and the SCR, respectively; and in Figs. 8.3 and 8.4 the MSEs under t-distributed clutter, also versus the pulse number and the SCR (defined in Eq. (6.56)), respectively.

From Figs. 8.1-8.4, it becomes obvious that the conventional algorithm (CMLE) becomes poor when the clutter is a SIRP, and all the three proposed algorithms lead to substantial superior performance.

Figs. 8.1-8.4 also show that as few as two iterations for the IMLE and the IMAPE, and generally only one iteration for the IEMLE, is enough for the respective estimators to have a satisfactory performance in terms of a resulting MSE appropriately close to the CRB, in asymptotic L and SCR cases.

Furthermore, one can see from Figs. 8.1-8.4 that the performance of the IEMLE, which is a theoretically optimum estimator, is superior to that of the IMLE and the IMAPE, especially in adverse scenarios (cf., e.g., Fig. 8.3). In asymptotic cases, the difference in performance between the IMEMLE and the other two proposed estimators becomes small, and in certain scenarios, this difference becomes negligible (cf., e.g., Fig. 8.2). On the other hand, the difference between the performance of the IMLE and the IMAPE is not obvious. In certain scenarios, e.g., in those for Figs. 8.2 and Fig. 8.4, the IMAPE has a slightly but almost constantly better performance than the IMLE. This (though slight) performance improvement comes from the exploitation of a priori knowledge of the texture distribution in the parameter estimation, despite the fact that the texture parameters in the distribution function are unknown and need to be estimated.

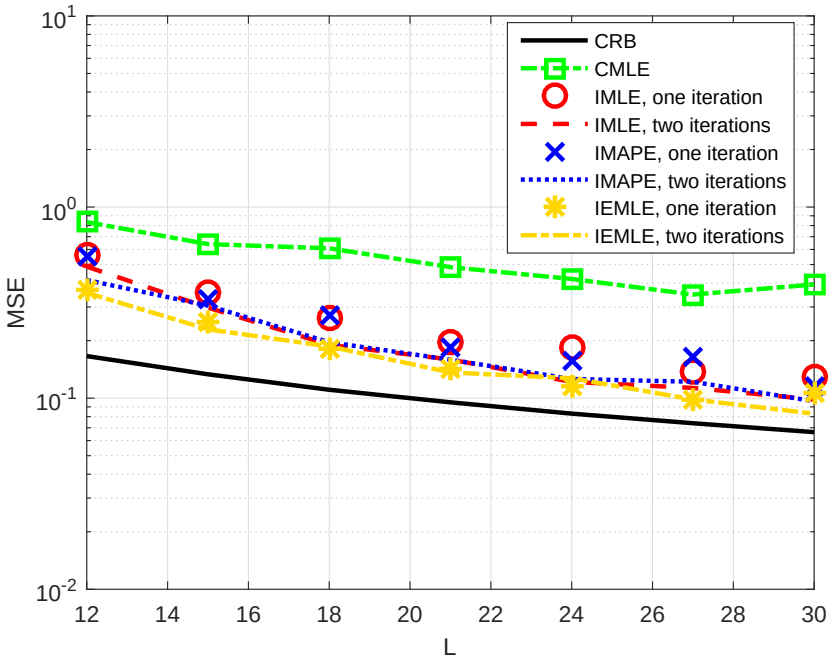

Figure 8.1: MSE vs. L under K-distributed clutter, SCR $= 15$dB.

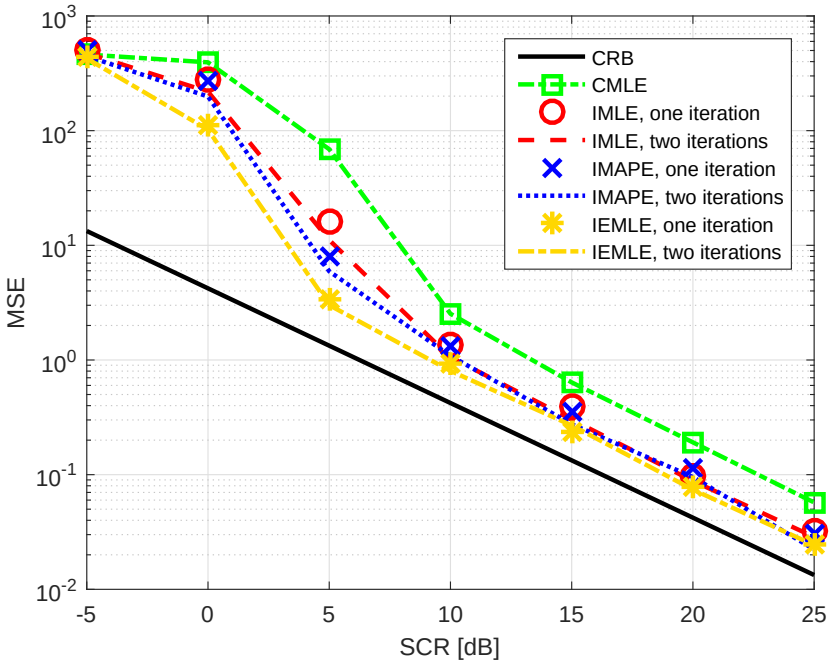

Figure 8.2: MSE vs. SCR under K-distributed clutter.

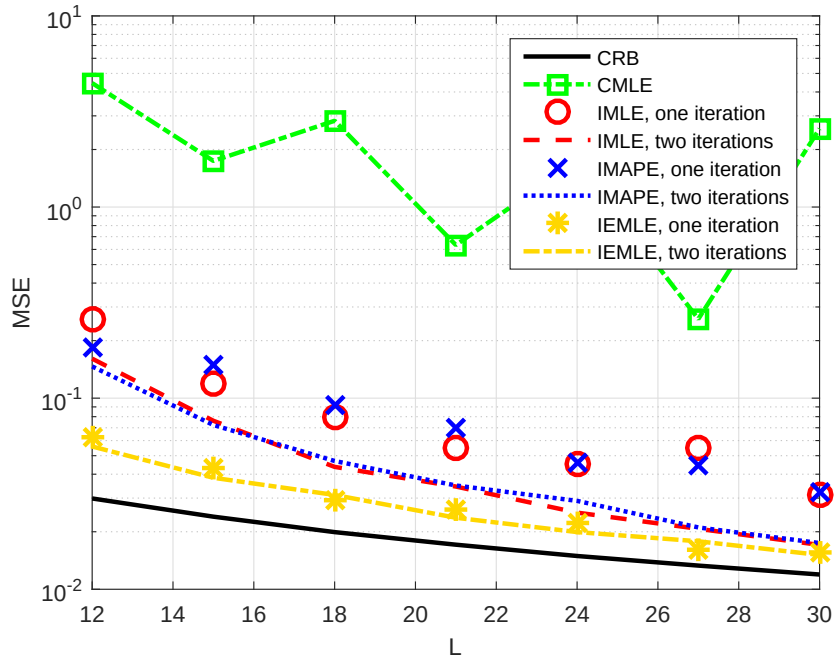

Figure 8.3: MSE vs. L under t-distributed clutter, SCR $= 15$dB.

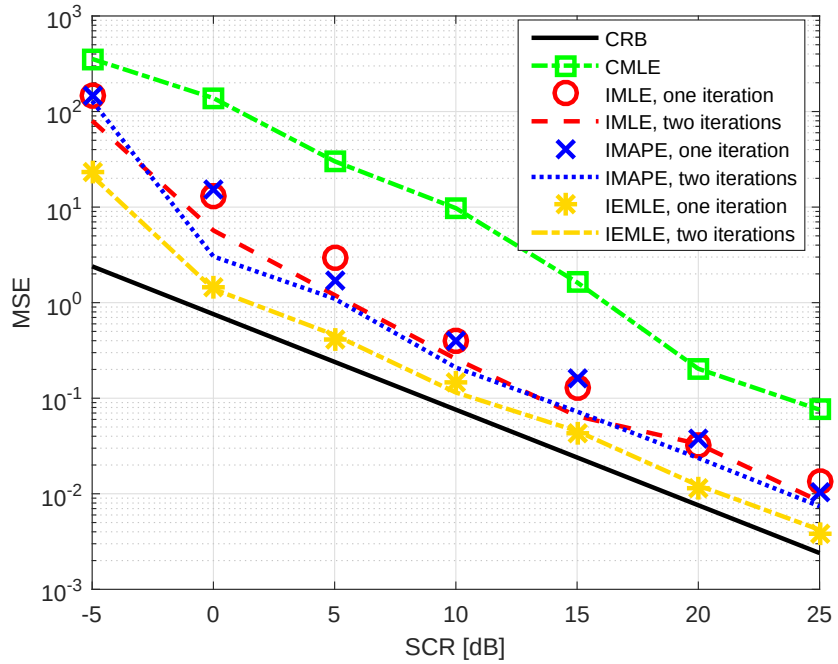

Figure 8.4: MSE vs. SCR under t-distributed clutter.

8.1.3 Simulation Results on the CRTBs

In Fig. 8.5 are plotted the CRTBs derived in Ch. 6 under K-distributed clutter, and in Fig. 8.6 under t-distributed clutter, versus L and MN, respectively. In both figures are also added, for comparison, the CRB under Gaussian clutter assumption (for which $\kappa = MN$).

From Figs. 8.5 and 8.6, one can observe that these bounds exhibit exactly the same relationships as were explained in Sec. 6.3, namely, that both the EMCB/MCB and the CRB is larger than the MCRB/HCRB, to which the EMCB/MCB approaches as L gets larger, or the CRB approaches as MN does. Furthermore, the EMCB is indifferent to the change of MN, and the CRB to that of L, in terms of their relative distance to the MCRB/HCRB. Which of the two is larger is then *indefinite* and depends on the specific choice of L and MN. Furthermore, one can see that the CRB under a SIRP clutter assumption is lower than that under the Gaussian one, which is in accordance with the result in [134], where it was proved that the CRB under the Gaussian data assumption is the *worst-case* one.

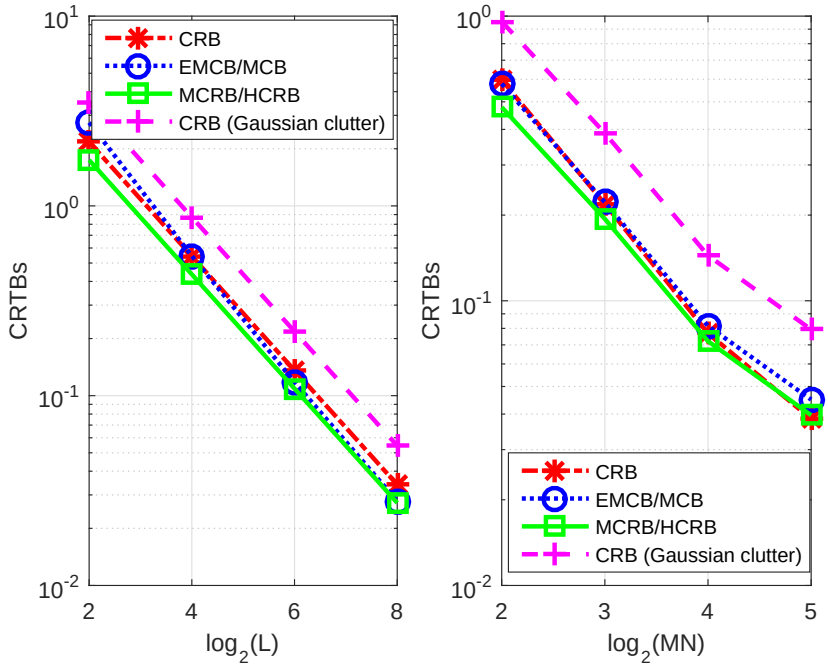

Figure 8.5: Left: CRTBs vs. L, $M = 2$, $N = 2$; right: CRTBs vs. MN. Both under K-distributed clutter, SCR $= 20$dB.

The respective impacts of the texture parameters on the CRTBs are examined in Fig. 8.7

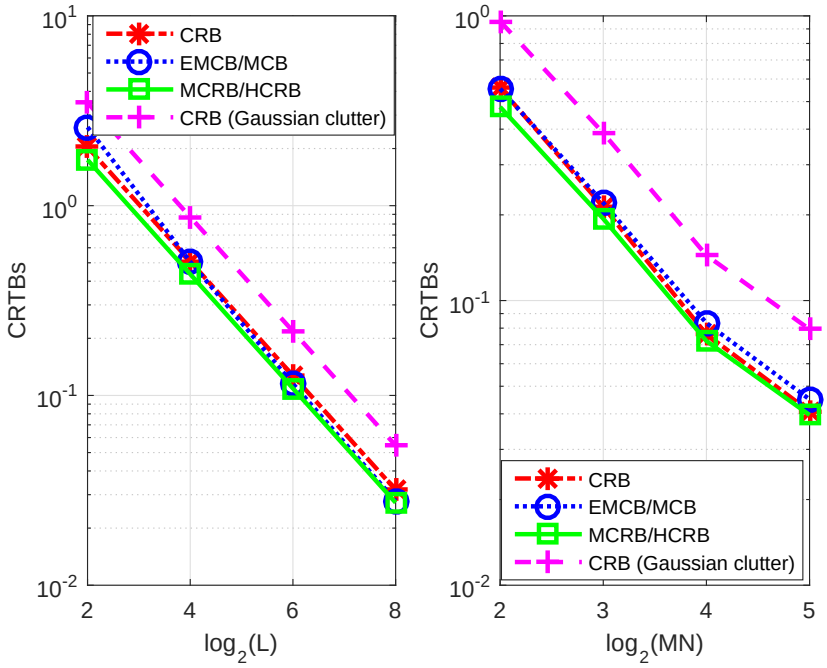

Figure 8.6: Left: CRTBs vs. L, $M = 2$, $N = 2$; right: CRTBs vs. MN. Both under t-distributed clutter with $a = 2$, $b = 10$, SCR $= 20$dB.

under K-distributed clutter, and in Fig. 8.8 under t-distributed clutter, by plotting, in the left part of both figures, the CRTBs versus a under fixed b, and in the right versus b under fixed a (the CRB under Gaussian clutter assumption is also plotted in all the four cases for comparison).

The results shown in Figs. 8.7 and 8.8 are in exact accordance with what has been discussed in Sec. 6.4, that for both clutter distributions, the CRTBs increase with a and remain indifferent to the change of b. It is noticable that the EMCB under K-distributed clutter, whose relationship with a and b has not been analytically established, also follows the same rule as the other CRTBs.

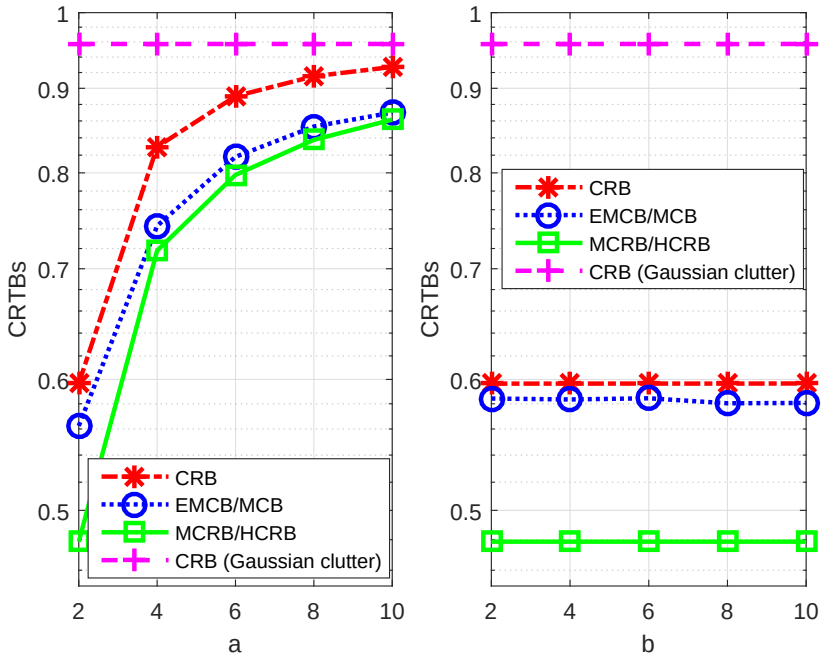

Figure 8.7: Left: CRTBs vs. a; right: CRTBs vs. b. Both under K-distributed clutter, SCR $= 20$dB.

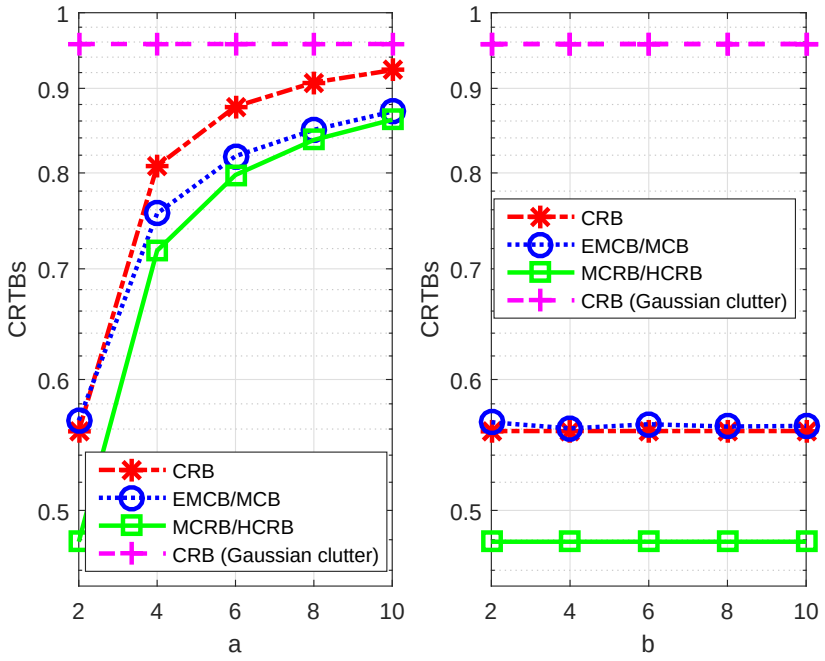

Figure 8.8: Left: CRTBs vs. a; right: CRTBs vs. b. Both under t-distributed clutter with $a = 2$, $b = 10$, SCR $= 20$dB.

8.2 The ARL

8.2.1 Simulation Context

The context for simulations concerning the proposed ARL expressions in Ch. 7 is one based on the simplified model in Sec. 7.1. specifically, consider a monostatic collocated MIMO radar comprising $M = 6$ sensors at the transmitter and $N = 8$ at the receiver, both with half-wave length inter-element spacing. The DOD/DOA of the first target is $60°$, and the angular spacing Δ between the targets has the value of 1. Furthermore, the coefficients α_1 and α_2 are chosen to be $2 + 0.5j$ and $1 - 3j$, respectively. The snapshot number $T = 6$. Both the real and imaginary parts of the entries of the target source vectors $\boldsymbol{s}(t)$ are generated within the interval $[-1, 1]$. For K-distributed clutter, choose $a = 2$ and $b = 10$; and for t-distributed clutter, $a = 1.1$ and $b = 2$. The entries of the speckle CM $\boldsymbol{\Sigma}$ are generated, similar to Eq. (8.1) in Sec. 8.1, by $[\boldsymbol{\Sigma}]_{m,n} = \sigma^2 \cdot 0.9^{|m-n|} e^{j\frac{\pi}{2}(m-n)},\ m, n = 1, \ldots, N$.

8.2.2 Simulation Results on the ARL

Fig. 8.9 verifies, under both K-distributed and t-distributed clutters, the proposed analytical expressions of the ARL in Eqs. (7.44) and (7.58) (denoted in the figure by δ_2 and δ_3, respectively), by plotting them versus the SCR together with the *exact* ARL (denoted in the figure by δ_1), which is obtained by numerically solving Smith's equation based on the model Sec. 7.1 before linearization, thus without any approximation.

Fig. 8.9 shows clearly that the values of the three curves essentially coincide in asymptotic cases (above 0 dB in the context) for both distributions of clutter, thereby demonstrates the validity of the proposed analytical expressions for the ARL in Eqs. (7.44) and (7.58).

In Figs. 8.10 and 8.11, the respective impacts of the texture parameters a and b on the ARL are investigated under K-distributed and t-distributed clutters, respectively. Again, by fixing one of the two parameters and varying the other, one compares the resulting ARLs.

It can be seen from Figs. 8.10 and 8.11 that δ increases with a, but remains invariant w.r.t. changes in b, as discussed in Sec. 7.7. The ARL under Gaussian clutter assumption is also plotted for comparison, which upper-bounds all the ARL results obtained under the

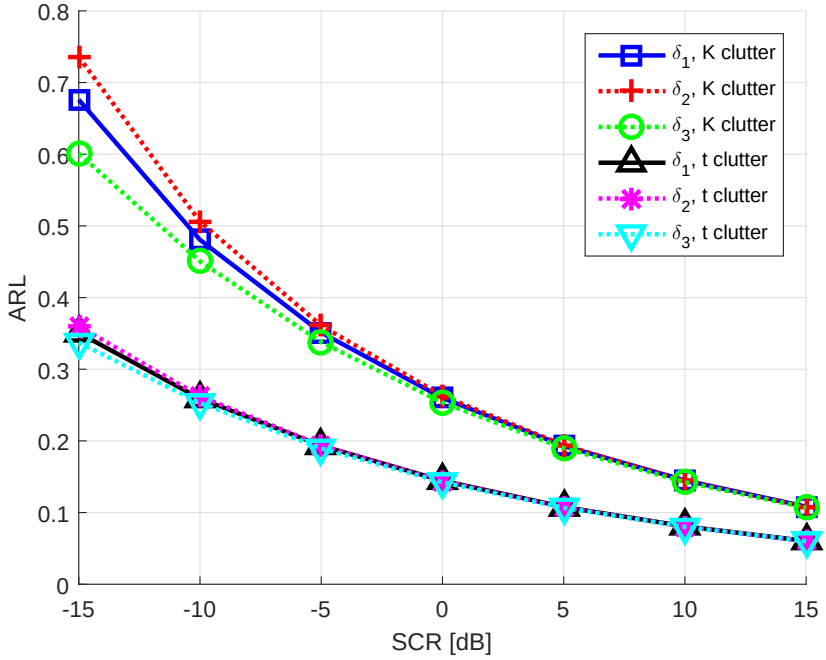

Figure 8.9: ARL vs. SCR under K-distributed and t-distributed clutters.

various SIRP clutter models considered. In fact it can be stated, as a direct generalization to the conclusion in [134], that for given noise power, the targets under Gaussian noise are the most difficult to be correctly resolved.

Finally, Fig. 8.12 examines the respective impacts of the power of the two targets on the ARL, by plotting the exact ARL (denoted by δ_1) and the analytical ARL in Eqs. (7.44) (denoted by δ_2) for both distributions of clutter, with the power (represented by the absolute value of the RCS factor) of one of the sources fixed and the other varying. From Fig. 8.12 one may observe that, while the ARL decreases with an increasing $|\alpha_2|$, it is independent of the value of $|\alpha_1|$. One may also gain insight into this from our expression in Eq. (7.43a), which is only dependent on $|\alpha_2|$. This follows from the fact that in the model in Sec. 7.1 the DOD/DOA of the first source is considered to be known, and the second unknown. Thus, increasing the power of the known source is of no avail in meliorating the resolvability of the sources, and the ARL depends solely on the concrete value of the power of the unknown source, rather than the relative ratio between the power of the two sources.

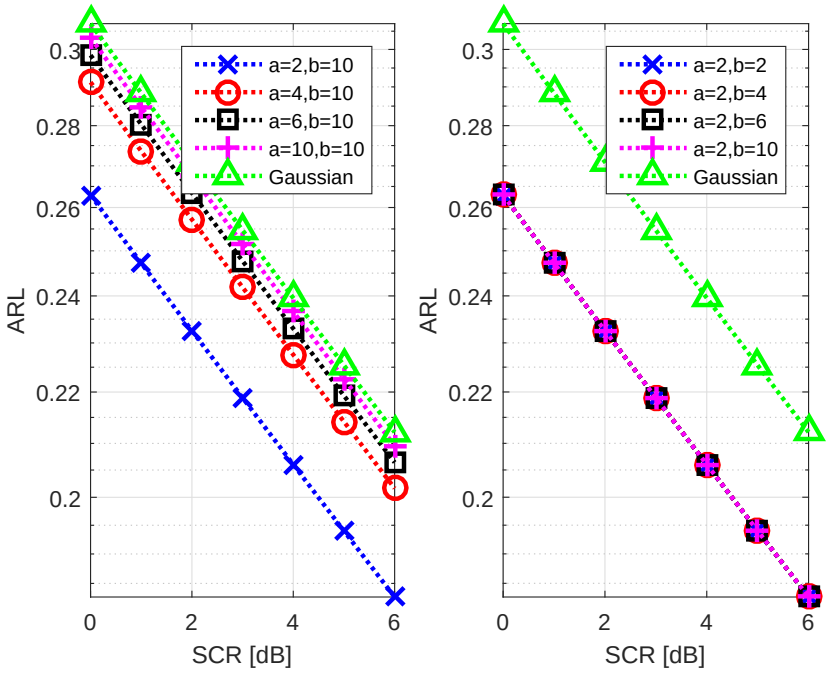

Figure 8.10: ARL vs. SCR. Left: varying a, fixed b; right: varying b, fixed a. Both under K-distributed clutter.

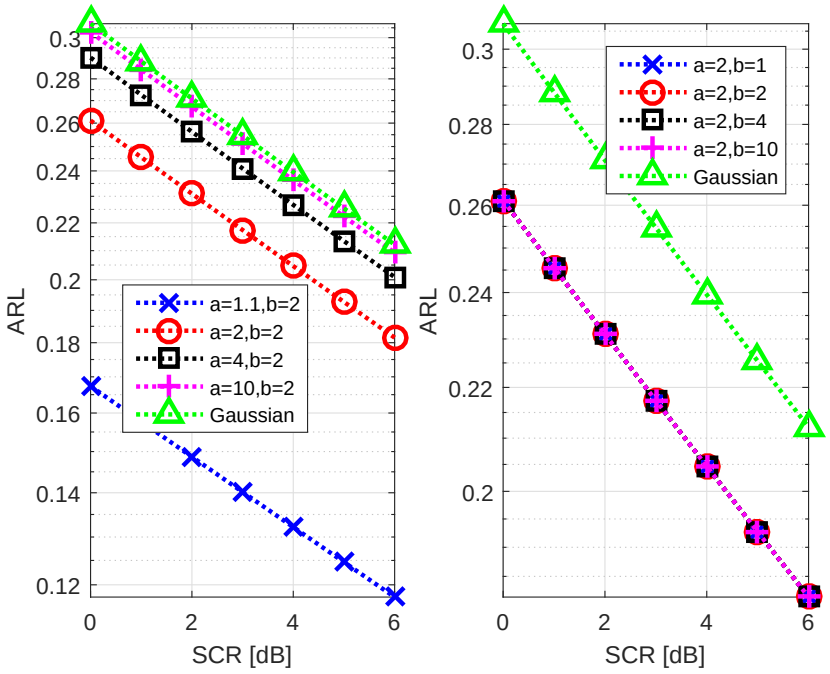

Figure 8.11: ARL vs. SCR. Left: varying a, fixed b; right: varying b, fixed a. Both under t-distributed clutter.

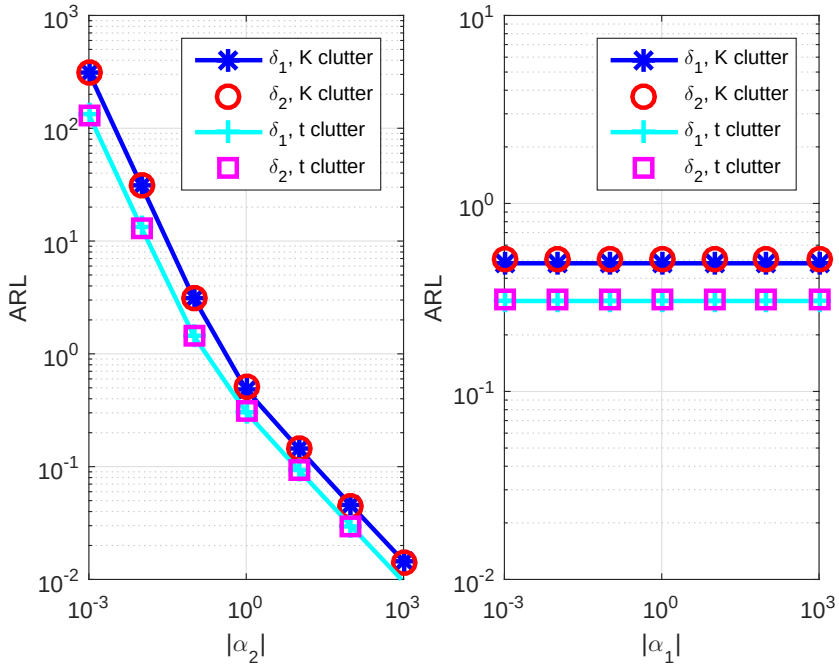

Figure 8.12: Left: ARL vs. $|\alpha_2|$, $|\alpha_1| = 1$; right: ARL vs. $|\alpha_1|$, $|\alpha_2| = 1$. Both under K-distributed and t-distributed clutters.

Chapter 9

Conclusions and Outlook

9.1 Conclusions

This thesis is dedicated to a systematic and comprehensive investigation into the DOD/DOA estimation problem for MIMO radar targets in the presence of SIRP clutter, both in respect of algorithm design and of performance analysis. The three proposed independent but interconnected estimators in Chs. 3, 4 and 5, which employ the stepwise numerical concentration approach, are proved by the simulation results in Ch. 8 to be both performant and considerably computationally efficient, as all of them require only a few iterations to attain convergence, and lead to significantly superior performance than the conventional ML approach.

The IMLE proposed in Chs. 3 considers the texture realizations as unknown parameters and ignores the statistical distribution of the texture. Thus it is the most robust among the three proposed estimators, as it does not require any knowledge of the texture distribution. By using the estimated texture realizations as weighting factors in its objective function, it achieves significantly better performance than the conventional ML estimator. Furthermore, it is the computationally simplest among the three proposed estimators, because it does not entail any numerical calculation of integrals, nor does it need to numerically solve nonlinear equations to obtain the estimates of the texture parameters.

The IMAPE proposed in Chs. 4, on the other hand, can be seen as a generalization of the IMLE from a Bayesian point of view. It also considers texture realizations, but exploits

at the same time the information from the texture distribution to improve the estimation accuracy. Furthermore, unlike the IMLE, the IMAPE can also be used to estimate the texture parameters if this is a task.

The IEMLE proposed in Chs. 5, by considering the exact LLF, is a theoretically optimum estimator. The IEMLE does not consider the texture realizations, but only the texture distribution (in terms of the texture parameters). The objective function of the IEMLE, by taking the form of multiplication other than summation, is essentially different from the one of the IMLE and the IMAPE. In such a way, it can focus on the best pulses, while the IMLE and the IMAPE treat all pulses equally. Thus, it has the superior performance among the three proposed estimators, especially in adverse scenarios.

As measures of performance for the proposed algorithms, expressions for various CRTBs w.r.t. DOD/DOA parameters are derived in Ch. 6, and their relationships are analytically compared. Furthermore, inspection of the texture parameters' respective effects on the CRTBs reveals that all of the CRTBs have a positive correlation with the shape parameter, but are all independent of the scale parameter. Thus the achievable estimation accuracy diminishes as the shape parameter increases, but is not affected by the change of the scale parameter. The reason for this is that, with fixed clutter power, an increase in the value of the shape parameter causes the clutter to become more heavy-tailed, signifying a larger portion of clutter power being decentralized; on the other hand, changing the scale parameter's value does not result in any change in the PDF of the clutter. Moreover, the CRTBs under a SIRP clutter model are upper-bounded by those under a Gaussian one (with the same clutter power), meaning that the achievable performance for estimation problems in the presence of the SIRP clutter is always better than that in the presence of the Gaussian clutter.

Apart from the CRTBs, this thesis also studies another important performance measure of estimation problems, namely, the target resolvability quantified by the RL. Based on the non-matrix form expression for the CRB w.r.t. the target spacing, which is derived as a by-product, two analytical expressions for the ARL are obtained in Ch. 7. The effects of the texture parameters on the ARL are then explored, which are analogous to their effect on the CRTBs. Furthermore, the proposed ARL expressions reveal that increasing the power of

the known source cannot meliorate the resolvability of the sources, and the ARL depends solely on the concrete value of the power of the unknown source, rather than the relative ratio between the power of the two sources.

The analytical findings on the CRTBs and the ARL are also numerically corroborated by simulations in Ch. 8.

9.2 Outlook

Proceeding from the contributions of this thesis summarized above, possible future works may include, first of all, finding appropriate, more competent numerical analysis methods for the calculation of numerical integrals involved in the IEMLE for K-distributed clutter case, as well as for the numerical nonlinear equation solving problems involved both in the IMAPE and the IEMLE. These numerical calculations constitute a major factor that adds to the computational costs of the proposed algorithms (though they are generally already substantially more computationally efficient as compared with some other iterative, e.g., PX-EM-based algorithms).

The proposed algorithms can also be applied to MIMO radar detection problems with unknown target DOD/DOA parameters and other research topics based on such detection problems, e.g., the RL based on the GLRT.

Furthermore, as generalizations of the DOA estimation algorithms in [106] and [123] to the SIRP clutter case, the proposed algorithms in this thesis also have the potential to be generalized, in their turn, to more complicated clutter cases. One such possibility is the case where the whole radar noise is modeled as a mixture of SIRP and Gaussian clutter/noise. This modeling not only becomes necessary in scenarios where the thermal noise (modeled as Gaussian) cannot be ignored compared with the clutter (modeled as a SIRP) [135, 136], but can also be used to describe contemporaneous backscattering by ground/clouds (whose clutter is modeled as Gaussian) and sea (whose clutter is modeled as a SIRP) [28, 137]. A main challenge of the generalization of the proposed algorithms to such a SIRP-Gaussian mixture clutter context is that, under this model, the expressions of the LLFs become more complicated, therefore many of the unknown parameter estimates that have closed-form ex-

pressions under SIRP clutter model can no longer have them, if no approximation is made to the LLFs. However, at least for certain special cases, e.g., the case of white Gaussian speckle, this problem disappears, and the generalization in question becomes rather straightforward.

Besides the SIRP-Gaussian mixture clutter model above, there are also two important non-Gaussian clutter models related to the SIRP model, to which the proposed algorithms have the potential to be generalized. One of them is the so-called generalized Bessel K (GBK) distributed clutter, proposed in [138], the class of which partially overlaps that of the SIRPs, but covers a wider variety of distributions. The other is the so-called complex elliptically symmetric (CES) distributed clutter [139], which constitutes a broader class to which SIRPs belong. Both models have till now attracted considerable research interest concerning radar detection/estimation problems [138, 140–145], and the generalization of the proposed algorithms to these more general non-Gaussian clutter models is of significant practical value.

In parallel to the proposed algorithms, the expressions for the CRTBs w.r.t. DOD/DOA paramters and for the ARL are also worth investigation under the framework of the SIRP-Gaussian mixture, the GBK and the CES clutter models.

Bibliography

[1] E. Fishler, "MIMO radar: an idea whose time has come," in *Proc. IEEE Radar Conference*, Philadelphia, PA, Apr. 2004, pp. 71–78.

[2] J. Li and P. Stoica, "MIMO radar with colocated antennas," *IEEE Signal Processing Mag.*, vol. 24, no. 5, pp. 106–114, Sep. 2007.

[3] ——, *MIMO radar Signal Processing*. New York: Wiley-Interscience, Oct. 2008.

[4] A. Haimovich, R. Blum, and L. Cimini, "MIMO radar with widely separated antennas," *IEEE Signal Processing Mag.*, vol. 25, pp. 116–129, Jan. 2008.

[5] E. Fishier, A. Haimovich, R. Blum, L. Cimini, D. Chizhik, and R. Valenzuela, "Statistical MIMO radar," in *Proc. Adaptive Sensor Array Processing (ASAP) Workshop*, Lexington, MA, Mar. 2004.

[6] D. W. Bliss and K. W. Forsythe, "Multiple-input multiple-output (MIMO) radar and imaging: Degrees of freedom and resolution," in *Proc. 37th Asilomar Conf. Signals, Syst. Comput.*, vol. 1, Pacifc Grove, CA, Nov. 2003, pp. 54–59.

[7] D. J. Rabideau and P. Parker, "Ubiquitous MIMO multifunction digital array radar," in *Proc. 37th Asilomar Conf. Signals, Syst. Comput.*, vol. 1, Pacifc Grove, CA, Nov. 2003, p. 1057–1064.

[8] E. Fishler, A. M. Haimovich, R. S. Blum, J. L. J. Cimini, D. Chizhik, and R. A. Valenzuela, "Spatial diversity in radars-models and detection performance," *IEEE Trans. Signal Processing*, vol. 54, no. 3, p. 823–838, Mar. 2006.

[9] N. H. Lehmann, A. M. Haimovich, R. S. Blum, and L. J. Cimini, "High resolution capabilities of MIMO radar," in *Proc. 40th Asilomar Conf. Signals, Syst. Comput.*, Pacifc Grove, CA, Nov. 2006, pp. 25–30.

[10] E. F. Knott, J. F. Schaeffer, and M. T. Tulley, *Radar Cross Section*, 2nd ed. Boston: Artech House, 1993.

[11] I. Bekkerman and J. Tabrikian, "Target detection and localization using MIMO radars and sonars," *IEEE Trans. Signal Processing*, vol. 54, no. 10, pp. 3873–3883, Oct. 2006.

[12] C.-Y. Chen and P. P. Vaidyanathan, "MIMO radar space-time adaptive processing using prolate spheroidal wave functions," *IEEE Trans. Signal Processing*, vol. 56, no. 2, pp. 623–635, Feb. 2008.

[13] X. Wang, W. Wang, J. Liu, X. Li, and J. Wang, "A sparse representation scheme for angle estimation in monostatic MIMO radar," *Signal Processing*, vol. 104, pp. 258–263, Nov. 2014.

[14] W. Wang, X. Wang, H. Song, and Y. Ma, "Conjugate ESPRIT for DOA estimation in monostatic MIMO radar," *Signal Processing*, vol. 93, no. 7, p. 2070–2075, Jul. 2013.

[15] M. Jin, G. Liao, and J. Li, "Joint DOD and DOA estimation for bistatic MIMO radar," *Signal Processing*, vol. 89, no. 2, pp. 244–251, Feb. 2009.

[16] J. Chen, H. Gu, and W. Su, "A new method for joint DOD and DOA estimation in bistatic MIMO radar," *Signal Processing*, vol. 2, pp. 714–718, Feb. 2010.

[17] H. W. Chen, D. Yang, H.-Q. Wang, X. Li, and Z. Zhuang, "Direction finding for bistatic MIMO radar using EM maximum likelihood algorithm," *Progress In Electromagnetics Research*, vol. 141, pp. 99–116, Jul. 2013.

[18] T.-Q. Xia, "Joint diagonalization based DOD and DOA estimation for bistatic MIMO radar," *Signal Processing*, vol. 108, pp. 159–166, Mar. 2015.

[19] B. R. Mahafza, *Radar Systems Analysis and Design Using MATLAB*, 3rd ed. CRC Press, 2013.

[20] J. B. Billingsley, "Ground clutter measurements for surface-sited radar," Massachusetts Inst. Technol., Cambridge, MA, Tech. Rep. 780, Feb. 1993.

[21] F. Gini, M. V. Greco, M. Diani, and L. Verrazzani, "Performance analysis of two adaptive radar detectors against non-Gaussian real sea clutter data," *IEEE Trans. Aerosp. Electron. Syst.*, vol. 36, no. 4, pp. 1429–1439, Oct. 2000.

[22] K. Yao, "Spherically invariant random processes: Theory and applications," in *Communications, Information and Network Security*, V. K. B. *et al.*, Ed., 2002, pp. 315–332.

[23] ——, "A representation theorem and its applications to spherically invariant random processes," *IEEE Trans. Inf. Theory*, vol. 19, no. 5, pp. 600–608, Sep. 1973.

[24] M. Rangaswamy, D. D. Weiner, and A. Ozturk, "Non-Gaussian vector identification using spherically invariant random processes," *IEEE Trans. Aerosp. Electron. Syst.*, vol. 29, no. 1, pp. 111–124, Jan. 1993.

[25] A. M. Vershik, "Some characteristic properties of Gaussian stochastic processes," *Theory Probab. Appl.*, vol. 9, no. 2, pp. 353–356, 1964.

[26] E. Jakeman and P. N. Pusey, "A model for non-Rayleigh sea echo," *IEEE Trans. Antennas Propag.*, vol. 24, no. 6, pp. 806–814, Nov. 1976.

[27] E. Conte and G. Ricci, "Performance prediction in compound-Gaussian clutter," *IEEE Trans. Aerosp. Electron. Syst.*, vol. 30, no. 2, pp. 611–616, Apr. 1994.

[28] F. Gini, "Sub-optimum coherent radar detection in a mixture of K-distributed and Gaussian clutter," *IEE Proceedings - Radar, Sonar and Navigation*, vol. 114, no. 1, pp. 39–48, Feb. 1997.

[29] M. Greco, F. Bordoni, and F. Gini, "X-band see-clutter nonstationarity: Influence of long waves," *IEEE J. Ocean. Eng.*, vol. 29, no. 2, pp. 269–283, Apr. 2004.

[30] M. Rangaswamy, "Spherically invariant random processes for modeling non-Gaussian radar clutter," in *Proc. 27th Asilomar Conf. Signals, Syst. Comput.*, vol. 2, Pacifc Grove, CA, Nov. 1993, pp. 1106–1110.

[31] H. Krim and M. Viberg, "Two decades of array signal processing research: the parametric approach," *IEEE Signal Processing Mag.*, vol. 13, no. 4, pp. 67–94, 1996.

[32] D. H. Johnson and D. E. Dudgeon, *Array Signal Processing: Concepts and Techniques*, 1st ed. Prentice-Hall, 1993.

[33] P. Stoica and R. L. Moses, *Spectral Analysis of Signals*. NJ: Prentice Hall, 2005.

[34] R. Schmidt, "Multiple emitter location and signal parameter estimation," *IEEE Trans. Antennas Propagat.*, vol. 34, no. 3, pp. 276–280, Mar. 1986.

[35] P. Stoica and A. Nehorai, "MUSIC, maximum likelihood and Cramer-Rao bound," *IEEE Trans. Acoust., Speech, Signal Processing*, vol. 37, no. 5, pp. 720–741, May 1989.

[36] H. Krim, P. Forster, and J. G. Proakis, "Operator approach to performance analysis of root-MUSIC and root-min-norm," *IEEE Trans. Signal Processing*, vol. 40, no. 7, pp. 1687–1696, Jul. 1992.

[37] B. Rao and K. Hari, "Performance analysis of root-MUSIC," *IEEE Trans. Acoust., Speech, Signal Processing*, vol. 37, no. 12, pp. 1939–1949, Dec. 1989.

[38] J. Mosher and R. Leahy, "Source localization using recursivaly applied and projected (rap) music," *IEEE Trans. Signal Processing*, vol. 47, pp. 332–340, Feb. 1999.

[39] R. Roy, A. Paulraj, and T. Kailath, "ESPRIT a subspace rotation approach to estimation of parameters of cisoids in noise," *IEEE Trans. Acoust., Speech, Signal Processing*, vol. 34, pp. 1340–1342, 1986.

[40] N. Yuen and B. Friedlander, "Performance analysis of higher order ESPRIT for localization of near-field sources," *IEEE Trans. Signal Processing*, vol. 46, pp. 709–719, Mar. 1998.

[41] K. Wong and M. Zoltowski, "Uni-vector-sensor ESPRIT for multisource azimuth, elevation, andpolarization estimation," *IEEE Trans. Antennas Propagat.*, vol. 45, no. 10, pp. 1467–1474, Oct. 1997.

[42] J. Li and R. Compton, "Angle and polarization estimation using esprit with a polarizationsensitive array," *IEEE Trans. Antennas Propagat.*, vol. 39, no. 9, pp. 1376–1383, Sep. 1991.

[43] M. Haardt and J. Nossek, "3-D unitary ESPRIT for joint 2-D angle and carrier estimation," in *Proc. of IEEE Int. Conf. Acoust., Speech, Signal Processing (ICASSP)*, vol. 1, Munich, Germany, 1997, pp. 255–258.

[44] S. M. Kay, *Fundamentals of Statistical Signal Processing : Estimation Theory*. NJ: Prentice Hall, 1993, vol. 1.

[45] J. F. Böhme, "Estimation of source parameters by maximum likelihood and non linear regression," in *Proc. of IEEE Int. Conf. Acoust., Speech, Signal Processing (ICASSP)*, 1984, pp. 731–734.

[46] M. Wax, "Detection and localization of multiple sources in noise with unknown covariance," *IEEE Trans. Signal Processing*, vol. 40, no. 1, pp. 245–249, Jan. 1992.

[47] A. G. Jaffer, "Maximum likelihood direction finding of stochastic sources: a separable solution," in *Proc. of IEEE Int. Conf. Acoust., Speech, Signal Processing (ICASSP)*, New York, 1988.

[48] J. F. Böhme, "Estimation of spectral parameters of correlated signals in wavefields," *Signal Processing*, vol. 10, pp. 329–337, 1986.

[49] H. L. VanTrees, *Detection, Estimation and Modulation Theory*. New York: Wiley, 1968, vol. 1.

[50] A. Renaux, P. Forster, E. Chaumette, and P. Larzabal, "On the high SNR conditional maximum-likelihood estimator full statistical characterization," *IEEE Trans. Signal Processing*, vol. 12, no. 54, pp. 4840–4843, Dec. 2006.

[51] B. Ottersten, M. Viberg, P. Stoica, and A. Nehorai, "Exact and large sample maximum likelihood techniques for parameter estimation and detection in array processing," in *Radar Array Processing*, S. Haykin, J. Litva, and T. J. Shepherd, Eds. Berlin: Springer-Verlag, 1993, ch. 4, pp. 99–151.

[52] F. Gini and R. Reggiannini, "On the use of Cramér-Rao-like bounds in the presence of random nuisance parameters," *IEEE Trans. Commun.*, vol. 48, no. 12, pp. 2120–2126, Dec. 2000.

[53] R. W. Miller and C. B. Chang, "A modified Cramér-Rao bound and its applications," *IEEE Trans. Inform. Theory*, vol. 24, no. 3, pp. 398–400, May 1978.

[54] I. Reuven and H. Messer, "A Barankin-type lower bound on the estimation error of a hybrid parameter vector," *IEEE Trans. Inform. Theory*, vol. 43, no. 3, pp. 1084–1093, May 1997.

[55] S. Narasimhan and J. Krolik, "Fundamental limits on acoustic source range estimation performance in uncertain ocean channels," *J. Acoust. Soc. Am.*, vol. 97, no. 1, pp. 215–226, Jan. 1995.

[56] A. N. D'Andrea, U. Mengali, and R. Reggiannini, "The modified Cramér-Rao bound and its application to synchronization problems," *IEEE Trans. Commun.*, vol. 42, no. 2/3/4, pp. 1391–1399, Feb./Mar./Apr. 1994.

[57] F. Gini, R. Reggiannini, and U. Mengali, "The modified Cramér-Rao bound in vector parameter estimation," *IEEE Trans. Commun.*, vol. 46, no. 1, pp. 52–60, Jan. 1998.

[58] S. T. Smith, "Statistical resolution limits and the complexified Cramér Rao bound," *IEEE Trans. Signal Processing*, vol. 53, no. 5, pp. 1597–1609, May 2005.

[59] M. Shahram and P. Milanfar, "On the resolvability of sinusoids with nearby frequencies in the presence of noise," *IEEE Trans. Signal Processing*, vol. 53, no. 7, pp. 2579–2588, Jul. 2005.

[60] M. N. El Korso, R. Boyer, A. Renaux, and S. Marcos, "Statistical resolution limit for multiple parameters of interest and for multiple signals," in *Proc. of IEEE Int. Conf. Acoust., Speech, Signal Processing (ICASSP)*, Dallas, TX, Mar. 2010, pp. 3602–3605.

[61] H. Cox, "Resolving power and sensitivity to mismatch of optimum array processors," *J. Acoust. Soc.*, vol. 54, no. 3, pp. 771–785, Mar. 1973.

[62] K. Sharman and T. Durrani, "Resolving power of signal subspace methods for fnite data lengths," in *ICASSP*, Florida, USA, 1995, pp. 1501–1504.

[63] M. Shahram and P. Milanfar, "Imaging below the diffraction limit: A statistical analysis," *IEEE Trans. Image Processing*, vol. 13, no. 5, pp. 677–689, May 2004.

[64] Z. Liu and A. Nehorai, "Statistical angular resolution limit for point sources," *IEEE Trans. Signal Processing*, vol. 55, no. 11, pp. 5521–5527, Nov. 2007.

[65] A. Amar and A. Weiss, "Fundamental limitations on the resolution of deterministic signals," *IEEE Trans. Signal Processing*, vol. 56, no. 11, pp. 5309–5318, Nov. 2008.

[66] M. N. El Korso, R. Boyer, A. Renaux, and S. Marcos, "Statistical analysis of achievable resolution limit in the near field source localization context," *Signal Processing*, vol. 92, no. 2, pp. 547–552, Feb. 2012.

[67] ——, "On the asymptotic resolvability of two point sources in known subspace interference using a GLRT-based framework," *Signal Processing*, vol. 92, no. 10, pp. 2471–2483, Oct. 2012.

[68] H. B. Lee, "The Cramér-Rao bound on frequency estimates of signals closely spaced in frequency," *IEEE Trans. Signal Processing*, vol. 40, no. 6, pp. 1507–1517, Jun. 1992.

[69] M. N. El Korso, R. Boyer, A. Renaux, and S. Marcos, "Statistical resolution limit of the uniform linear cocentered orthogonal loop and dipole array," *IEEE Trans. Signal Processing*, vol. 59, no. 1, pp. 425–431, Jan. 2011.

[70] X. Zhang, M. N. El Korso, and M. Pesavento, "On the asymptotic resolvability of far-field stochastic sources," in *Proc. EUSIPCO*, Bucharest, Romania, Aug. 2012, pp. 889–893.

[71] ——, "Angular resolution limit for deterministic correlated sources," in *Proc. of IEEE Int. Conf. Acoust., Speech, Signal Processing (ICASSP)*, Vancouver, Canada, May 2013, pp. 5539–5543.

[72] H. B. Lee, "The Cramér-Rao bound on frequency estimates of signals closely spaced in frequency (unconditional case)," *IEEE Trans. Signal Processing*, vol. 42, no. 6, pp. 1569–1572, Jun. 1994.

[73] E. L. Lehmann, *Theory of Point Estimation*. New York: Wiley, 1983.

[74] M. Kaveh and A. J. Barabell, "The statistical performance of the MUSIC and the minimum-norm algorithms in resolving plane waves in noise," *IEEE Trans. Acoust., Speech, Signal Processing*, vol. 34, no. 2, pp. 331–341, Apr. 1986.

[75] E. Dilaveroglu, "Nonmatrix Cramér-Rao bound expressions for high-resolution frequency estimators," *IEEE Trans. Signal Processing*, vol. 46, no. 2, pp. 463–474, Feb. 1998.

[76] R. Boyer, "Performance bounds and angular resolution limit for the moving co-located MIMO radar," *IEEE Trans. Signal Processing*, vol. 59, no. 4, pp. 1539–1552, Apr. 2011.

[77] M. N. El Korso, R. Boyer, A. Renaux, and S. Marcos, "Statistical resolution limit for source localization with clutter interference in a MIMO radar context," *IEEE Trans. Signal Processing*, vol. 60, no. 5, pp. 987–992, Feb. 2012.

[78] M. N. El Korso, F. Pascal, and M. Pesavento, "On the resolvability of closely spaced targets using a colocated MIMO radar," in *Proc. 46th Asilomar Conference on Signals, Systems and Computers*, Pacific Grove, Nov. 2012, invited paper.

[79] M. Einemo and H. C. So, "Weighted least squares algorithm for target localization in distributed MIMO radar," *Signal Processing*, vol. 115, pp. 144–150, Oct. 2015.

[80] S. Hong, X. Wan, and H. Ke, "Spatial difference smoothing for coherent sources location in MIMO radar," *Signal Processing*, vol. 109, pp. 69–83, Apr. 2015.

[81] Y.-H. Tang, X.-F. Ma, W.-X. Sheng, and Y. Han, "Transmit beamforming for DOA estimation based on Cramer-Rao bound optimization in subarray MIMO radar," *Signal Processing*, vol. 101, pp. 42–51, Aug. 2014.

[82] L. Xu, J. Li, , and P. Stoica, "Target detection and parameter estimation for MIMO radar systems," *IEEE Trans. Aeronaut. Navig. Electron.*, vol. 44, no. 3, p. 927–939, Jul. 2008.

[83] L. Xu and J. Li, "Iterative generalized-likelihood ratio test for MIMO radar," *IEEE Trans. Signal Processing*, vol. 55, no. 6, pp. 2375–2385, Jun. 2007.

[84] Y. Jin, J. Huang, and J. M, "Least square DOA estimator fast algorithm by MIMO sonar," *Acta Electronica Sinica*, vol. 37, no. 9, pp. 2041–2045, Sep. 2009.

[85] W. Shi, J. Huang, and C. He, "Fast algorithm for maximum likelihood DOA estimation in MIMO array," in *Proc. World Congress on Engineering and Computer Science (WCECS)*, San Francisco, USA, Oct. 2011.

[86] W. Shi, J. Huang, and Y. Hou, "Fast DOA estimation algorithm for MIMO sonar based on ant colony optimization," *J. Syst. Eng. Electron.*, vol. 23, no. 2, pp. 173–178, Apr. 2012.

[87] C. Duofang, C. Baixiao, and Q. Guodong, "Angle estimation using ESPRIT in MIMO radar," *Electron. Lett.*, vol. 44, no. 12, p. 770–771, Jun. 2008.

[88] C. Jinli, G. Hong, and S. Weimin, "Angle estimation using ESPRIT without pairing in MIMO radar," *Electron. Lett.*, vol. 44, no. 24, p. 1422–1423, Nov. 2008.

[89] D. Nion and N. D. Sidiropoulos, "A PARAFAC-based technique for detection and localization of multiple targets in a MIMO radar system," in *Proc. of IEEE Int. Conf. Acoust., Speech, Signal Processing (ICASSP)*, Taipei, Taiwan, R.O.C., 2009, pp. 2077–2080.

[90] A. Hassanien and S. A. Vorobyov, "Transmit energy focusing for DOA estimation in MIMO radar with colocated antennas," *IEEE Trans. Signal Processing*, vol. 59, no. 6, pp. 2669–2682, Jul. 2011.

[91] C. Wen and G. Shi, "A unitary ESPRIT scheme of joint angle estimation for MOTS MIMO radar," *Sensors (Basel)*, vol. 14, pp. 14 411–14 422, Aug. 2014.

[92] J. Li, X. Zhang, and T. Hu, "Compressive sensing-based angle estimation for MIMO radar with multiple snapshots," in *Proc. Int. Conf. Comp. Sci. Electron. Eng. (ICCSEE)*, Hangzhou, China, Mar. 2013, pp. 2344–2347.

[93] X. Zhang, L. Xu, L. Xu, and D. Xu, "Direction of departure (DOD) and direction of arrival (DOA) estimation in MIMO radar with reduced-dimension MUSIC," *IEEE Commun. Lett.*, vol. 14, no. 12, pp. 1161–1163, Dec. 2010.

[94] X. Zhang and D. Xu, "Angle estimation in MIMO radar using reduced-dimension Capon," *Electron. Lett.*, vol. 46, no. 12, pp. 860–861, Jul. 2010.

[95] J. Li, X. Zhang, and W. Chen, "Root-MUSIC based angle estimation for MIMO radar with unknown mutual coupling," *Int. J. Antennas Propagat.*, vol. 2014, no. 1, pp. 1–8, Jan. 2014.

[96] C. Liu and D. B. Rubin, "ML estimation of the t distribution using EM and its extensions, ECM and ECME," *Statistica Sinica*, vol. 5, pp. 19–39, 1995.

[97] F. Pascal, Y. Chitour, J.-P. Ovarlez, and P. Forster, "Covariance structure maximum-likelihood estimates in compound Gaussian noise: Existence and algorithm analysis," *IEEE Trans. Signal Processing*, vol. 56, no. 1, pp. 34–48, Jan. 2008.

[98] J. Wang, A. Dogandžić, and A. Nehorai, "Maximum likelihood estimation of compound Gaussian clutter and taget parameters," *IEEE Trans. Signal Processing*, vol. 54, no. 10, pp. 3884–3897, Oct. 2006.

[99] Y. Chitour and F. Pascal, "Exact maximum-likelihood estimates for SIRV covariance matrix: Existence and algorithm analysis," *IEEE Trans. Signal Processing*, vol. 56, no. 10, pp. 4563–4573, Oct. 2008.

[100] P. Lombardo and C. J. Oliver, "Estimation of texture parameters in K-distributed clutter," *IEE Proceedings - Radar, Sonar and Navigation*, vol. 141, no. 4, pp. 196–204, Aug. 1994.

[101] M. Akcakaya and A. Nehorai, "Adaptive MIMO radar design and detection in compound-Gaussian clutter," *IEEE Trans. Aerosp. Electron. Syst.*, vol. 47, no. 3, pp. 2200–2207, Jul. 2011.

[102] A. Dogandžić and A. Nehorai, "Generalized multivariate analysis of variance: A unified framework for signal processing in correlated noise," *IEEE Signal Processing Mag.*, vol. 20, no. 5, pp. 39–54, Sep. 2003.

[103] M. Haardt, M. Pesavento, F. Röemer, and M. N. El Korso, *Subspace Methods and Exploitation of Special Array Structures, Electronic Reference in Signal Processing: Array and Statistical Signal Processing (M. Viberg, ed.).* Academic Press Library in Signal Processing, Elsevier Ltd., 2014, vol. 3.

[104] P. Stoica and A. Nehorai, "Performance study of conditional and unconditional direction of arrival estimation," *IEEE Trans. Acoust., Speech, Signal Processing*, vol. 38, pp. 1783–1795, Oct. 1990.

[105] A. J. Weiss and B. Friedlander, "On the Cramér-Rao bound for direction finding of correlated sources," *IEEE Trans. Signal Processing*, vol. 41, no. 1, pp. 495–499, Jan. 1993.

[106] M. Pesavento and A. B. Gershman, "Maximum-likelihood direction-of-arrival estimation in the presence of unknown nonuniform noise," *IEEE Trans. Signal Processing*, vol. 49, no. 7, pp. 1310–1324, Jul. 2001.

[107] H. Ye and R. D. DeGroat, "Maximum likelihood DOA estimation and asymptotic Cramér-Rao bounds for additive unknown colored noise," *IEEE Trans. Signal Processing*, vol. 43, no. 4, pp. 938–949, Apr. 1995.

[108] A. B. Gershman, P. Stoica, M. Pesavento, and E. Larsson, "Stochastic Cramér-Rao bound for direction estimation in unknown noise fields," *IEE Proceedings-Radar, Sonar and Navigation*, vol. 149, pp. 2–8, Jan. 2002.

[109] Y. Abramovich, O. Besson, and B. Johnson, "Bounds for maximum likelihood regular and non-regular DoA estimation in K-distributed noise," *IEEE Trans. Signal Processing*, vol. 63, no. 21, pp. 5746–5757, Nov. 2015.

[110] M. N. El Korso, A. Renaux, and P. Forster, "CRTB under K-distributed observation with parameterized mean," in *Proc. IEEE International Sensor Array and Multichannel Signal Processing Workshop (SAM)*, A Coruña, Spain, May 2014, pp. 461–464.

[111] P. Woodward, *Probability and Information Theory with Applications to Radar*. MA : Artech House: Norwood, 1980.

[112] X. Zhang, M. N. El Korso, and M. Pesavento, "Maximum likelihood and maximum a posteriori direction-of-arrival estimation in the presence of SIRP noise," in *Proc. of IEEE Int. Conf. Acoust., Speech, Signal Processing (ICASSP)*, Shanghai, China, Mar. 2016.

[113] S. Watts, "Radar detection prediction in sea clutter using the compound K-distribution model," *Proc. Inst. Electr. Eng. F*, vol. 132, no. 7, pp. 613–620, Dec. 1985.

[114] T. Nohara and S. Haykin, "Canada east coast trials and the K-distribution," *Proc. Inst. Electr. Eng. F*, vol. 138, no. 2, pp. 82–88, Apr. 1991.

[115] K. J. Sangston and K. R. Gerlach, "Coherent detection of radar targets in a non-Gaussian background," *IEEE Trans. Aerosp. Electron. Syst.*, vol. 30, no. 2, pp. 330–340, Apr. 1994.

[116] K. L. Lange, R. J. A. Little, and J. M. G. Taylor, "Robust statistical modeling using the t distribution," *J. Amer. Stat. Assoc.*, vol. 84, no. 408, pp. 881–896, Dec. 1989.

[117] E. Jay, J.-P. Ovarlez, D. Declercq, and P. Duvaut, "Bayesian optimum radar detector in non-Gaussian noise," in *Proc. of IEEE Int. Conf. Acoust., Speech, Signal Processing (ICASSP)*, Orlando, FL, May 2002, pp. 1289–1292.

[118] ——, "BORD: Bayesian optimum radar detector," *Signal Processing*, vol. 83, no. 6, pp. 1151–1162, Jun. 2003.

[119] E. Conte, A. D. Maio, and G. Ricci, "Recursive estimation of the covariance matrix of a compound-Gaussian process and its application to adaptive CFAR detection," *IEEE Trans. Signal Processing*, vol. 50, no. 8, pp. 1908–1915, Aug. 2002.

[120] T. W. Anderson, *An Introduction to Multivariate Statistical Analysis*, 3rd ed. New York: Wiley-Interscience, 2003.

[121] F. Gini and M. Greco, "Covariance matrix estimation for CFAR detection in correlated heavy tailed clutter," *Signal Processing*, vol. 82, no. 12, pp. 1847–1859, Dec. 2002.

[122] T. Jiang, N. D. Sidiropoulos, and J. M. F. ten Berge, "Almost-sure identifiability of multidimensional harmonic retrieval," *IEEE Trans. Signal Processing*, vol. 49, no. 9, pp. 1849–1859, Sep. 2001.

[123] S. A. Vorobyov, A. B. Gershman, and K. M. Wong, "Maximum likelihood direction-of-arrival estimation in unknown noise fields using sparse sensor arrays," *IEEE Trans. Signal Processing*, vol. 53, no. 1, pp. 34–43, Jan. 2005.

[124] P. Tseng, "Convergence of a block coordinate descent method for nondifferentiable minimization," *Journal of Optimization Theory and Applications*, vol. 109, no. 3, pp. 475–494, Jun. 2001.

[125] D. P. Bertsekas, *Nonlinear Programming*, 2nd ed. Nashua: Athena Scientific, 1999.

[126] B. Anderson, J. Jackson, and M. Sitharam, "Descartes' rule of signs revisited," *Amer. Math. Monthly*, vol. 105, pp. 447–451, 1998.

[127] R. A. Thisted, *Elements of Statistical Computing: Numerical Computation*. New York: Chapman & Hall, 1988.

[128] X. Zhang, M. N. El Korso, and M. Pesavento, "MIMO radar performance analysis under K-distributed clutter," in *Proc. of IEEE Int. Conf. Acoust., Speech, Signal Processing (ICASSP)*, Florence, Italy, May 2014, pp. 5287–5291.

[129] T. Groves and T. Rothenberg, "A note on the expected value of an inverse matrix," *Biometrika*, vol. 56, no. 3, pp. 690–691, Dec. 1969.

[130] A. Papoulis and S. U. Pillai, *Probability, random variables, and stochastic processes*. New York: McGraw-Hill, 1965.

[131] K. Petersen and M. Pedersen, "The matrix cookbook," *Citeseer*, 2006.

[132] H. L. V. Trees, *Optimum Array Processing: Part IV of Detection, Estimation, and Modulation Theory*. New York: John Wiley & Sons Inc., 2002.

[133] M. Viberg, P. Stoica, and B. Ottersten, "Maximum likelihood array processing in spatially correlated noise fields using parameterized signals," *IEEE Trans. Signal Processing*, vol. 45, no. 4, pp. 996–1004, Apr. 1997.

[134] P. Stoica and P. Babu, "The Gaussian data assumption leads to the largest Cramér-Rao bound [lecture notes]," *IEEE Signal Processing Mag.*, vol. 28, no. 3, pp. 132–133, May 2011.

[135] Y. Abramovich and O. Besson, "Fluctuating target detection in fluctuating K-distributed clutter," *IEEE Signal Processing Lett.*, vol. 22, no. 10, p. 1791–1795, Oct. 2015.

[136] O. Besson and Y. Abramovich, "Sensitivity analysis of likelihood ratio test in K distributed and/or Gaussian noise," *IEEE Signal Processing Lett.*, vol. 22, no. 12, pp. 2329–2333, Dec. 2015.

[137] A. Farina, F. Gini, M. V. Greco, and P. Lombardo, "Coherent radar detection of targets against a combination of K-distributed and Gaussian clutter," in *Proc. IEEE National Radar Conference*, Piscataway, NJ, 1995, pp. 83–88.

[138] D. R. Iskander and A. M. Zoubir, "Estimating the parameters of the K-distribution using the ML/MoM approach," in *Proc. TENCON. Digital Signal Processing Applications*, Perth, Australia, Nov. 1996, pp. 769–774.

[139] E. Ollila, D. E. Tyler, V. Koivunen, and H. V. Poor, "Complex elliptically symmetric distributions: Survey, new results and applications," *IEEE Trans. Signal Processing*, vol. 60, pp. 5597–5625, Nov. 2012.

[140] D. R. Iskander, "The generalised Bessel function K distribution and its application to the detection of signals in the presence of non-Gaussian interference," Ph.D. dissertation, Queensland University of Technology, Signal Processing Research Centre, Brisbane, Australia, Feb. 1997.

[141] D. R. Iskander, A. M. Zoubir, and B. Boashash, "A method for estimating the parameters of the K distribution," *IEEE Trans. Signal Processing*, vol. 47, no. 4, pp. 1147–1151, Apr. 1999.

[142] E. Ollila and D. E. Tyler, "Distribution-free detection under complex elliptically symmetric clutter distribution," in *Proc. IEEE International Sensor Array and Multichannel Signal Processing Workshop (SAM)*, Hoboken, NJ, Jun. 2012, pp. 413–416.

[143] M. Greco, S. Fortunati, and F. Gini, "Maximum likelihood covariance matrix estimation for complex elliptically symmetric distributions under mismatched conditions," *Signal Processing*, vol. 104, pp. 381–386, Nov. 2014.

[144] Y. Abramovich and O. Besson, "Regularized covariance matrix estimation in complex elliptically symmetric distributions using the expected likelihood approach — Part 1: The over-sampled case," *IEEE Trans. Signal Processing*, vol. 61, no. 23, pp. 5807–5818, Jul. 2013.

[145] O. Besson and Y. Abramovich, "Regularized covariance matrix estimation in complex elliptically symmetric distributions using the expected likelihood approach — Part 2: The under-sampled case," *IEEE Trans. Signal Processing*, vol. 61, no. 23, pp. 5819–5829, Oct. 2013.

Publications

Internationally Refereed Journal Articles

- X. Zhang, M. N. El Korso, and M. Pesavento, "MIMO radar target localization and performance evaluation under SIRP clutter," *Signal Processing*, January 2017, pp. 217-232.

Internationally Refereed Conference Papers

- X. Zhang, M. N. El Korso, and M. Pesavento, "Maximum Likelihood and Maximum A Posteriori Direction-of-Arrival Estimation in the Presence of SIRP Noise," in *Proc. 41th IEEE International Conference on Acoustics, Speech, and Signal Processing (ICASSP 2016)*, Shanghai, China, March 2016, pp. 3081-3085.

- X. Zhang, M. N. El Korso, and M. Pesavento, "MIMO Radar Performance Analysis under K-Distributed Clutter," in *Proc. 39th IEEE International Conference on Acoustics, Speech, and Signal Processing (ICASSP 2014)*, Florence, Italy, May 2014, pp. 5287-5291.

- X. Zhang, M. N. El Korso, and M. Pesavento, "Angular Resolution Limit for Deterministic Correlated Sources," in *Proc. 38th IEEE International Conference on Acoustics, Speech, and Signal Processing (ICASSP 2013)*, Vancouver, Canada, May 2013, pp. 5539-5543.

- X. Zhang, M. N. El Korso, and M. Pesavento, "On the Asymptotic Resolvability of

Far-Field Stochastic Sources," in *Proc. 20th European Signal Processing Conference (EUSIPCO 2012)*, Bucharest, Romania, August 2012, pp. 889-993.

Curriculum Vitae

Name:	Xin ZHANG
Date of birth:	19.11.1987
Place of birth:	Henan, China
Family status:	married

Education

09/2009 - 10/2012	Technische Universität Darmstadt, Germany Information and Communication Engineering (ICE), M.Sc. Master thesis: "*On the Asymptotic Resolvability of Far-Field Targets in Gaussian and Non-Gaussian Clutter*"
08/2005 - 07/2009	Tsinghua University, Beijing, China Electronic Engineering, B.Sc. Bachelor thesis: "*Software Development on Mobile Terminal Operating System*"
09/2002 - 06/2005	Xuchang High School, Xuchang, China High school degree (Abitur)

Work Experience

11/2012 - 05/2016	Research associate at Communication Systems Group, Technische Universität Darmstadt, Germany
10/2010 - 08/2011	Student research assistant at Fraunhofer Institute SIT, Darmstadt, Germany